Volume 2

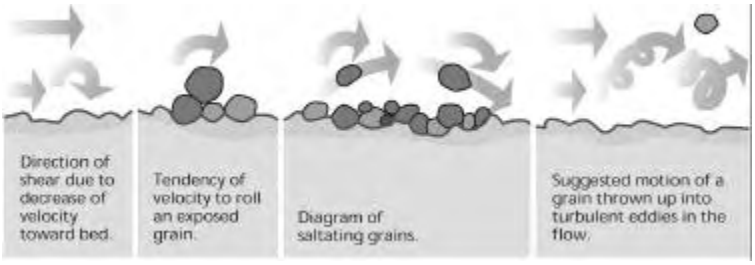

V. Processes

V. Processes

TABLE OF CONTENTS

	Page
FIELD AND LABORATORY JET TESTING METHOD FOR DETERMINING COHESIVE MATERIAL ERODIBILITY: Gregory J. Hanson, USDA-ARS, Stillwater, OK	V – 1
PREDICTING INTERPARTICLE BOND SHEAR STRENGTH NUMBER OF THE HEADCUT ERODIBILITY INDEX FROM SOIL INDEX TESTS: John S. Moore, USDA-NRCS, Washington, DC	V – 9
HEADCUT EROSION RESEARCH: Kerry M. Robinson and Gregory J. Hanson, USDA-ARS, Stillwater, OK	V – 15
EPHEMERAL GULLY EROSION MODEL (EGEM), NEXT STEP: Donald E. Woodward, USDA-NRCS, Washington, DC	V – 23
EVALUATING MECHANICS OF EMBANKMENT EROSION DURING OVERTOPPING: Gregory J. Hanson and Darrel M. Temple, USDA-ARS, Stillwater, OK	V – 24
COMPUTATION OF SEDIMENT EROSION FROM THE BASE OF CUT BANKS IN RIVER BENDS: Jason W. Kean and J. Dungan Smith, USGS, Boulder, CO	V – 31
USING THE PHOTO-ELECTRONIC EROSION PIN (PEEP) AUTOMATIC MONITORING SYSTEM TO DEFINE BANK EROSION EVENT TIMINGS: THE R. WHARFE, UK: Damian Lawler and ; J. S. Couperthwaite, The University of Birmingham, UK; G. J. L. Leeks, Centre for Ecology & Hydrology, Wallingford, Oxfordshire, UK	V – 39
SCIENTIFIC BASIS FOR STREAMBANK STABILIZATION USING RIPARIAN VEGETATION: Andrew Simon, USDA-ARS, NSL, Oxford, MS; and Andrew Collison, King's College, London, UK	V – 47
AN ANALYTICAL APPROACH TO ESTIMATE SOIL EROSION IN ROADSIDE DITCHES IN MOUNTAIN FOREST: Jennifer G. Duan, Desert Research Institute, Las Vegas, NV	V – 55
SEDIMENT DYNAMICS AND CONTAMINANT ACCUMULATION IN NEW YORK BIGHT: Marilyn Buchholtz ten Brink, Bradford Butman, Courtney Harris, Ellen Mecray, and William Schwab USGS, Woods Hole, MA	V – 63
EFFECTS OF TRAFFIC AND DITCH MAINTENANCE ON FOREST ROAD SEDIMENT PRODUCTION: Charles H. Luce and Thomas A Black, USDA-FS, Boise, ID	V – 67
MODELING THE EFFECTIVENESS OF SILT FENCE: Sherry L. Britton, Oklahoma State U., Stillwater, OK; Kerry M. Robinson, USDA-ARS NSL, Oxford, MS; and Billy Barfield, Oklahoma State U., Stillwater, OK	V – 75
EROSION AND SEDIMENT YIELDS IN TWO SUBBASINS OF CONTRASTING LAND USE, RIO PUERCO, NEW MEXICO: Allen Gellis, USGS, Albuquerque, NM; Milan Pavich, USGS, Reston, VA; and Amy Ellwein, Geologist, Austin, TX	V – 83
FACTORS CONTROLLING STORM-GENERATED SUSPENDED-SEDIMENT CONCENTRATIONS AND LOADS IN A HUMID-TROPICAL BASIN, QUEBRADA BLANCA, PUERTO RICO: Allen Gellis, USGS, Albuquerque, NM	V – 91
LONG-TERM SUSPENDED SEDIMENT MEASUREMENTS, REYNOLDS CREEK EXPERIMENTAL WATERSHED IN SOUTHWEST IDAHO: Frederick B. Pierson, Jr., Charles W. Slaughter, and Clayton L. Hanson, USDA-ARS, Boise, ID	V – 99

FIELD AND LABORATORY JET TESTING METHOD FOR DETERMINING COHESIVE MATERIAL ERODIBILITY

By Gregory J. Hanson, Research Hydraulic Engineer,
USDA-ARS Hydraulic Engineering Unit, Stillwater, Oklahoma

Author contact point: USDA-Agricultural Research Service, Plant Science and Water Conservation Research Laboratory, 1301 N. Western Street, Stillwater, OK 74075. Phone number (405) 624-4135, Fax number (405) 624-4136, e-mail address: ghanson@pswcrl.ars.usda.gov.

Abstract: *This paper provides a summary of the progress made in development and use of a submerged jet test for measurement of soil erodibility. The apparatus and methodology have been developed as a tool to measure the erodibility of cohesive materials. A submerged jet is directed at the material surface and amount of scour is measured. The two orifices used to produce the jets have been 6 mm and 13 mm diameter, respectively. The orifice height above the material surface used in testing has been from 6 to 20 times the diameter of the orifice. The method of analysis has progressed from use of a jet index to a physical analysis of the hydraulic excess stress parameters based on jet diffusion principles. The test device is capable of producing boundary shear stresses from less than 1 Pa to 1000 Pa. The methodology has been used to determine erodibility of materials in headcuts, embankments, scour holes, rills, compacted soils, streambeds, and stream banks. Erodibilities of cohesive materials have been found to vary over several orders of magnitude. This apparatus and methodology can be a useful tool for scientists, consultants, and government agencies interested in quantifying erodibility of cohesive materials.*

INTRODUCTION

Historically, it was hoped to find simple design rules for water erosion of cohesive soil channels based on easily determined criteria such as soil indexes, and flow velocity or stress applied. However, as more knowledge was gained it was revealed that erosion of cohesive soils is a complex system dependent on many parameters, including plasticity index, percent clay, density, moisture content, dispersion, and structure. Due to the complexity of erosion resistance and often subtle dependencies of one parameter to another, soil classification indexes have not proved useful as erosion predictors (Paaswell 1973).

The design method for stable channel boundaries in continuous open channel flow in erodible materials was initially based on an "allowable velocity." Generally, this method has been replaced by the concept of an "allowable stress." Allowable stress is the maximum stress that the channel bed can experience without excessive erosion. Research on stable channel boundary design has concentrated on the correlation of the allowable stress to fundamental soil and water properties (Dunn 1959, Smerdon and Beasley 1959, Carlson and Enger 1963, Lyle and Smerdon 1965, Kamphius and Hall 1983). Allowable stress is determined primarily by either one of two ways: visually assessing failure at a measured stress, or by plotting the erosion rate against stress and taking the allowable stress as the point at which the slope changes. In the literature, the stress at this point is commonly referred to as the critical stress. The latter approach, along with the need for understanding soil erodibility in unstable channel boundaries, has led researchers to not only observe fundamental soil and water properties in correlation to the allowable stress but also to observe the erosion rate at various stresses. This approach has led to the development of the excess stress equation to represent the detachment process of soil materials:

$$\varepsilon = k_d(\tau_e - \tau_c)^a \qquad [1]$$

where

ε = the erosion rate in volume of soil per unit time per unit area,
τ_e= the local effective stress, Pa
τ_c= the critical stress, Pa
k_d= the detachment coefficient, and
a = exponent (often assumed to be = 1).

This equation, although controversial as a mathematical representation of the detachment process, has proven useful as a simple equation to characterize soils. The terms k_d and τ_c are soil parameters, whereas the term τ_e is a hydraulic parameter.

Because soil indexes such as clay content, and dispersion, have not been conclusive predictors of erodibility there has been a need for the development of direct testing methods. The most dependable erosion test is a large open channel flow test with the material of interest forming the entire bed. However, this testing procedure poses many problems, including the effects of remolding and the large amounts of material required for testing. This dilemma has led to the development of smaller laboratory and in-situ devices such as linear flumes, annular flumes, sucking funnels, rotating cylinders, and jet probes (Liem et al. 1997, Grissinger 1982).

This paper provides a summary of the progress made in use and development of a submerged jet test. The apparatus and methodology have been developed as a tool to measure the erodibility of cohesive materials. The purpose of this paper is to describe a jet test apparatus and the research that has been conducted on measuring the erodibility of cohesive soils

DEVELOPMENT OF APPARATUS

Submerged Jet Testing: Jet testing of cohesive materials has been conducted in the laboratory (Dunn 1958, Moore and Masch 1962, Hollick 1976, Hanson 1992) as well as in-situ (DelVecchio and Moonen 1980, Hanson 1990). The laboratory jet testing has consisted of a submerged circular jet oriented perpendicular to the soil surface. The initial testing in the laboratory, even though scour was monitored, focused on critical stress determination. DelVecchio and Moonen (1980) utilized a non-submerged circular jet oriented perpendicular to the soil surface for site- specific testing of earthen spillway materials. They made relative comparisons of erosion resistance based on volume of material removed over time. Hanson (1991, 1992) used a submerged jet apparatus in the laboratory and in-situ, focusing on the rate of scour to characterize soils. Analysis of the jet test results has progressed to its present usage in three major steps: 1) analysis of the volume of material removed during scour; 2) analysis of the maximum depth of scour directly beneath the jet and determination of a jet index; and 3) analysis based on the diffusion characteristics of the jet to determine the excess stress parameters, detachment coefficient, and critical stress (Equation 1). These changes as well as changes in the apparatus are described below.

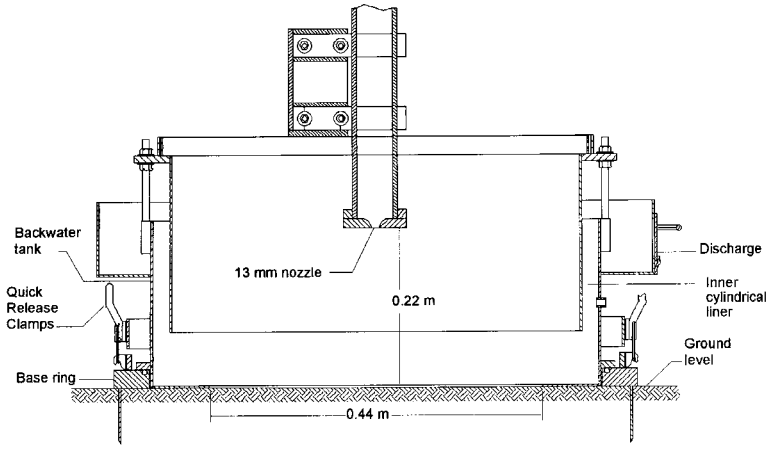

Figure 1. Submerged jet device for in-situ testing (Hanson, 1990).

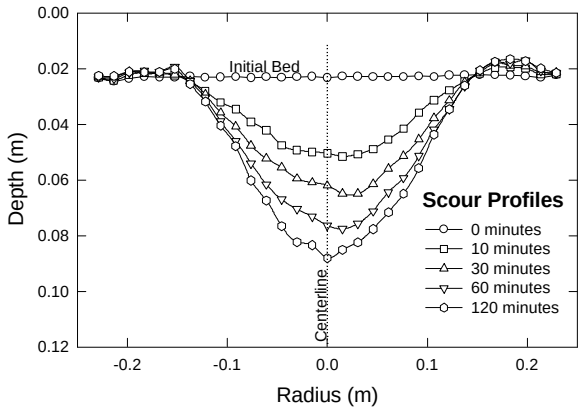

Figure 2. Measured scour profiles.

Hanson (1990) described a submerged jet device for in-situ testing of cohesive soils (Fig. 1). The device was mounted on a base ring with a sealing ring to prevent leakage and piping. A cylindrical tank was attached to the base ring to act as a weir while maintaining the water level required to submerge the jet. The soil surface inside the device was 0.46 m in diameter. Attached to the tank was an inner cylindrical liner that acted as a baffle to minimize return turbulence to the jet. The jet tube and pin profiler can be interchangeably mounted to the upper surface of this liner. A 51-mm diameter plexiglas tube, the lower end of which is fitted with a 13-mm diameter nozzle, is mounted in a hanger that can be set on the inner cylinder. The volume and maximum depth of scour during a jetting event were determined using a pin profiler. Measurements were typically taken at: 10, 30, 60, and 120 minutes of testing time, but could have been conducted for longer times depending on the resistance of the soil being tested. A typical set of profiles is shown in

Figure 2. The functional relationship used in the analysis of the results was similar to Moore and Masch (1962) and Hollick (1976), with the exception that the emphasis of the analysis was on incorporating the detachment coefficient rather than the critical tractive stress. The results of this study, based on a comparison of open channel results and jet tests results, indicated that the scour volume data could be collapsed by incorporating the coefficient of erodibility and using a fixed H_i and d:

$$\frac{\sqrt[3]{Vol}}{H_i} = 0.00436\left(\frac{\rho U_o d}{\mu}\right)^{0.67}\left(\frac{\mu t}{\rho d^2}\right)^{0.065}\left(\frac{k_d \mu}{d}\right)^{0.138} \qquad [2]$$

where

Vol = volume of material removed during scour,
H_i = height of nozzle above the initial surface (Fig. 3),
d = diameter of the jet nozzle,
U_o= jet velocity at the nozzle
k_d = detachment coefficient, and
μ = viscosity of the fluid
ρ = the fluid density.

Hanson (1991) developed a soil-dependent jet index based on the change in maximum scour depth caused by an impinging jet versus time. Based on results of multiple in-situ tests of four soil materials it was concluded that a simplified function based on the jet velocity U_o, maximum scour depth (D_s=H-H_i), dimensionless time function time t/t_1 (where t_1 = 1 second), and a jet index J_i could be used to characterize the erosion resistance of a soil material.

$$\frac{D_s}{t} = J_i U_o \left(\frac{t}{t_1}\right)^{-0.931} \qquad [3]$$

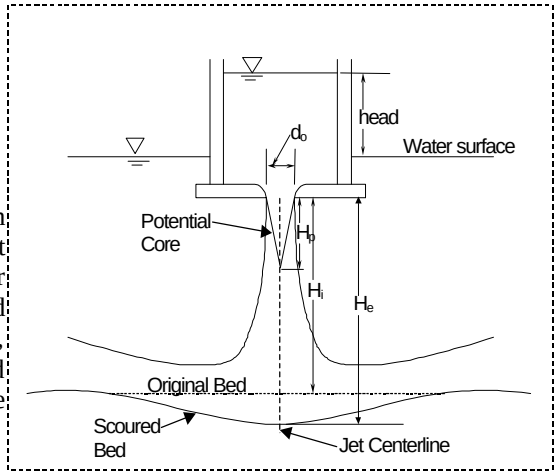

Figure 3. Definition of scour parameters.

The scour results for several in-situ tests of a CL-ML soil with 16% clay at different jet nozzle velocities U_o, are shown in Figure 4. It was observed that the scour depth increased with an increase in U_o, and the rate of scour depth decreased with time. A comparison of these results with Equation 3 is shown in Figure 5. The jet index for this soil is therefore a soil characteristic. The jet index was then empirically correlated to the k_d values obtained from open channel tests of the four soil materials (Hanson 1991). The testing apparatus and jet index methodology are described in ASTM Standard D5852-95, Standard Test Method for Erodibility Determination of Soil in the Field or in the Laboratory by the Jet Index Method.

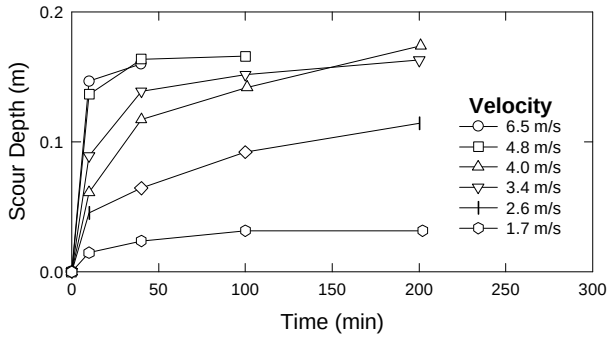

Figure 4. Maximum depth of scour versus time for a CL-ML soil at different velocities.

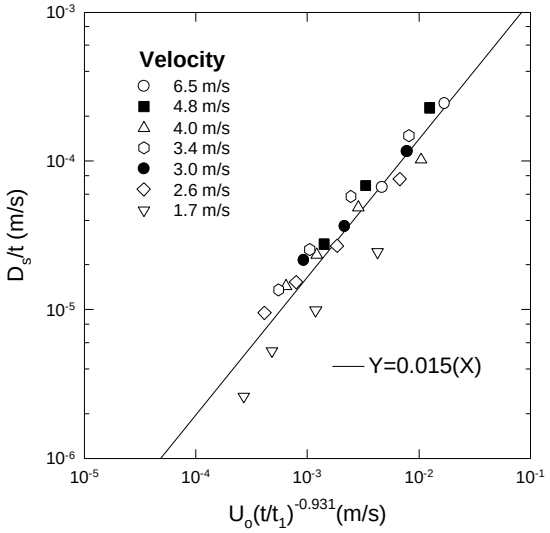

Figure 5. Jet Index J_i determination for a CL-ML soil.

In an attempt to remove empiricism and obtain direct measurements of the parameters τ_c and k_d, Hanson and Cook (1997) and Hanson et al. (2000) developed analytical procedures for determining soil erodibility based on the diffusion principles of a submerged circular jet, and scour beneath an impinging jet. These procedures are based on analytical procedures developed by Stein and Net (1997) for a planar jet at an overfall. Stein and Nett validated this approach in the laboratory using six different soil types. The diffusion principles of a circular jet are slightly different from those of a planar jet and therefore have resulted in differences in the final equations, but the basic concepts are the same.

In a submerged jet erosion test the height of the test varies with time. The jet origin is at an initial height H_i above the soil bed. As scour continues, an equilibrium depth is eventually reached, which results in a distance from the jet origin to the maximum point of scour H_e. The equilibrium depth is the scoured depth at which the hydraulic stresses created by the jet are no longer sufficient to cause additional downward erosion. As the jet travels toward the soil boundary, it spreads radially and diffuses throughout the surrounding fluid, decreasing the velocity. There is an initial reach length in which the centerline velocity U_o remains constant. This distance defines the potential core length from the jet origin H_p. Beyond this point, the velocity U remains at maximum along the jet centerline but the entire velocity field is reduced by diffusion.

If it is assumed that 1) the rate of change in the depth of scour dH/dt is the erosion rate as a function of the maximum stress at the boundary, and 2) the distance from jet origin to the initial bed surface is greater than H_p, then the erosion rate equation for the jet scour test is expressed similar to Equation 1 (Hanson and Cook 1997):

$$\frac{dH}{dt} = k_d \left[\frac{\tau_o H_p^{\,2}}{H^2} - \tau_c \right] \qquad [4]$$

When the rate of scour diminishes to dH/dt=0, equilibrium depth H_e is attained and critical stress is calculated as:

$$\tau_c = \tau_o \left(\frac{H_p}{H_e} \right)^2 \qquad [5]$$

A dimensionless form incorporating Equations 4 and 5 is expressed as:

$$\frac{dH^*}{dT^*} = \frac{(1 - H^{*2})}{H^{*2}} \qquad [6]$$

The dimensionless terms are defined as $H^* = H/H_e$, and $H_p^* = H_p/H_e$, and dimensionless time $T^* = t/T_r$, where t is time, and T_r is a reference time defined by Stein and Nett (1997):

$$T_r = \frac{H_e}{k_d \, \tau_c} \qquad [7]$$

Equation 6 indicates that the change in scour depth with time is expressed as a continuous function of the appropriate scour depth ratios for any time T^* from the jet origin $H^*=0$ to the equilibrium scour depth $H^*=1$. The integration of Equation 6 is:

$$T^* = 0.5 \ln \left(\frac{1 + H^*}{1 - H^*} \right) - H^* - 0.5 \ln \left(\frac{1 + H_i^*}{1 - H_i^*} \right) + H_i^* + T_i^* \qquad [8]$$

The function for Equation 8 is plotted in terms of H* versus T* in Figure 6 for H_p^* = 0.0, 0.1, 0.4, and 0.8, respectively. As seen from Figure 6, scour depth initially increases rapidly, especially for large values of H_p^*. Scour rate decreases rapidly as the equilibrium scour depth is approached and depth asymptotically approaches the equilibrium depth. Also note that for values of T*>0.001, the function of H* is very similar for values of H_p^*=0.0 and 0.1.

The parameters τ_c and k_d are determined by curve fitting measured values of H versus t to Equation 8 and minimizing the error of the measured time t_m and the predicted time t_p. Application of the same results shown in Figure 4 to equation 8 are shown in Figure 7. The advantage of this approach is that the excess stress parameters τ_c and k_d are determined independently. The jet index determination of k_d is dependent on the empirical relationship developed by Hanson (1991). This relationship was based on a comparison of open channel erosion tests on four

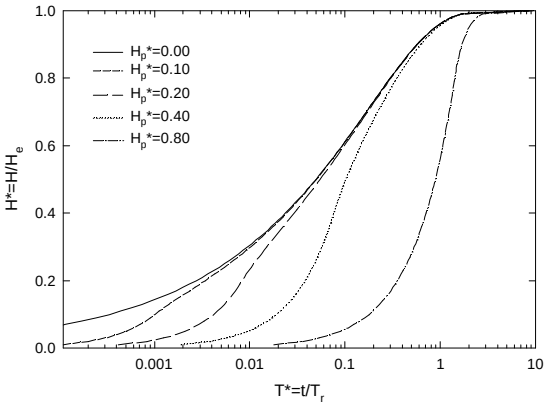

Figure 6. Theoretical dimensionless scour depth versus dimensionless time.

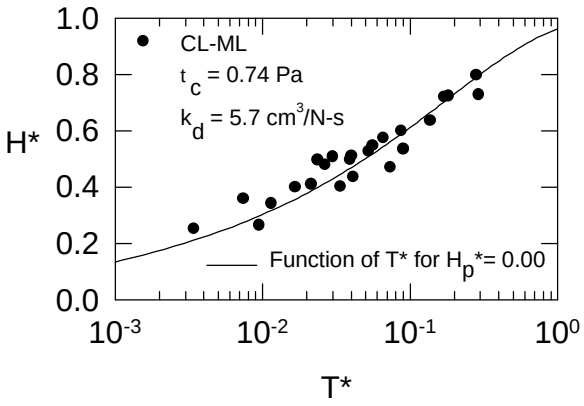

Figure 7. Dimensionless time function analysis for a CL-ML soil.

soils conducted in 1986 and 1987. In-situ jet tests for the same soils were conducted in 1988. Although the soil samples were prepared in the same manner for both tests, Hanson (1992) observed from laboratory tests that moisture content can have a significant effect on test results.

Soil samples for laboratory submerged jet testing were prepared by dynamic compaction attained by dropping a 79.4-kg hammer 0.30 m and controlling the number of blows. The soils were compacted in three layers, using 24 blows per layer, with the compaction effort of 603 kN-m/m^3. Moisture content was also controlled at the time of compaction. Tests were conducted on circular soil samples 0.44 m in diameter with a volume of 0.03 m^3. Water was fed under a constant head of 0.91 m, U_o = 4.2 m/s. The plot of τ_c and k_d versus moisture content (Figure 8, a-b) indicates that the compaction moisture content at the same compactive effort can have a significant impact on the erosion resistance. The k_d determined from the open channel tests and from the in-situ jet tests are shown in Figure 8 b with the laboratory jet test results to indicate that small changes in the moisture content at compaction could have potentially altered the erodibility determinations.

In an effort to compare open channel test results with equivalent in-situ jet test results, Hanson and Cook (1999) conducted: 1) a series of laboratory jet tests on compacted samples of a CL material at various moisture contents; 2) two open channel flow tests in a large outdoor flume; and 3) in-situ jet tests in the flume during the open channel flow tests. The two open channel erosion tests were conducted on this soil in a flume 1.8 m wide by 29 m long with 2.4-m sidewalls. A flat-bottomed channel 1.8 m wide and 21 m long was constructed in the flume for each test. Soil was placed in the flume on a 1% slope for test 1, and 3% slope for test 2. The average water content of the placed soil for tests 1 and 2 was 15.1% and 13.9%, respectively. Soil was placed in 15-cm loose lifts and compacted with 4 passes of a vibratory roller compactor, 2 passes without vibration and 2 with vibration. The resulting average dry unit weight for test 1 and 2 was 1.80 g/cm^3 and 1.85 g/cm^3, respectively.

The depth of erosion and average effective stress were determined from the data collected for each test. The effective stress range for tests 1 and 2 varied from 12 to 55 Pa. The τ_c for this soil, determined from Agricultural Handbook 667 (Temple et al. 1987), was 2.8 Pa for test 1 and 2.9 Pa for test 2. The k_d determined from the data was 0.06 cm^3/N-s for test 1 and 0.08 cm^3/N-s for test 2.

Following open channel testing, the flow was continued and in-situ jet tests were conducted on the channel bed. Three jet tests were conducted on the channel bed of test 1 and two jet tests were conducted on the channel bed of test 2. Average values of τ_c and k_d were determined from the jet tests run on channel tests 1 and 2: for test 1, τ_c = 2.1 Pa and k_d =0.12 cm^3/N-s; for test 2, τ_c = 1.1 Pa and k_d =0.09 cm^3/N-s. A comparison of the laboratory results, open channel results, and in-situ jet test results are shown in Figure 9 a and b. This example indicates the utility of the jet test for determining optimum placement conditions as well as corroboration of laboratory jet test, in-situ jet test, and channel erosion results.

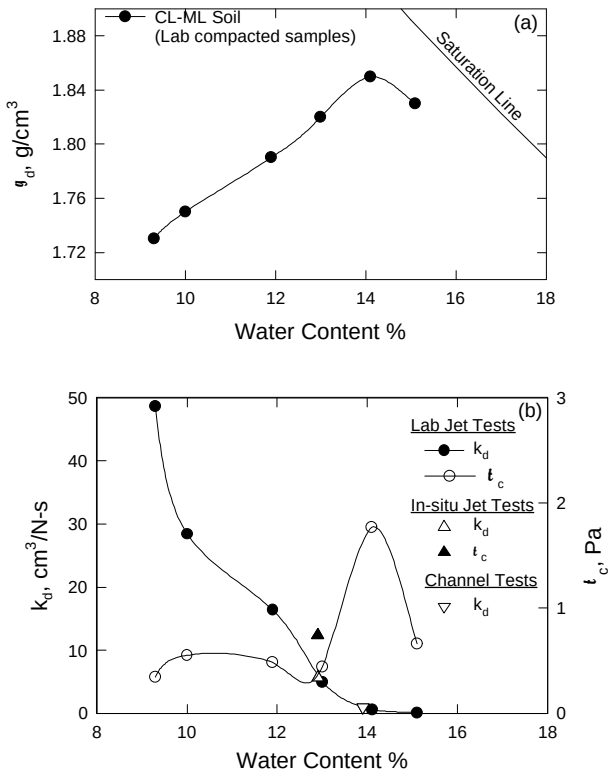

Figure 8. CL-ML Soil (a) Water content-dry unit weight relationship. (b) Water content – k_d and τ_c relationship for tested material.

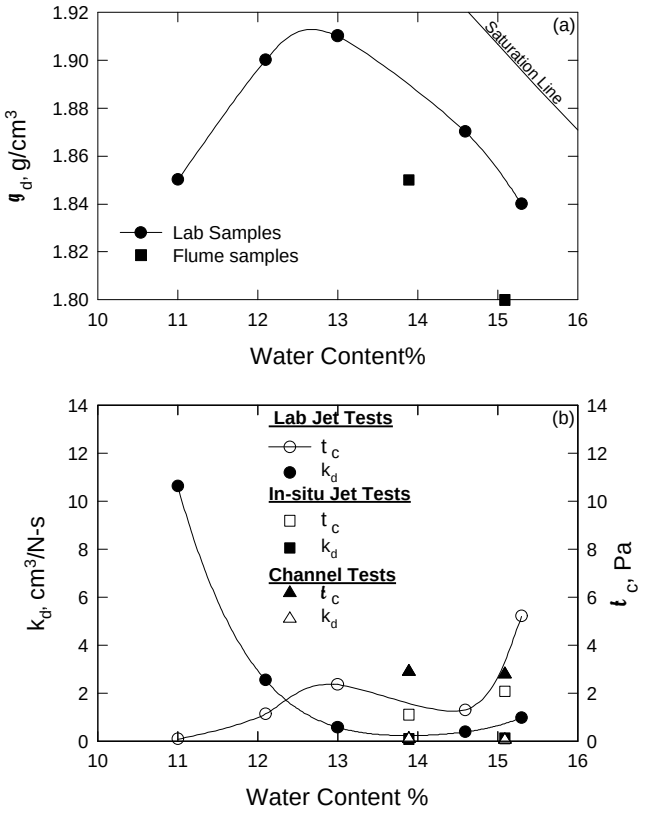

Figure 9. CL Soil (a) Water content– dry unit weight relationship. (b) Water content – k_d and τ_c relationship for tested material.

Jet Test Apparatus: Not only have the analytical procedures changed but there have also been changes in the apparatus due to differences in applications. The original apparatus (Hanson 1990) as described earlier (Fig. 1) has been modified into a smaller more portable version (Hanson and Cook 1999) for in-situ testing in open channel flow (Fig. 10). This later apparatus consists of a pump, adjustable head tank, jet submergence tank, jet nozzle (6.4-mm diameter), delivery tube, and point gage. Water is pumped directly from the channel bed into an adjustable head tank. The head and nozzle height are parameters adjusted to control the initial stress on the boundary. An initial stress of 1 Pa to 1000 Pa can be applied to the bed with this apparatus. Once the test is started scour readings are taken with a point gage aligned with the jet nozzle so that the point gage can pass through the nozzle to the bed to read depth of scour. The point gage is nominally equivalent to the nozzle diameter so that when the point gage rod passes through the nozzle opening flow is effectively shut off. Scour depth readings are typically taken at 10-minute intervals over a total duration of 120 minutes of testing.

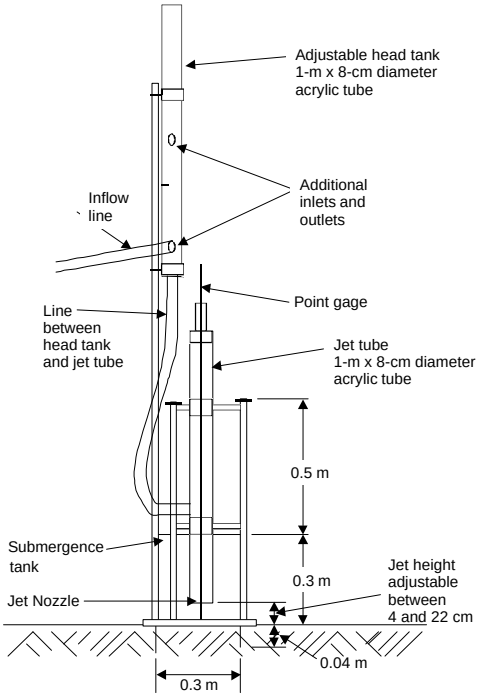

Figure 10. Schematic of a modified version of the in-situ jet test device.

Application: The submerged jet apparatus has been used to determine erodibility of cohesive soils in the open channel flow environment (Hanson and Cook 1999, Allen et al. 1999, Hanson and Simon 2000), to predict headcut migration (Hanson et al. 1999),

scour at an overfall (Hanson et al. 2000), and soil weathering (Robinson et al 2000). It may also prove useful in other applications, such as determining the erodibility of earthen embankments, agricultural fields, or bridge abutments.

CONCLUSIONS

The processes involved in erosion of cohesive materials in concentrated flow are complex. This paper presents the development of a submerged jet testing apparatus, procedure, and analytical methodology for characterizing the erosion resistance of cohesive soil materials. Research conducted to date has included tests conducted in large flumes for the purpose of developing a laboratory and in-situ jet device for measuring soil erodibility. Defining the parameters for the excess stress erodibility equation, and the factors that affect these parameters, such as water content, density, compaction, and roughness, has been the main focus of the research. Factors such as water content and density have been observed to affect τ_c and k_d by as much as 200 fold. Such observations point out the importance of using in-situ tests rather than relying solely upon empirical estimates, based on material classification to determine soil erodibility.

REFERENCES

Allen, P. M., Arnold, J., and Jakubowski, E., 1999, Prediction of Stream Channel Erosion Potential. Environmental and Engineering Geoscience V(3):339-351.

Carlson, E. J., and Enger, P. F., 1963, Studies of tractive forces of cohesive soils in earth canals. Hydraulic Branch Report No. Hyd-504, Bureau of Reclamation, Denver, CO.

DelVecchio, J. R., and Moonen, H. F., 1980, Measurement of erosion resistance of selected soils in New York utilizing the jet erosion tool. Soil Conservation Service, Syracuse, NY.

Dunn, I. S., 1959, Tractive resistance of cohesive channels. In Proc. Journal of the Soil Mechanics and Foundation Division, ASCE 85(SM3):1-24

Grissinger, E.H., 1982, Bank erosion of cohesive materials. In *Gravel-bed Rivers*. Hey, R. D., Bathurst, J. C., and Thorne, C. R., (eds.). Wiley: Chichester; 237-287.

Hanson, G. J., 1990, Surface erodibility of earthen channels at high stresses. Part II – Developing an in-situ testing device. Transactions of the ASAE 33(1):132-137.

Hanson, G. J., 1991, Development of a jet index to characterize erosion resistance of soils in earthen spillways. Transactions of the ASAE 36(5):1349-1352.

Hanson, G. J., 1992, Erosion resistance of compacted soils. Transportation Research Board, Transportation Research Record No. 1369:26-30.

Hanson, G. J. and Cook, K. R., 1997, Development of excess shear stress parameters for circular jet testing. Paper No. 97-2227. ASAE 2950 Niles Road, St. Joseph, MI 49085-9659 USA.

Hanson, G. J. and Cook, K. R., 1999, Procedure to estimate soil erodibility for water management purposes. Paper No. 99-2133. ASAE 2950 Niles Road, St. Joseph, MI 49085-9659 USA.

Hanson, G. J. and Simon, A., 2000, Erodibility of cohesive streambeds in the loess area of the Midwestern USA. Hydrological Processes. 2000 (*in press).*

Hanson, G. J., Robinson, K. M., and Cook, K. R. 1999, Prediction of headcut migration using a deterministic approach. ASAE Paper No. 002065. St. Joseph, MI. 22 pp.

Hanson, G. J., Robinson K. M., and Cook, K. R., 2000, Estimating free overfall jet scour of a cohesive soil. Paper No. 00-2065. ASAE 2950 Niles Road, St. Joseph, MI 49085-9659 USA.

Hollick, M., 1976, Towards a routine test for assessment of the critical tractive forces of cohesive soils. Transactions of the ASAE 19(6): 1076-1081.

Kamphius, W. J. and Hall, K. R.. 1983, Cohesive material erosion by unidirectional current. Journal of Hydraulic Engineering, ASCE 109(1):49-60.

Liem, R., Spork, V., and Kongeter, J., 1997, Investigations on erosional processes of cohesive sediment using an in-situ measuring device. Proceedings of the Conference on Management of Landscape Disturbed by Channel Incision, pp. 794-799.

Lyle, W. M., and Smerdon, E. T., 1965, Relation of compaction and other soil properties to erosion resistance of soils. Transactions of the ASAE 8(3):419-422.

Moore, W. L., and Masch, F. D., 1962, Experiments of the scour resistance of cohesive sediments. Journal of Geophysical Research. 67(4):1437-1446.

Paaswell, R. E., 1973, Causes and mechanisms of cohesive soil erosion: The state of the art. Highway Research Board Special Report No. 135. pp. 52-74.

Robinson, K. M., Bennett, S. J., Hanson, G. J., and Kadavy, K. C., 2000, The influence of weathering on headcut erosion. Paper No. 00-2066. ASAE 2950 Niles Road, St. Joseph, MI 49085-9659 USA.

Smerdon, E. T. and Beasley, R. P., 1959, The tractive force theory applied to stability of open channels in cohesive soil. Research Bulletin 715. University of Missouri. Ag. Exp. Station.

Stein, O. R. and Nett, D. D.. 1997, Impinging jet calibration of excess shear sediment detachment parameters. Transactions of the ASAE 40(6):1573-1580.

Temple, D. M., Robinson, K. M., Ahring, R. M., and Davis, A. G., 1987, Stability design of grass-lined open channels. USDA Agric. Handbook No. 667. Washington, D.C

PREDICTING INTERPARTICLE BOND SHEAR STRENGTH NUMBER OF THE HEADCUT ERODIBILITY INDEX FROM SOIL INDEX TESTS

By John S. Moore
National Hydrogeologist/Fluvial Geomorphologist
Natural Resources Conservation Service
Washington, DC

ABSTRACT. The US Department of Agriculture (USDA), Natural Resources Conservation Service (NRCS) uses the SITES software program to determine breach potential of auxiliary earth spillways of dams. One component of the computational model predicts the rate of headcut advance within the spillway. The component utilizes an energy-based parameter to represent hydraulic attack and a headcut erodibility index to describe resistance of geologic materials to that attack. The headcut erodibility index applies across a broad spectrum of geologic materials ranging in strength from soft cohesive soil through hard massive rock. One of the parameters that comprise the index is the discontinuity or interparticle bond shear strength number, K_d. Although for rock and rock-like materials the number can be estimated reliably by simple field tests, the results for soil materials are typically less consistent, and therefore, less dependable unless backed up by laboratory shear testing. Because shear strength testing is costly, a rational method is described to predict the effective residual friction angle from less expensive soil index tests. Specifically, the liquid limit of cohesive soil material is used to predict the effective residual friction angle at an assumed effective normal stress of 100 kPa, for three broad ranges of clay size-fraction. The K_d factor is then taken to be represented by the tangent of the effective residual friction angle of the material.

INTRODUCTION

The earth spillway erosion model (called SITES) that is incorporated into the NRCS Water Resource Site Analysis Program (NRCS, 1997a) predicts erosion from a given outflow hydrograph through auxiliary earth spillways of dams. The intended uses of the model are to minimize spillway erosion damages and evaluate the potential for the flow to breach the spillway. One component of the computational model predicts the rate of headcut advance within the spillway. The component utilizes an energy-based parameter to represent hydraulic attack and a headcut erodibility index to describe resistance of geologic materials to that attack (Temple and Moore, 1997). The logarithmically scaled geologic parameters that constitute the Headcut Erodibility Index, K_h, include earth material strength number, M_s, block or particle size number, K_b, discontinuity or interparticle bond shear strength number, K_d, and relative ground structure number, J_s, which accounts for both the shape of material units and their orientation relative to stream flow. The headcut erodibility index to a broad spectrum of geologic materials ranging in strength from loose granular or soft cohesive soils through extremely hard, massive rock. NRCS (1997b) uses field procedures developed by Moore (1997) to determine the index.

CURRENT PROCEDURE FOR DETERMINING K_d FOR COHESIVE MATERIALS

The interparticle bond shear strength number for cohesive material was originally defined by Barton et. al. (1974) to be approximately represented by the tangent of the effective residual friction angle, ϕ'_r, of the material. The NRCS Field Procedures Guide (1997b) provides a subjective methodology for estimating K_d for cohesive materials. Clay mineralogy, relative plasticity, and particle size gradation are used subjectively to provide a table of logarithmically scaled values from which one can, by using an appropriate measure of professional judgement, arrive at a rough approximation of an effective residual friction angle. The Guide suggests that field estimates of K_d be backed up with laboratory determinations of ϕ'_r [1/] Because laboratory shear strength testing of cohesive soils is costly and time-consuming and is often considered impractical by the field practitioner, an alternative method for predicting K_d is examined that uses standard soil index properties that correlate with the effective residual friction angle.

REVIEW OF SOIL INDEX PROPERTIES THAT INFLUENCE RESIDUAL SHEAR STRENGTH OF COHESIVE MATERIALS

Correlations between drained residual shear strength and various soil index properties are widely reported in the literature. An exhaustive review is beyond the scope of this paper; however, papers by Lupini et. al. (1981), Collotta et. al. (1989) and, more recently, Stark and Eid (1994 and 1997), examine most of the available, practical correlations that have been developed from case histories and laboratory tests performed by various researchers since the mid-1960's.

The clay size fraction (CF), plasticity index (PI), liquid limit (LL), and (to some extent) clay mineralogy are the parameters that generate particular interest because they are routine tests performed in most geotechnical soil investigation programs and are relatively fast and inexpensive. All of the correlations have a certain amount of scatter in the data, as would be expected from empirical relationships. The trends in the data are clear, however. High clay content, high plasticity indexes, and high liquid limits contribute to low residual shear strengths. Clay mineralogy, particularly type and shape, also influences residual strength. Smaller, more plate-shaped clay minerals contribute to low residual shear strengths. In this context, the most common clay minerals can be listed in the following order of decreasing residual strength: massive minerals (e.g. quartz, feldspar), kaolinite, micaceous minerals (e.g. chlorite, illite), and montmorillonite (Mesri et. al., 1986).

Stark and Eid (1994) conducted torsional ring shear tests on specimens of remolded, normally consolidated, cohesive clays at effective normal stresses ranging from 50 to 700 kPa. Liquid limit was used as an indicator of clay mineralogy, and clay-size fraction the quantity of particles smaller than 0.002 mm. The drained residual failure envelopes were nonlinear at all effective normal stresses for given liquid limits and clay-size fractions. They concluded that a drained residual strength correlation could be used to estimate the entire nonlinear failure envelope or ef-

[1/] The NRCS Soil Mechanics Center is equipped to conduct ASTM D 3080, Direct Shear Test of Soils Under Consolidated Drained Conditions, and ASTM D 6467, Torsional Ring Shear Test to Determine Drained Residual Shear Strength of Cohesive Soils.

fective residual friction angle that corresponds to the average effective normal stress on the slip surface. They describe an empirical correlation for the effective residual friction angle as a function of liquid limit, clay-size fraction, and effective normal stress.

Figure 1 is a plot of Stark and Eid's data for drained effective residual friction angle and soil index properties, at an effective normal stress of 100 kPa. This data set was selected because it reasonably represents the normal stress that would be characteristic of soil materials in NRCS earth spillways subject to headcut erosion. Power functions, R^2, and n for the three curves are given in Table 1.

Table 1.

Clay-size Fraction	R^2	n	Power Function of ϕ'_r	
< 20 %	0.9986	3	$169.58\ (LL)^{-0.4925}$	(1)
25 – 45 %	0.9891	5	$329.56\ (LL)^{-0.7100}$	(2)
≥ 50 %	0.9588	12	$234.73\ (LL)^{-0.6655}$	(3)

Figure 1. Residual Friction Angle vs. Liquid Limit for Three Ranges in Clay Content

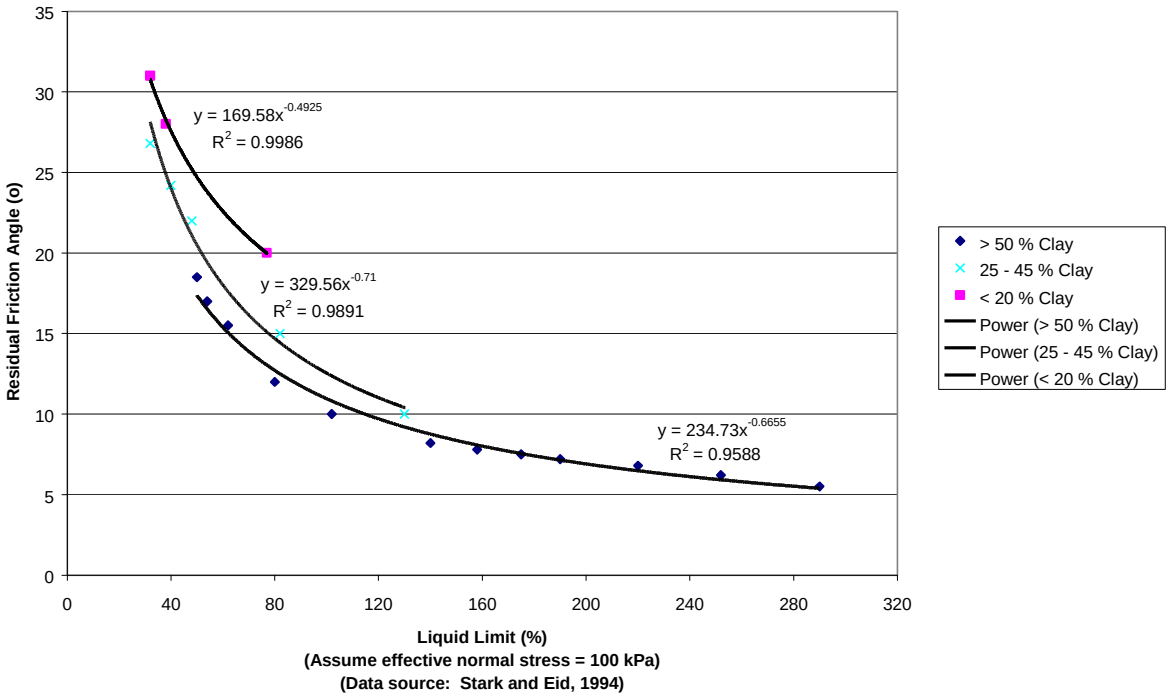

A METHOD FOR PREDICTING INTERPARTICLE BOND SHEAR STRENGTH NUMBER, K_d

The interparticle bond shear strength number (K_d) of a cohesive soil is predicted by a rational correlation between soil index properties and residual shear strength by the following method.

1. Determine the liquid limit by ASTM D 4318, Standard Test Method for Liquid Limit, Plastic Limit, and Plasticity Index of Soils, and report the result to the nearest one percent.
2. Determine clay content (the percent finer than 0.002 mm) by ASTM D 422, Standard Test Method for Particle-Size Analysis of Soils, and report the result to the nearest five percent.
3. Use the clay content value to select the appropriate equation (1, 2, or 3) to predict effective residual friction angle, ϕ'_r, and report the result to the nearest one-tenth degree.

For soil materials, the interparticle bond shear strength number, K_d, of the Headcut Erodibility Index is taken to be the tangent of the effective residual friction angle, ϕ'_r:

$$K_d = \tan \phi'_r \qquad (4)$$

EXAMPLE PREDICTIONS OF K_d

Results of NRCS soil mechanics laboratory testing on seven fine-grained soil samples are summarized in Table 2. Because all the soil samples contained greater than 50 percent clay, effective residual friction angles are predicted by using equation 3. Figure 2 is a plot of the effective residual friction angle versus liquid limit for the seven samples with respect to the equation 3 curve. Figure 3 shows the plot of the K_d predicted from soil index tests versus the laboratory determination of residual shear strength.

Table 2. NRCS Soil Mechanics Laboratory Data

State	Watershed	Sample #	LL	PI	Clay (%)	Lab Shear, ϕ'_r? (°)	Calculated*, ϕ'_r (°)	K_d (From Lab Shear)	K_d (From Curve)
AL	Old Town Creek 37	1939	70	44	>50	10.6	13.9	0.185	0.242
AR	Ozan Creek 20	673	56	27	>50	21.0	16.1	0.367	0.281
AL	Mush Creek 2	85-1726	70	45	>50	12.0	13.9	0.209	0.242
TX	Auds Creek 8A	79-1855	50	26	>50	13.7	17.4	0.239	0.303
TX	Elm Creek	2365	88	65	>50	10.5	11.9	0.183	0.208
TX	Elm Creek	2378	75	53	>50	9.4	13.3	0.164	0.232
TX	Greys	None	76	51	>50	15.7	13.1	0.274	0.229

* $\phi'_r = 234.73\ (LL)^{-0.6655}$

Figure 2. NRCS Lab Data vs. Stark and Eid Data

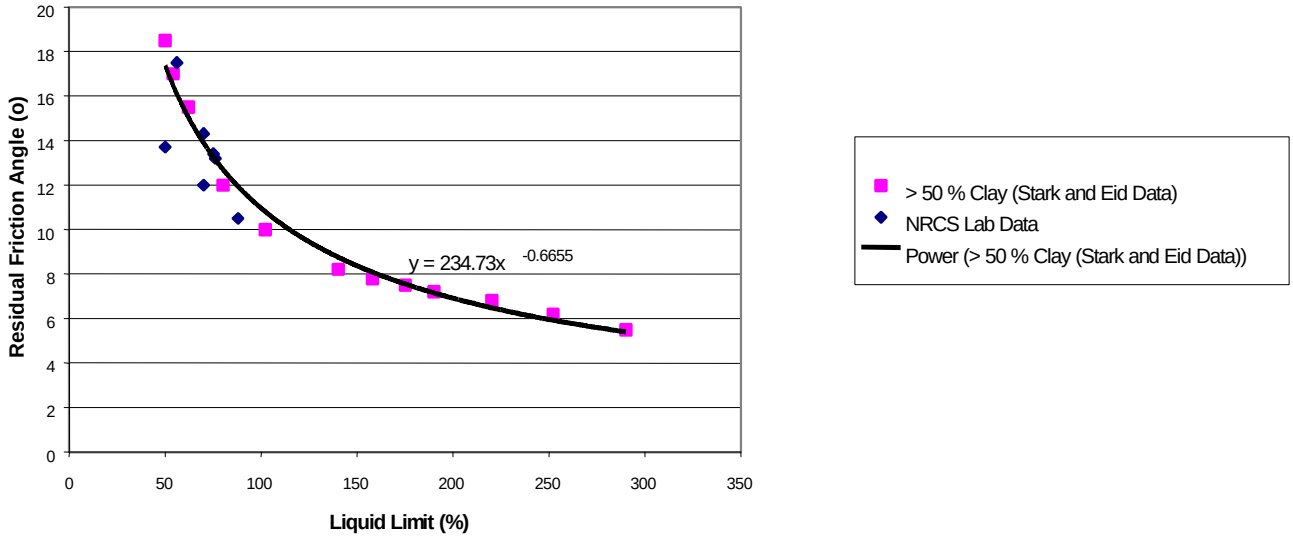

Figure 3. Predicted vs. Measured Kd

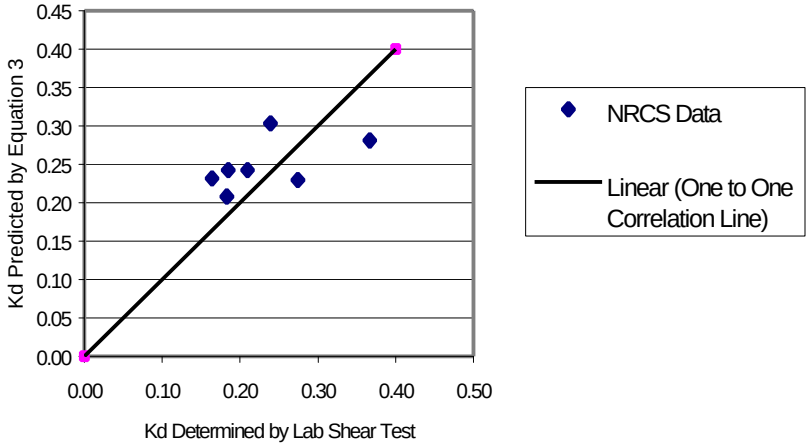

CONCLUSION

A method is considered for predicting the interparticle bond shear strength number of the Headcut Erodibility Index according to a rational correlation (Stark and Eid, 1994) of soil index properties with the effective residual friction angle. A limited number of NRCS data show reasonably good correlation by this approach; however, additional data are being collected from the NRCS soil mechanics laboratories to further test the apparent relationship between the effective residual friction angle and soil index tests. Use of a rational correlation in lieu of a traditional laboratory determination of residual shear strength is under consideration by the NRCS to expedite field classification of the hydraulic erodibility of materials in earth auxiliary spillways.

REFERENCES CITED

American Society for Testing and Materials, Annual Book of ASTM Standards: Section 4, Construction, vol. 04.08 and 04.09 (Standards D 422, D 2487, D 3080, D 4318, and D 6467), 100 Barr Harbor Drive, West Conshohocken, PA, 19428.

Barton, Nick, Lien, R., and Lunde, J., 1974, Engineering classification of rock masses for the design of tunnel support: Rock Mechanics, vol. 6, no. 4, pp. 189-236.

Collotta, T., Cantoni, R., Pavesi, U., Ruberl, E., and Moretti, P.C., 1989, A correlation between residual friction angle, gradation, and the index properties of cohesive soils: Géotechnique, London, England, vol. 39, no. 2, pp. 343-346.

Lupini, J.F., Skinner, A.E., and P.R. Vaughn, 1981, The drained residual strength of cohesive soils: Géotechnique, London, England, vol. 31, no. 2, pp. 181-213.

Mesri, G., and Cepeda-Diaz, A.F., 1986, Residual shear strength of clays and shales: Géotechnique, London, England, vol. 36, no. 2, pp. 269-274.

Moore, John S., 1997, Field procedures guide for the headcut erodibility index: Transactions, American Society of Agricultural Engineers, vol. 40, no. 2, pp. 325-336.

Natural Resources Conservation Service, USDA, 1997a, Earth spillway erosion model: National Engineering Handbook, 210-VI, Part 628, Chapter 51 (NEH-628-51), 10 p.

_____ 1997b, Field procedures guide for the headcut erodibility index: National Engineering Handbook, 210-VI, Part 628, Chapter 52 (NEH-628-52), 31 p.

Ralston, David C., and Brevard, John A., 1988, SCS's 40 year experience with earth auxiliary spillways: Proceedings of 5th Annual Conference, Association of State Dam Safety Officials, Manchester, NH, September, 1988, 19 p.

Stark, Timothy D., and Eid, Hisham T., 1994, Drained residual strength of cohesive soils: Journal of Geotechnical Engineering, American Society of Civil Engineers, vol. 120, no. 5, May, 1994, pp. 856-871.

_____, 1997, Slope stability analysis in stiff fissured clays: Journal of Geotechnical and Geoenvironmental Engineering, American Society of Civil Engineers, vol. 123, no. 4, pp. 335-343.

Temple, Darrel M., and Moore, John S.,1997, Headcut advance prediction for earth spillways: Transactions, American Society of Agricultural Engineers, vol. 40, no. 3, pp. 557-562.

HEADCUT EROSION RESEARCH

Authors: **Kerry M. Robinson and Gregory J. Hanson, Research Hydraulic Engineers, USDA-ARS Hydraulic Engineering Research Unit, Stillwater, Oklahoma**

Authors contact point: USDA-Agricultural Research Service, Plant Science and Water Conservation Research Laboratory, 1301 N. Western Street, Stillwater, Oklahoma, 74075. Phone number (405)624-4135, Fax number (405)624-4136, e-mail addresses: krobinson@pswcrl.ars.usda.gov and ghanson@pswcrl.ars.usda.gov.

Abstract: A comprehensive research program was conducted to examine headcut erosion processes in compacted cohesive soils. A headcut test facility was constructed, and a systematic examination of the dominant parameters that influence headcut erosion was performed. Major findings from the last seven years of headcut erosion research using this facility are briefly described. The influence of soil properties, hydraulic forces, overfall geometry, and multiple soil layers in the profile were examined. The influence of weathering and fractured materials was also investigated. Predictive relationships are discussed that allow the user to predict the headcut advance rate and the rate of vertical scour downstream of a headcut.

INTRODUCTION

Headcut erosion occurs worldwide, causing major problems such as dissection of the landscape, channel instability, and earth spillway damage. Headcut erosion occurs as rills, ephemeral gullies, field gullies, large headcuts, and stream knickpoints. As water passes over an overfall, or abrupt drop in bed elevation, the impinging nappe attacks the channel bed and creates a reverse roller (Fig. 1). This flow circulation transfers hydraulic shear stress to the near-vertical overfall face. The impinging nappe and flow circulation typically cause deepening and undercutting of the headcut face causing the headcut to retreat upstream. Headcut erosion delivers vast quantities of sediment to receiving streams, with attendant negative environmental impacts.

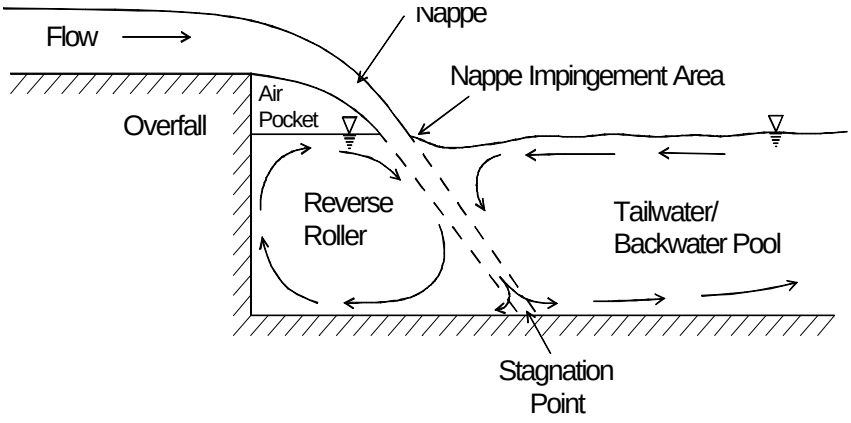

Figure 1. Definition sketch (Robinson et al., 2000b)

In order to learn more about fundamental headcut erosion processes, a research program was conceived by the authors in 1992. A large-scale flume was constructed for the primary purpose of conducting headcut erosion tests. The flume and appurtenant flow measurement and tailwater control structures were completed in 1993. Since then, numerous tests have been conducted that enhance our present knowledge of headcut erosion. The objective of this paper is to summarize the major findings from the last seven years of headcut erosion research using this facility. Investigation of this challenging topic is on-going.

EXPERIMENTAL SETUP

Test Facility: The headcut erosion test facility is composed of three concrete structures connected by earthen dikes. While not drawn to scale, a centerline profile of the test facility is provided (Fig. 2). Flow measurement is provided with a 2.4-m (8-ft) wide modified Parshall flume. Immediately downstream of this flume is a 2.7-m (9-ft) wide straight drop spillway with a 3.0-m (10-ft) vertical drop. An earth forebay connects the drop structure with the test flume. The drop structure and forebay provide subcritical flow to the test flume.

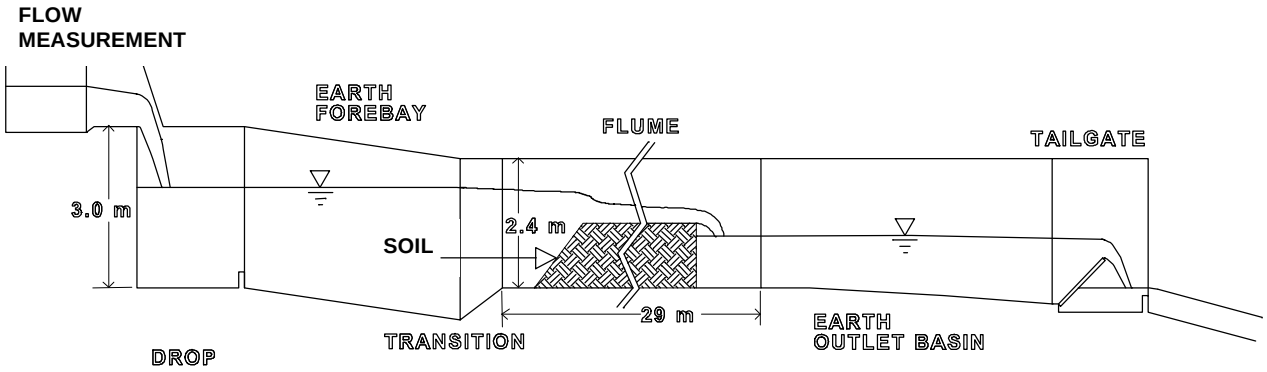

Figure 2. Test facility centerline profile (Robinson and Hanson, 1995).

A 2.4-m (8-ft) long concrete transition section is located at the upstream end of the flume to provide uniform approach flow conditions. The 29-m (96-ft) long horizontal test flume is 1.8 m (6 ft) wide and has 2.4-m (8-ft) tall sidewalls. A rail-mounted carriage on top of the flume walls allows rapid water surface and bed profile measurement, and the flume wall also has two windows that allow a side view of the erosion process.

The flume exits into an earthen outlet basin where the majority of sediment is deposited after a test. An outlet structure, located at the downstream end of the outlet basin, is equipped with a 2.3-m (7.5-ft) wide overflow tailgate. This tailgate allows tailwater control within the flume. The outlet basin is also connected to a supply canal, so it can be filled to a desired tailwater level before beginning a test flow. A more detailed description of the test facility is provided in Robinson and Hanson (1995).

EXPERIMENTAL PROCEDURE

Soil Material and Sampling: The primary soil examined in this study exhibited a liquid limit of 26 and a plasticity index of 15. Using the Unified Soil Classification System, this red sandy clay (CL) exhibited 25% clay, 40% silt, and 35% sand. This soil was selected primarily because large quantities with uniform soil properties could be obtained locally. Standard Proctor tests displayed a maximum dry density of 1.9 Mg/m^3 (119 lb/ft^3) at an optimum moisture of 12%. Soil strength is an important parameter in headcut advance, and a strong relationship exists between the density and strength for this soil. In the initial tests, strength and density data were intentionally varied over a wide range (Robinson and Hanson, 1995). Following placement of the soil in the flume and before testing, samples were taken from the downstream end of the placed soil. Density samples were taken with 76-mm (3-in) diameter push tubes at

approximately 152-mm (6-in) intervals in the profile. Unconfined compressive strength samples were taken at 305-mm (12-in) intervals with 51-mm (2-in) diameter push tubes. Compacted soil densities typically ranged from 70 to 100% of Standard Proctor density.

Fill Preparation: The test flume was filled by placing soil in horizontal loose lift layers ranging in thickness from 100 to 150 mm (4 to 6 in). Typically, water was added to achieve the desired soil moisture. A PTO-operated tiller was used to mix the soil layer and to reduce aggregate sizes. A 0.9-m (34-in) wide self-propelled vibratory sheepsfoot roller was used to compact each soil layer. The fill was compacted with repeated passes of the roller over the fill layer. A vibratory load could also be used to increase compactive effort. A hand-held pneumatic compactor was used to compact the soil next to the concrete walls. The compacted soil surface was then scarified with a tiller to improve bonding with subsequent layers. These fill placement procedures were repeated until the desired fill depth was obtained. As the fill depth increased, a ramp was constructed at each end of the fill. This ramp allowed equipment access to the top of the fill. Before testing, the downstream ramp was removed, and a vertical headcut was prepared at the end of the test section. The fill section included additional horizontal length to allow for soil sampling at the downstream end of the test section. The total length of horizontal fill varied depending on test objectives. Overfall heights up to 1.55 m (5.1 ft) were tested.

For the headcut advance tests, a soil cement treatment was added to the fill surface to minimize soil erosion upstream of the headcut. Portland cement at a rate of 4% (by weight) was mixed into the top 75 mm (3 in) of the soil surface and then compacted. The soil cement treatment served to retard surface detachment without restricting the headcut erosion processes. The weathering tests did not have a soil cement treatment.

Testing: Flume tests were conducted following a routine sequence of events. Soil sampling was conducted, and the headcut was preformed. The tailgate was set to the desired position, and the flow was introduced into the forebay. Once the forebay was filled and the flow reached the overfall, the headcut position was monitored with time. Water surface and bed profiles were taken periodically during the test, as were discharge measurements. Normally, the test continued until the horizontal fill section was completely breached.

RESULTS

A systematic plan of attack was formulated for the headcut erosion problem. It was understood from the beginning that this complex erosion behavior could be influenced by many parameters. Hydraulic parameters such as the shear stress, flow rate, and tailwater level were thought to be important. The resisting forces of the compacted cohesive soil such as soil strength, dry density, moisture content, and overfall geometry were also considered important. Certainly other parameters such as seepage and weathering were also believed to be important. Test objectives were proposed recognizing that all possible parameters could not be isolated. The large test facility also imposed some real limits. For instance, two-dimensional approach flow conditions were a limitation, as was the limited overfall height. Though limited, this comprehensive database is one of the few to examine field-scale headcut erosion processes. Brief descriptions are provided for most of the tests conducted in this study. An in-depth treatment can be found in the supporting references.

Varying Soil Moisture and Density: Initial headcut testing was conducted while varying the moisture and dry density of the compacted cohesive soil. These initial tests were performed with a constant flow rate of 1.55 m^3/s (55 ft^3/s) and an overfall height of 1.2 m (4 ft). No additional tailwater depth was imposed on the fill. The soil materials tested exhibited a strong relationship between the unconfined compressive strength and the dry density. The soil strength increased as the density increased. Flow over the headcut created a reverse roller that acted to remove material from the overfall base. When sufficient material was removed, a mass wasting event would occur, and the headcut would retreat upstream. Even though the headcuts moved in an episodic fashion, the headcut position versus time is well represented by a linear fit. The same soil exhibited widely different headcut advance depending on the dry density (Fig. 3). Observed advance rates for the CL soil ranged from 0 to 18 m/hr (59 ft/hr) (Robinson and Hanson, 1995).

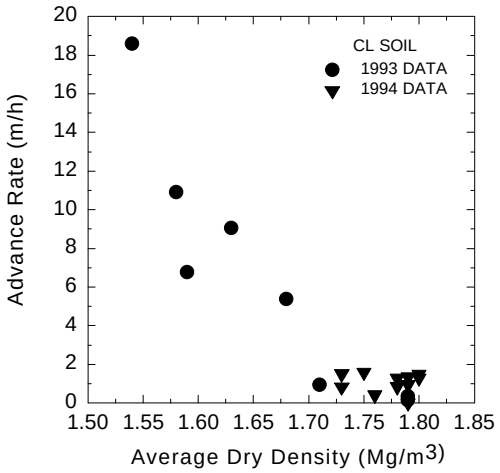

Figure 3. Advance rate vs. dry density (Robinson and Hanson, 1996a)

Influence of a Sand layer: To evaluate the influence of a more erodible layer of material in the soil profile a 0.3-m (1-ft) thick sand layer was placed at the bottom of a 1.2-m (4-ft) tall overfall. The sand layer extended horizontally 4.6 m (15 ft) into a 9.2-m (30-ft) long fill section. This configuration allowed the headcut migration to be examined with and without the sand layer in the profile. The sand layer did not appear to influence the rate of advance when a highly erodible soil was the overlying material. However, when the overlying material was more erosion resistant, the sand layer dramatically accelerated the headcut advance rate (Fig. 4). As a worst case, the sand layer caused the headcut advance rate to increase by an order of magnitude. The presence of even a relatively thin layer of erodible material in the soil profile can dramatically alter headcut movement (Robinson and Hanson, 1995).

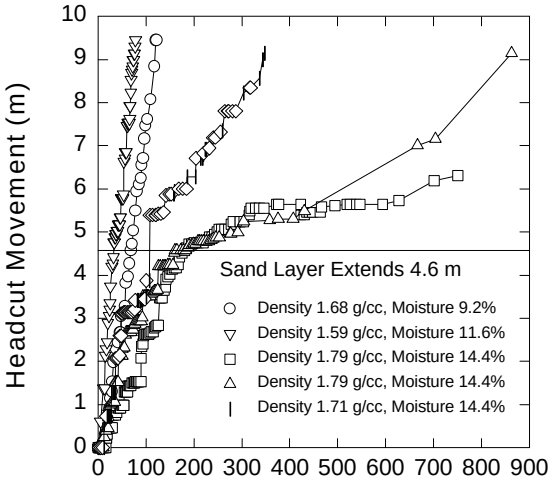

Figure 4. Movement with and without a sand layer (Robinson and Hanson, 1995)

Influence of Overfall Height and Flow Rate: The influence of overfall height and flow rate were examined while attempting to hold the soil moisture and soil density constant. Preformed overfalls with average heights of 0.96, 1.25, and 1.55 m (3.1, 4.1, and 5.1 ft) were tested to failure at average discharges of 0.75, 1.59, and 2.42 m^3/s (26.5, 56.1, and 85.5 ft^3/s). While an individual fill material could be placed quite uniformly, it was more difficult to place multiple fills at the same moisture content. The variation in weather conditions caused some variation in the moisture content of the soil

stockpile. While the dry densities were similar, the average moisture contents ranged from 12.6 to 15.9% for eleven tests. The variation in placed soil conditions appeared to have as much influence on headcut advance as did the overfall height and discharge variations. Typically the tests exhibited advance rates of 0.5 to 1.5 m/h (1.6 to 4.9 ft/hr). A subset of the data with less variability in density and moisture content indicated that the advance rate increased slightly as the overfall height increased at a constant discharge. This subset of data also suggests that the advance rate is not greatly affected by discharge over the tested range.

The air pocket below the nappe became smaller as the overfall height decreased and as the discharge increased. The headcuts eroded with both sloping and vertical faces. The lower moisture content tests were more likely to erode with a sloping face. Typically the erosion occurred along placed soil layers with relatively small-sized failure blocks. The higher moisture tests exhibited erosion along a near-vertical face. Undercutting, tension cracking, and mass failure of relatively large blocks of soil were common (Robinson and Hanson, 1996a).

Influence of Tailwater: Tests were conducted to evaluate the influence of tailwater level on the observed rate of headcut advance. The discharge, overfall height, and soil type were held constant and the tailwater level was varied. Four tests, each prepared with different soil moisture and density conditions, were conducted that each examined four different tailwater conditions. Low moisture and low density conditions produced the largest headcut advance rate, while high moisture and high density conditions produced the lowest advance rate. The intermediate tailwater levels produced the largest headcut advance rate for a given soil condition. The maximum headcut advance rate was observed for a tailwater to overfall height ratio of approximately 0.8. The tailwater level was observed to vary the advance rate by a factor of 2.6 to 7.5 over the range of soil conditions tested. This study suggests that an accurate prediction of headcut advance must incorporate tailwater information (Robinson and Hanson, 1996b).

Influence of Scour Below an Overfall: Scour below an overfall contributes to headcut instability and gully advance. Thirteen tests were conducted by preforming an overfall in a compacted cohesive soil bed. A typical plot of the scour at the base of an overfall versus time is provided (Fig. 5). Moisture and density variations in the placed soil were observed to influence the scour rate. The scour rate was observed to decrease as the soil density increased, and the scour rate also increased as the moisture content at the time of compaction decreased. For the conditions examined, the vertical scour rate ranged from near 0 to 1.98 m/hr (6.5 ft/hr) (Robinson et al., 1996, 1999a).

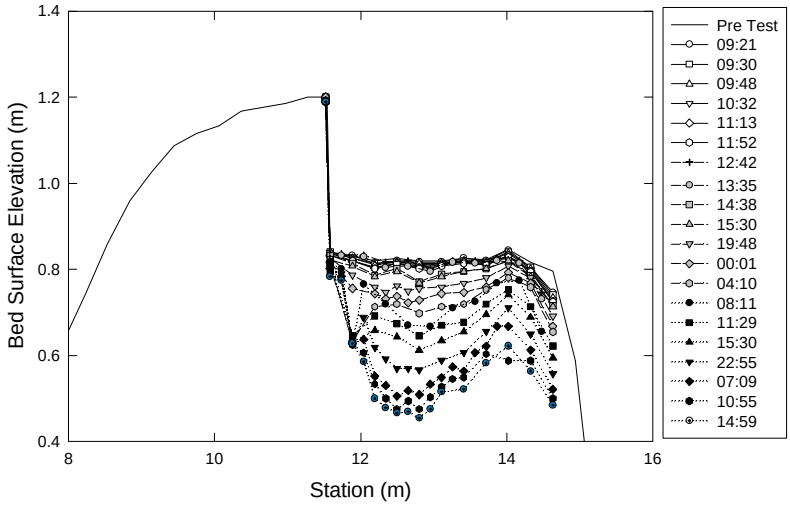

Figure 5. Bed surface profiles for test 13 (Robinson et al., 1999a)

None of these scour tests reached an equilibrium or ultimate depth. As equilibrium conditions are approached, the rate of scour should be expected to decrease. The scour in a cohesive soil caused by an impinging nappe was compared with the scour of a submerged circular jet device. Relationships were developed to predict the scour below an overfall based on the jet test performance (Hanson et al., 2000). Figure 6 displays the measured and calculated vertical scour rate versus time for the test shown in figure 5.

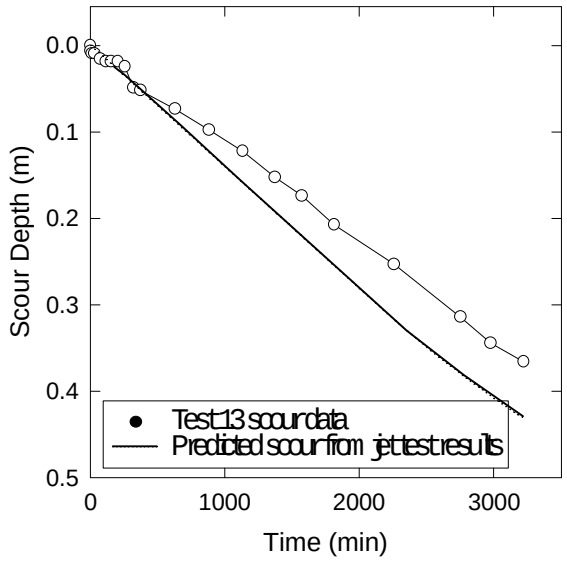

Figure 6. Measured and predicted scour for test 13 (Hanson et al., 2000)

Influence of Weathering: Surface weathering has been shown to accelerate soil erosion, and weathering processes can contribute to increased scour in the vicinity of a headcut. A preformed headcut in a compacted cohesive soil was exposed to intermittent flows. The soil surface was allowed to weather for periods of approximately one month between subsequent flow events. Processes such as wet-dry cycles, freeze-thaw cycles, desiccation cracking, tension cracking, and crust development were observed to weaken the surface and accelerate observed erosion. As flows were introduced over weathered material, a surface layer 25 to 50 mm (0.1 to 0.2 ft) deep was quickly removed. After this initial period of rapid erosion, the erosion rate stabilized at a constant but much lower rate. Desiccation cracks formed polygonal peds in the soil surface. The crack locations remained constant, and the cracks enlarged during subsequent flows. Jet tests correlated well with the observed scour and indicate that weathering increased the surface erodibility 160 times over that of the unweathered soil. These tests suggest that weathering can substantially accelerate the erosion of cohesive soils exposed to intermittent flow conditions (Robinson et al., 2000a).

Other Topics: Various other topics were investigated to enhance our understanding of headcut erosion. The velocity field was measured in the vicinity of an overfall for a range of flow rates and tailwater elevations. The observed flow circulation was similar to that shown in figure 1. The near boundary velocities did not change appreciably as the flow rate changed (Robinson et al., 2000b)

The presence of fracture patterns or cracks in soil and rock materials can accelerate the movement of headcuts. Studies examined the erosion of fractured materials. Blocks of known size were placed downstream of an overfall, and the discharge was increased incrementally until the block matrix failed. The failure discharge was observed to decrease as the overfall height increased. The failure discharge also increased as the block dimension orthogonal to the bed surface increased (Hanson et al., 1998).

Pressure within the a block matrix is also considered to be a dominant failure parameter. Pressure measurements suggest that the block matrix dramatically dampens the peak pressures measured at the floor even with a relatively large crack spacing. The pressure also increased as the overfall flow rate increased. Pressures were largest when the nappe impingement occurred directly over a crack (Robinson et al., 1999b). Additional pressure testing is on-going.

Tests are being planned to examine the influence of seepage on headcut advance.

Prediction of Headcut Migration Rate: This database can be used to develop or evaluate headcut advance prediction models (Hanson et al., 1997). A deterministic headcut advance model was developed that used a nappe profile component, a boundary stress component, and a mass wasting component (Robinson and Hanson, 1994). While numerous assumptions were required, this process-based model can incorporate future advances. More recently Hanson et al; (1999) developed a simplified deterministic equation to predict headcut advance. This relationship uses the stress prediction model (Robinson, 1992) to determine effective stress. The submerged jet test device (Hanson et al., 2000) is used to determine critical shear stress and the erodibility coefficient. This simplified prediction technique does a good job of fitting the headcut erosion data (Fig. 7). It is important to note that the data were not used to develop this relationship. While some scatter is observed, particularly for low tailwater conditions, this relationship looks very promising.

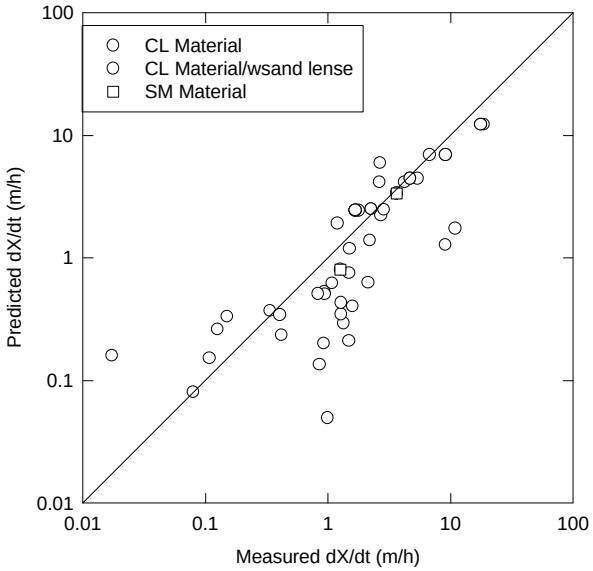

Figure 7. Predicted vs. measured migration rate (Hanson et al., 1999).

SUMMARY

A comprehensive research program was established to learn more about headcut erosion processes. A large-scale flume was constructed to test compacted cohesive soils of different geometry. Variations in soil moisture content and dry density on headcut movement were examined, as were variations in overfall height and flow rate. A sand layer was observed to dramatically affect the rate of headcut movement. Intermediate tailwater levels caused the most rapid headcut movement. Flow circulation in the vicinity of a headcut was described, and studies found weathering to be important when a headcut is exposed to intermittent flows. Predictive relations were developed that do a good job of predicting the headcut advance rate and

the vertical rate of scour at the base of an overfall. Pertinent references are provided for those wanting additional details.

REFERENCES

Hanson, G. J., K. M. Robinson, and K. R. Cook, 1997, Headcut migration analysis of a compacted soil. Trans. of the ASAE Vol. 40(2):355-361.

Hanson, G. J., K. M. Robinson, and K. R. Cook, 1998, Erosion of structured material due to impinging jet. Proc. of the 1998 ASCE International Water Resources Engineering Conference. Memphis, TN, August 3-7, 1998. Pp. 1101-1107.

Hanson, G. J., K. M. Robinson, and K. R. Cook, 1999, Prediction of headcut migration using a deterministic approach. ASAE Paper No. 992160. St. Joseph, MI. 12 pp.

Hanson, G. J., K. M. Robinson, and K. R. Cook, 2000, Estimating free overfall jet scour of a cohesive soil. ASAE Paper No. 002065. St. Joseph, MI. 22 pp.

Robinson, K. M., 1992, Predicting stress and pressure at an overfall. Trans. of the ASAE Vol. 35(2):561-569.

Robinson, K. M. and G. J. Hanson, 1994, A deterministic headcut advance model. Trans. of the ASAE Vol. 37(5):1437-1443.

Robinson, K. M. and G. J. Hanson, 1995, Large-scale headcut erosion testing. Trans. of the ASAE Vol. 38(2):429-434.

Robinson, K. M. and G. J. Hanson, 1996a, Gully headcut advance. Trans. of the ASAE Vol. 39(1):33-38.

Robinson, K. M. and G. J. Hanson, 1996b, Influence of backwater on headcut advance. Proc. ASCE Water and Environment Congress, Anaheim, CA. June 22-28, 1996. CD-ROM.

Robinson, K. M., G. J. Hanson, and K. R. Cook, 1996, Scour below an overfall. ASAE Paper No. 962121. St. Joseph, MI. 13pp.

Robinson, K. M., G. J. Hanson, and K. R. Cook, 1999a, Investigation of scour below an overfall. ASAE Paper No. 992037. St. Joseph, MI. 14 pp.

Robinson, K. M., G. J. Hanson, K. R. Cook, and K. C. Kadavy, 1999b, Erosion of fractured materials. ASAE Paper No. 992038. St. Joseph, MI. 13 pp.

Robinson, K. M., S. J. Bennett, G. J. Hanson, and K. C. Kadavy, 2000a, The influence of weathering on headcut erosion. ASAE Paper No. 002066. St. Joseph, MI. 10 pp.

Robinson, K. M., K. R. Cook, and G. J. Hanson, 2000b, Velocity field measurements at an overfall. Trans. of the ASAE Vol. 43(3):665-670.

EGEM, Next Step

By
Donald E. Woodward
National Hydraulic Engineer
USDA-NRCS
Washington, DC

ABSTRACT

The Natural Resources Conservation Service (NRCS) developed a computer program with the assistance of the Agricultural Research Service (ARS) to estimate the average annual erosion from an ephemeral gully in 1992. The computer program, Ephemeral Gully Erosion Model (EGEM), has been used in Europe to estimate ephemeral gully erosion. The NRCS strategic plan has established a goal of furnishing a tool to estimate ephemeral gully erosion and the impact of various management practices on the average annual erosion rate. NRCS has determined that the ephemeral gully erosion rates vary from 24 to 273 percent of the sheet and rill erosion, depending on the location.

In May of 2000, NRCS put together an international team of scientist to help meet the deadline of 2002. This team is working together to develop a tool that can be used to determine the impact of management practices on ephemeral gully erosion rates. This presentation will explain how this team was organized and the results of their effort.

Contact
Donald E. Woodward
National Hydraulic Engineer
US Department of Agriculture
Natural Resources Conservation Service (NRCS)
P.O. Box 2890, 1400 Independence Ave., SW
Washington DC 20013-2890
Email don.woodward@usda.gov Telephone: 202-720-0772, fax 202-720-0428

EVALUATING MECHANICS OF EMBANKMENT EROSION DURING OVERTOPPING

By Gregory J. Hanson, Research Hydraulic Engineer and Darrel M. Temple, Research Leader, USDA-ARS Hydraulic Engineering Research Unit, Stillwater, Oklahoma

Authors contact point: USDA-Agricultural Research Service, Plant Science and Water Conservation Research Laboratory, 1301 N. Western Street, Stillwater, Oklahoma, 74075. Phone number (405)624-4135, Fax Number (405)624-4136, e-mail addresses: **ghanson@pswcrl.ars.usda.gov** and **dtemple@pswcrl.ars.usda.gov**.

Abstract: *Thousands of dams built in the United States have a potential to be overtopped by flood flows. Therefore it is necessary to understand the mechanics of embankment erosion in order to evaluate the safety risk that overtopping represents. This paper describes tests conducted at the USDA-ARS Hydraulic Engineering Research Laboratory in Stillwater, Oklahoma, using an embankment 3 m high and 37 m long with 3:1 slopes. Measured bed profiles and velocity profiles for four 1--m wide channels, two vegetated and two non-vegetated, are compared. The tests were conducted at discharges of 0.2 m^3/s and 0.6 m^3/s. The tests in the vegetated condition were run for 75 hours, and the tests in the non-vegetated condition for 73 hours and 52 hours, respectively. The maximum overall erosion rate in the non-vegetated channels was 25 and 50 times greater than that in the vegetated channels. The erosion in the non-vegetated channels was not uniform spatially along the length of the channel or temporarily over the duration of the tests. The erosion progressed into stair-stepped overfalls. It is anticipated that the results of these studies will provide the basis for improved evaluation of the erosion of embankments subjected to overtopping. This study will provide a tool for evaluating dam rehabilitation needs, as well as accessing the risk to human and livestock life and property loss downstream.*

INTRODUCTION

When the inflow exceeds the outflow of a reservoir, the water level will build up and water storage will increase. In the case where the auxiliary spillway and other outlet structures fail to provide a successful passage of the flood, the water level will rise and overtop the dam. For earth embankments, erosion will begin once the forces exerted by the flowing water exceed the resistive forces of the exposed materials. The extent of damage depends on the vegetation, the properties of the dam fill, the degree of compaction of the fill materials, the dam geometry, the location of any impervious element, and the quantity and duration of flow over the dam.

Ralston (1987) in his discussions of dam overtopping distinguishes between cohesive and non-cohesive soils and the characteristic erosion of each. For cohesive soils in embankments with backslopes in the range of 2.0 or 3.0 horizontal to 1.0 vertical, overtopping results in the eventual degradation of the surface, formation of a discontinuity, and development of an overfall. The overfall advances progressively headward as the base of the overfall deepens and widens. Failure and breach occur when the overfall migrates through the upstream crest of the dam. This process is quite different from that described for embankments in non-cohesive soils. With non-cohesive soil embankments, the erosion occurs on a uniform but gradually flattening gradient.

This form of erosion pattern is consistent with the theory of sediment transport and can be modeled by it. Fread (1991) developed a physically based mathematical model. This breach model assumes that the eroded slope is parallel to the original downstream face of the dam, and the erosion rate is consistent with the assumption of steady uniform flow in the eroding channel. The following discussions will focus on the erosion of a cohesive embankment rather than that of a non-cohesive one.

An earth embankment typically consists of an upstream and downstream slope of 2 or 3 horizontal to 1 vertical and a level crest. Flow over the embankment, with minimal or no tailwater, progresses through three zones (Powledge et al. 1989): 1) beginning upstream in the calm reservoir, accelerating to a subcritical flow state over a portion of the embankment crest; 2) through critical flow on the crest, and supercritical flow over the remainder of the crest; and 3) supercritical flow on the downstream slope. The hydraulic stresses remain relatively low in zone 1. Hydraulic stress increases through zone 2 due to the changing energy slope as the flow approaches the downstream end of the crest. In zone 3, the flow accelerates down the slope, increasing the shear stress on the slope to comparatively large values. Erosion begins when these forces exceed the forces resisting detachment of the exposed material.

Determination of the erosion inception is based on a combination of the embankment geometry, depth of overtopping, vegetal condition, and embankment material. Powledge et al. (1989) observed that the erosion process begins most commonly at a point of slope discontinuity, such as the toe or base of the dam. However, depending on the condition and configuration of the embankment the initial erosion may begin anywhere within the supercritical flow region. The type of erosion that does occur is typically that of the formation of a headcut, or multiple headcuts, on the downstream slope (AlQaser and Ruff, 1993). This erosion pattern may be shown to be consistent with the stress pattern associated with acceleration of the flow on the slope. Once formed these headcuts tend to deepen, combine, and migrate upstream. This has been described for earth spillway erosion in terms of a three-phase process (Temple and Hanson, 1994). These phases are vegetal cover failure, concentrated flow erosion, and headcut advance. When well-maintained vegetation exists on the embankment the headcut formation and migration process typically begins at the toe of the slope (Temple and Hanson, 1998; Ralston, 1987) where high velocities impact the base material due to the sudden flattening of the slope. Erosion associated with phase one failure may also begin where other discontinuities in the slope or cover result in locally increased stress on the erodible material. AlQaser and Ruff (1993), in studies on bare soil embankments, observed the formation of multiple stair steps on the downstream slope and concluded that formation occurs when the shear stresses exceed the resistive forces of the material comprising the surface.

Phase two of the erosion of headcut formation process begins when the vegetal cover fails or is non-existent, and ends when erosion is sufficient to cause plunging action in the flow with associated energy and stress concentrations at the base of the headcut. This results in the initiation of phase three, which involves both a headcut deepening and an upstream migration component. The beginning of phase three has been defined to occur when the overfall height is greater than the critical depth of flow (Temple and Hanson, 1994). As this process occurs, the flow regime transitions from open channel flow to a combination of open channel flow and plunging jets. Therefore, the stress environment cannot be defined only as a function of the

energy slope and depth, but must also include the stress distributions generated by the plunging jet.

The point of initial erosion and the occurrence of an overfall on the downstream slope are important in breach timing and in understanding the processes and the forces involved. Experiments have been and are being conducted on the erosion process associated with overtopping. The purpose of this research is multi-faceted: 1) to understand the mechanics; 2) to determine the effects of materials and vegetation on the rate of headcut development and migration; and 3) to determine the effects of the erosion process on the breach hydrograph. This paper describes tests conducted on steep channels, 3.0 horizontal to 1.0 vertical, and the observed results. Vegetated and non-vegetated test results are contrasted, and the temporal and spatial variation of the observed erosion is described.

EMBANKMENT TEST SETUP

The experiments were conducted at the USDA-ARS Hydraulic Engineering Research Unit's outdoor laboratory in Stillwater, Oklahoma, using an embankment 3 m high and 37 m long constructed for use in these tests. The embankment was constructed from a locally borrowed sandy silt that classed as a CL-ML soil under the Universal Soil Classification System, with some of the samples classifying as ML. The plasticity index ranged from 0 to 7 for the samples tested. The soil was placed in 0.15-m horizontal lifts and compacted to an average density of 1.8 Mg/m^3 at an average moisture content of 12%. Tests showed the optimum moisture content and density to be 12% and 1.9 Mg/m^3, respectively. Jet tests (ASTM D5852-95) were conducted on 0.028-m^3 laboratory-compacted samples and 0.028-m^3 undisturbed samples to determine erosion resistance of the material.

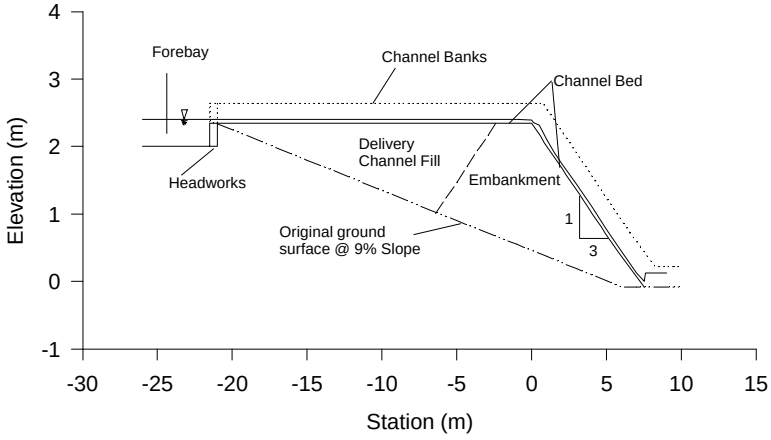

Figure 1. Schematic of cross-section view of embankment overtopping test set-up.

The embankment was initially constructed with slopes of 3 horizontal to 1 vertical both upstream and downstream, and a 2.4-m top width (Fig. 1). The embankment was constructed on a relatively impermeable erosion-resistant clay, sloping downstream at approximately 9%. After construction of this initial embankment, additional fill was placed on the upstream side to allow water to be delivered to six sections using an existing water delivery system. Trapezoidal channels 1 m wide and 1 m deep with 1:1 side slopes were cut through the crest and down the face of the embankment to contain the water during testing, and to allow separate tests to be run on each of the six sections. The embankment was initially used for testing the protective capability of bermuda grass as discussed by Temple and Hanson, (1998). These tests resulted in only minor damage to the portion of the embankment (test channels) used for the tests described herein. That damage was repaired prior to establishment of the fescue cover. The data gathered

from the two non-vegetated channels and the fescue grass-vegetated channels included centerline profiles of the water surface and channel bed, and velocity profiles at selected locations. The data collected from these tests provide insight on the erosion process in the bare condition, as well as the benefits of vegetation for increasing erosion resistance.

RESULTS AND DISCUSSION

The non-vegetated channels were tested for 72 hours and 51 hours at discharges of 0.2 m^3/s and 0.6 m^3/s, respectively. The fescue-vegetated channels were each tested for 75 hours at discharges of 0.2 m^3/s and 0.6 m^3/s. The 0.6 m^3/s test of the non-vegetated channel was terminated at 51 hours due to the extensive damage to the channel. Centerline profiles of the bed surface for each test provide significant information as to the nature of the erosion that occurred over the duration of the tests (Fig. 2 a-d). The vegetated channels tested at 0.2 m^3/s (Fig. 2a) and 0.6 m^3/s (Fig. 2c) showed very little degradation over the 75-hour duration of the tests. The erosion that did occur was most significant in the lower reaches of the channel, with a maximum of 0.045 m and 0.040 m of degradation occurring over 75 hours of testing for flows of 0.2 m^3/s and 0.6 m^3/s, respectively. This erosion occurred at about 4 m horizontal distance down the slope. This is near the toe of the slope, which was noted as the location of headcut development in previously tested vegetated channels (Temple and

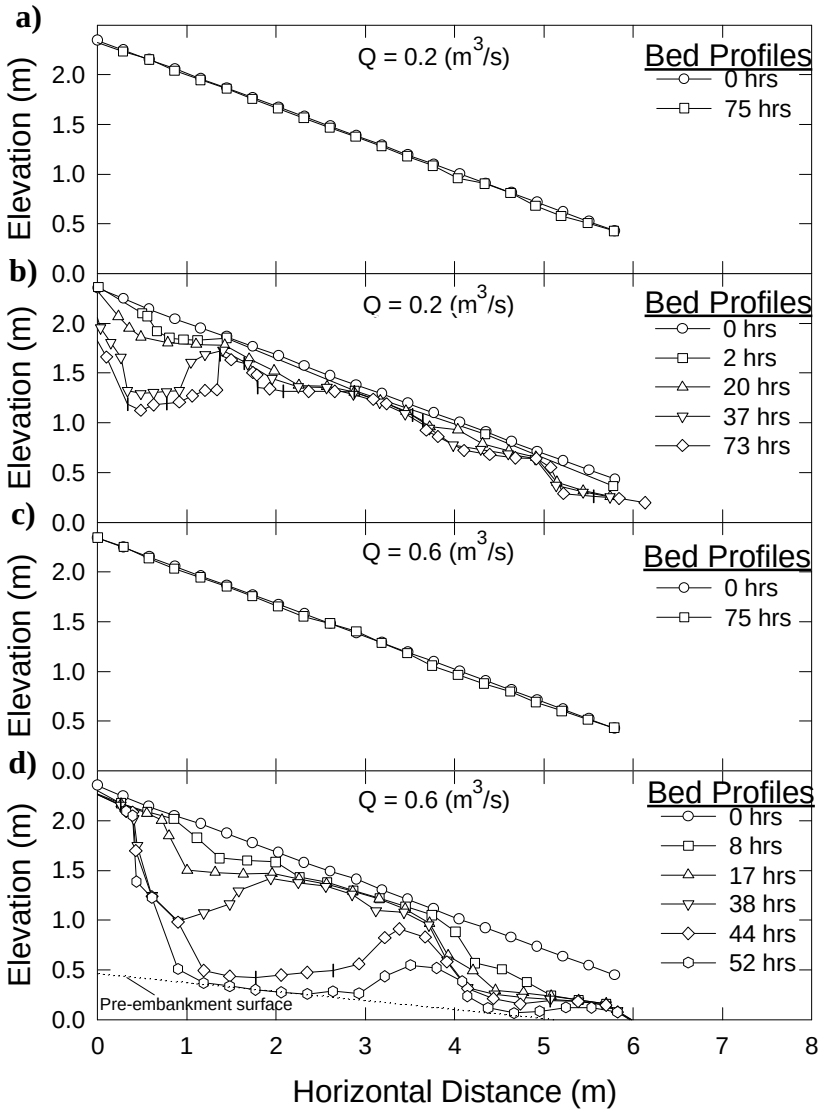

Figure 2. Centerline Bed profiles over test duration a) Vegetated channel at Q=0.2 m^3/s, b) Non-vegetated channel at Q=0.2 m^3/s, c) Vegetated channel at Q=0.6 m^3/s, and d) Non-vegetated channel at Q=0.6 m^3/s.

Hanson, 1998). The non-vegetated channels tested at 0.2 m^3/s (Fig 2b) and 0.6 m^3/s (Fig 2d) showed significant damage over the 73-hours and 52-hour durations of the tests, respectively. The erosion began immediately upon flow initiation, with a maximum erosion of 1.0 m and 1.6 m of degradation occurring over the duration of the tests for flows of 0.2 m^3/s and 0.6 m^3/s, respectively. The maximum erosion occurred near the upstream end of the test channels, immediately downstream of the embankment crest, in both cases. The degradation in the non-vegetated channel tested at 0.6 m^3/s reached the original base foundation materials in the last recorded profile (Fig 2d).

Velocity profiles taken at several stations during the tests give an indication of the effects of the vegetation and the degradation of the bare channels. Peak and average velocities are in Table 1. The velocity profiles in the vegetated state were consistently the same throughout the tests. The velocities were lower within the vegetal boundary and increased significantly once above it. The maximum velocities were attained at the lower reaches of the channel. The velocity profiles in the bare earth channels changed rapidly as erosion occurred. The measured velocities decreased at certain locations by as much as 500% because the flow changed from uniform open channel flow to a plunging jet. These changes in flow direction present some problems in measurement, because it was not always possible to align the pitot tube being used with the mean flow at the point of measurement. Even though these measurements are not representative of the true velocities and energy in the flow, they do show that the flow patterns changed significantly due to the degradation occurring in the channel.

Table 1. Summary of Tests.

Test #	1	2	3	4
Vegetation	Fescue	None	Fescue	None
Discharge (m^3/s)	0.2	0.2	0.6	0.6
Ave Flow Depth (m)	0.17	0.07	0.24	0.13
Mean Velocity (m/s)	2.6	3.0	4.5	5.4
Peak Velocity (m/s)	4.6	4.3	6.0	6.1
Test Duration (hrs)	75	72	75	51
Critical Specific Head (m)	0.3	0.3	0.7	0.7

The rate of erosion was not uniform over the length of the channel as shown in Figure 3. The average erosion rates over the entire duration of the flow were relatively high in the upstream reaches and low in the downstream reaches for the bare channel tests. The maximum time averaged rate of erosion for the 0.6 m^3/s flow rate test was 0.03 m/h, and for the 0.2 m^3/s flow rate test was 0.015 m/h. The rates were greater at the locations of discontinuities with the highest rate at the most upstream discontinuity. The maximum overall erosion rate for the vegetated channels was essentially the same for both tests, 0.0006 m/h.

The erosion rates varied not only spatially but also with time. Erosion was most dramatic during the initial stages of the bare channel runs just after flow was started (Figure 4 a, b). The rates reduced from 0.1 m/h or greater to less than 0.03 m/h in both test cases. The only exception to this was the most upstream discontinuity of the 0.6 m^3/s test where the rate increased dramatically toward the end of the test as the headcut deepened beneath the plunging jet. Prior to this increase in erosion, a headcut with overfall height of 1.6 m had developed. This resulted in erosion to the original foundation material by the end of the test, and a downstream cleaning action that removed the placed embankment material downstream of the headcut. The erosion rates at horizontal locations of 1.22, 2.13, and 3.05 m confirm this, with rates increasing to 0.10 to 0.15 m/h at 47 hours and then decreasing to 0.01 m/h at 52 hours. This reduction was due to the fact that the exposed foundation material was more erosion resistant than the placed material. The erosion rate at station 1.22 m for the 0.2 m^3/s flow rate test also increased significantly toward the end of the test because of the increased depth and resulting plunging action of the jet. The overfall at this location had reached a height of 1.0 m when flow was stopped.

SUMMARY

Erosion due to embankment dam overtopping is important because of the potential impacts that a dam breach may have on people and property downstream. The present investigation sought to collect data on the processes of

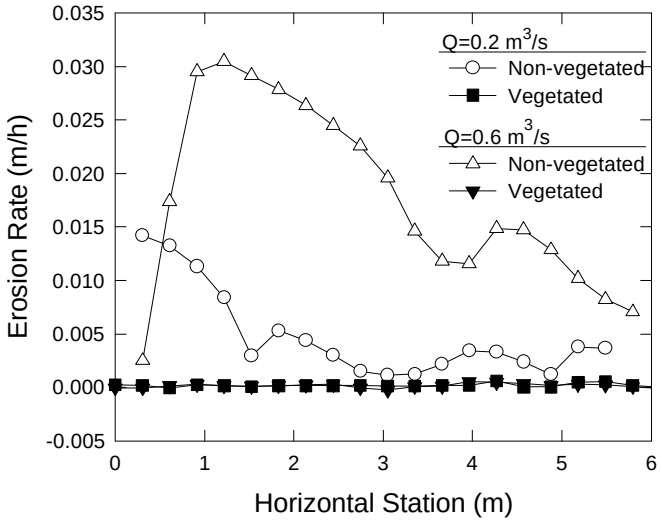

Figure 3. Time average erosion rate for vegetated and non-vegetated channels for duration of test along length of channel.

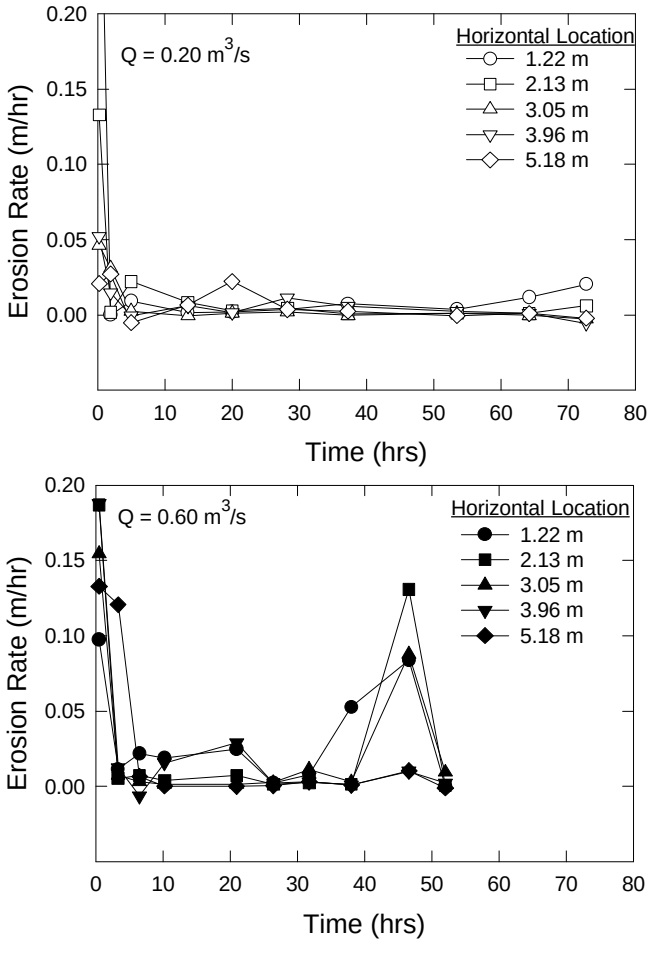

Figure 4 Erosion rate for a) Non-vegetated channel at Q=0.2 m^3/s, b) Non-vegetated channel at Q=0.6 m^3/s.

embankment overtopping erosion during initial stages of overtopping, both in the vegetated and non-vegetated condition. The experiments were conducted at the USDA-ARS Hydraulic Engineering Research Unit' s outdoor laboratory in Stillwater, Oklahoma, using an embankment 3 m high and 37 m long with a 3:1 downstream slope. The embankment was constructed from a locally borrowed sandy silt (CL-ML). Trapezoidal channels 1 m wide and 1 m deep with 1:1 side slopes were cut through the crest and down the face of the embankment to contain the water during testing, and to allow separate tests to be run on each of the six sections. Data gathered from two non-vegetated channels and two fescue grass-vegetated channels, including centerline profiles of water surface, bed elevations, and flow velocity profiles, are described in detail. The data collected from these tests provide insight to the erosion process in the bare condition, as well as document the benefits of the vegetation for erosion resistance.

One non-vegetated channel and one vegetated channel were tested using a flow of 0.2 m^3/s, which is equivalent to approximately 0.2 to0.3 m of overtopping head. The other two channels were tested at a flow of 0.6 m^3/s, equivalent to approximately 0.6-0.7 m of overtopping head. There was very little observed erosion in the vegetated channels for 75 hours of testing. The erosion that did occur was near the toe of the slope. The erosion in the non-vegetated channels was significantly greater, resulting in termination of the 0.6 m^3/s test after 52 hours. The maximum observed erosion was near the crest of the embankment, resulting in development of near-vertical overfalls. At the termination of these tests, the non-vegetated channel tested at 0.2 m^3/s had a classical stair-stepped appearance, and the section tested at 0.6 m^3/s had a single headcut. In both cases the highest vertical step at termination of the tests was at the crest.

These tests confirm the benefits of well-maintained vegetation in an embankment environment. The tests also confirm that erosion does not progress uniformly, with continuously degrading slopes or slopes parallel to the initial slope. Rather, the erosion develops into stair-stepped overfalls (headcuts), migrating upstream and scouring downward in a highly turbulent environment.

REFERENCES

AlQaser, G. and Ruff, J. F., 1993, Progressive failure of an overtopped embankment. Proceedings of the 1993 National Conference of Hydraulic Engineering, Hydraulics Division of ASCE. pp. 1957-1962.

Fread, D. L., 1991, BREACH: An erosion model for earthen dam failures. Revision 1. Hydrologic Research Laboratory, National Weather Service. Silver Spring, MD.

Powledge, G. R., Ralston, D. C., Miller P., Chen, Y. H., Clopper, P. E., and Temple, D. M., 1989, Mechanics of overflow erosion and embankments. II: Hydraulics and Design Considerations. Journal of Hydraulic Engineering 115(8),1056-1075.

Ralston, D. C., 1987, Mechanics of embankment erosion during overflow. Proceedings of the 1987 National Conference of Hydraulic Engineering, Hydraulics Div. of ASCE. pp. 751-757.

Temple, D. M. and Hanson, G. J., 1994, Headcut Development in Vegetated Earth Spillways. Applied Engineering in Agriculture. Vol. 10(5):677-682.

Temple, D. M. and Hanson, G. J., 1998, Overtopping of grassed embankments. Proceedings of the 1998 Annual conference of State Dam Safety Officials, Las Vegas, NV. (CD-ROM).

COMPUTATION OF SEDIMENT EROSION FROM THE BASE OF CUT BANKS IN RIVER BENDS

By J. W. Kean, Hydrologist, U.S. Geological Survey, Boulder, CO;
J. Dungan Smith, Hydrologist, U.S. Geological Survey, Boulder, CO

Abstract: This paper presents an approximate method for computing the boundary shear stress distribution on the cut banks and beds of meandering rivers. Such systems typically have cut banks that are irregular in planform geometry and the proposed method permits bank irregularities to be included in the computation of boundary shear stress and sediment transport at the base of the cut bank. Results are presented for a hypothetical meander bend containing bank irregularities that is typical of bends in the Clark Fork of the Columbia River in the Deer Lodge Valley of Montana.

INTRODUCTION

Computation of the rates of removal of sediment from the bases of cut banks in rivers is required for determining rates of cut bank erosion, and a comprehensive knowledge of the boundary shear stress distributions near the cut banks is necessary for these sediment transport calculations. Moreover, natural cut banks are irregular in planform geometry and the effects of bank irregularity in reducing flow in the neighborhood of the toes of banks must be taken into account in cut bank erosion calculations. We have developed methods for dealing with these facets of cut bank erosion over the past several years, and they have been applied to analyze the rapidly eroding cut banks on the Clark Fork of the Columbia River in the Deer Lodge Valley of Montana. To accomplish this task for meandering rivers, an algorithm for computing the form drag on bank irregularities and an algorithm for computing the near-bank boundary shear stress have been combined with a model for flow in a curved channel of prescribed curvature and bed topography.

BANK FORM DRAG ALGORITHM

Bank irregularities are approximated in planform geometry by a sequence of Gaussian shapes with appropriately chosen sequences of heights, spans, and spacings. These are attached to a more broadly curved basic channel boundary. The form drag on each of these Gaussian topographic elements is calculated in a streamwise averaged manner and separated from the spatially averaged shear stress primarily responsible for the forces on sediment particles comprising the banks. Drag on each topographic element is determined by calculating the velocity field at the site of the topographic element using a virtual-origin-adjusted wake and a growing internal boundary layer resulting from the upstream element and an appropriate drag coefficient. Drag coefficients were determined from laboratory measurements (Hopson, 1999) and the method for calculating the virtual origin adjustment was developed using laboratory data. The entire procedure for calculating drag on the Gaussian topographic elements was tested using laboratory measurements (Kean, 1998). As a consequence of determining the drag on the topographic elements, the spatially averaged total wall roughness length, y_o, is determined. This value is used in the near-bank shear stress algorithm, which is described below.

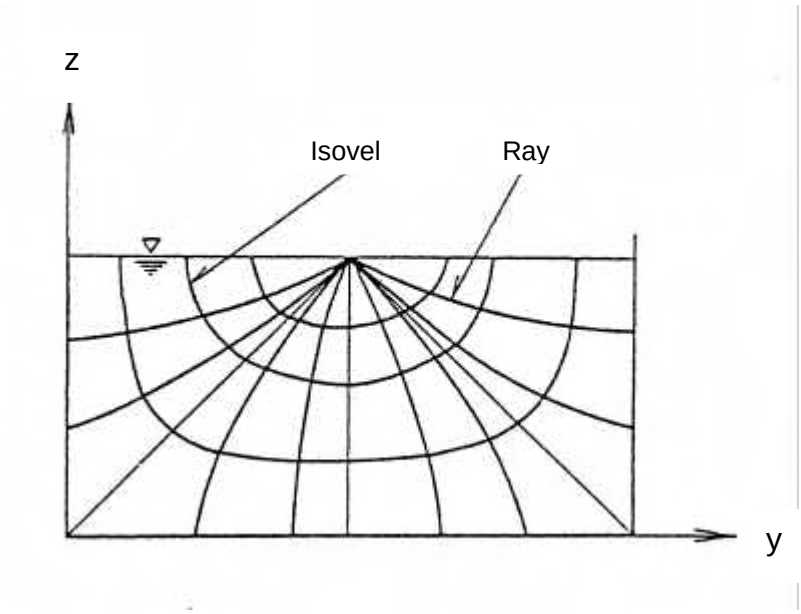

Figure 1. Diagram of orthogonal ray-isovel grid.

NEAR-BANK BOUNDARY SHEAR STRESS ALGORITHM

For steady, horizontally uniform flow in channel a force balance exists between friction along the wetted perimeter and the downstream component of the weight of water in the channel. A similar force balance exists for the friction along an incremental length of the wetted perimeter and the downstream component of the weight of a fraction of the water in the channel. This balance can be expressed in terms of shear stress in a manner similar to the familiar equation for the average boundary shear stress in the entire channel by the equation

$$t_{bi} = -r\, g\, S\, A_i / p_i \qquad (1)$$

where r is the density of water, g is the acceleration due to gravity, S is the channel slope, t_{bi} is the average boundary shear stress along the length of wetted perimeter, p_i, and A_i is the fraction of the cross-sectional area that produces this shear stress.

The mixing processes, which distribute fluid stress throughout the channel, act along lines (rays) perpendicular to lines of constant velocity (isovels) as shown in Figure 1. The rays, which are perpendicular to the boundary and extend to the water surface, define streamwise surfaces of zero shear. The area, A_i, responsible for producing the shear on a section of boundary of length p_i, is simply the area between two rays separated by a distance p_i along the boundary.

The shape of the rays in channels with well-defined corners between two boundaries, such as rivers with cut banks and rectangular and trapezoidal channels, is controlled by the location of a primary ray which originates from the corner and has nearly constant slope to the water surface. The rays from both boundaries defining the corner begin perpendicular to the boundary and eventually become tangent to and join the primary ray. The slope of the primary ray controls the distribution of shear stress between the two boundaries making the corner and is a function of the

relative roughness of the two boundaries. In a rectangular channel having the same roughness on the bed and the wall, the angle of the primary ray from the corner is 45 degrees. As a result, the shear stress distribution on the bed and wall near the corner will be the same. If the roughness on the walls of the channel is greater than the roughness of the bed, the primary ray will be pushed away from the bank, resulting in a lower shear stress on the bed and a higher shear stress on the wall.

Shimizu (1989) developed a physically based numerical model that calculates the ray, shear stress, and velocity fields in rectangular channels with known bed and bank roughnesses. The model involves solving the streamwise two-dimensional momentum equation for uniform flow together with equations for the appropriate eddy viscosity field. A draw back to this model is that it is computationally very intensive. The computational difficulty arises from the fact that the momentum equation is best solved in orthogonal *y*-*z* space, while the eddy viscosity must be solved in an orthogonal ray-isovel grid that is not known apriori.

An alternative approach consistent with the results of Shimizu is presented here. It has the advantage of being substantially less complex while still capturing the essential physics of the problem. The approach involves an approximate means of calculating the orientation of an essentially linear primary ray and uses an empirically developed equation for the shape of the other rays to calculate the distribution of boundary shear stress in the channel. This equation is developed such that the rays and resulting shear stress distribution are in reasonable agreement with the numerical results by Shimizu. The ray equation is a function of the width of the channel and the slope of the primary ray, which itself, is determined by the relative roughnesses of the bed and the wall. Given the roughnesses of the wall and the bed, the model first calculates the angle of the linearly approximated primary ray. As a result of employing an empirical equation for the rays, it is possible to have an analytic expression for the boundary shear stress along the bed and wall. This expression is found by taking the limit of A_i/p_i as p_i goes to zero, where, A_i is the area between two empirical rays separated by a distance p_i along the boundary.

The empirical function for the rays is described in a $x' - y'$ coordinate system normalized by the depth of the flow. This coordinate system is mapped to the boundary of the channel such that the y'-axis is parallel to the boundary. If the rays are to be calculated for the wall of the channel, the y'-axis corresponds to the *y*-axis of the channel. Alternatively, if the rays are to be calculated for the bed of the channel, the y'-axis for the rays corresponds to the *z*-axis of the channel. The equation for the primary ray is simply $y' = m\,x'$, where *m* is the slope of the primary ray in the $x' - y'$ coordinate system. The function for the rays has the form

$$y' = a\,x'^{\,c} + b \qquad (2)$$

where, $a = (m\,x_i - b)/\,x_i^c$ and

$$c = 1 + b^{3/4}$$

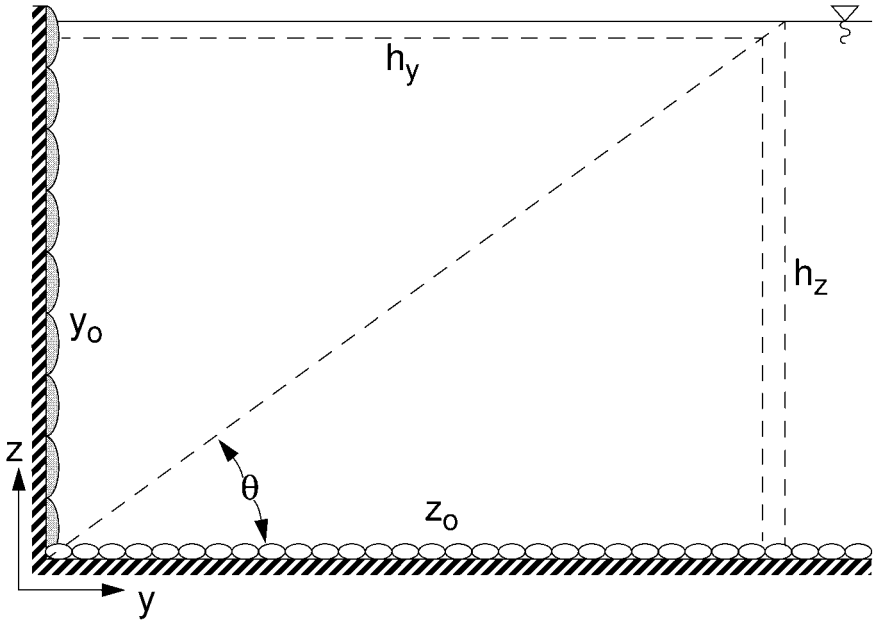

Figure 2. Diagram of method for determining the primary ray. The rays h_y and h_z are approximated to be linear.

In these equations, *b* is the non-dimensional distance from the origin to where the ray meets the boundary, and x_i corresponds to the location where the ray joins the primary ray and is, itself, a function of *b* and *m*.

The method used to calculate the slope of the primary ray is demonstrated in Figure 2. For a given point on a linear ray, the shear stress on the bed (t_{bed}) and wall (t_{wall}) are given by the following equations

$$t_{bed} = -r\, g\, S\, h_z \tag{3a}$$

$$t_{wall} = -r\, g\, S\, h_y \tag{3b}$$

where h_z is the length of the ray from the bed to the primary ray, and h_y is the length of the ray from the wall to the same point on the primary ray. Assuming that the velocity profiles coming off the bed and wall are logarithmic, the velocity at any point along the corresponding rays for the bed (u_{bed}) or wall (u_{wall}) are given by the equations

$$u_{bed} = \frac{\sqrt{t_{bed} / r}}{k} \ln \frac{z}{z_o} \tag{4a}$$

$$u_{wall} = \frac{\sqrt{t_{wall} / r}}{k} \ln \frac{y}{y_o} \tag{4b}$$

where k is von Karman' s constant (0.408). Equating u_{bed} and u_{wall} at the same point where they meet the primary ray yields the equation

$$\frac{t_{bed}}{t_{wall}} = \frac{h_z}{h_y} = \left(\frac{\ln \frac{h_y}{y_o}}{\ln \frac{h_z}{z_o}} \right)^2 \qquad (5)$$

Because the actual wall and bed rays have less curvature farther from the corner, the linear ray approximation works best if u_{bed} and u_{wall} are equated at the point on the primary ray where it meets the water surface. Substituting the depth of flow for h_z, (5) can by solved numerically for h_y. For channels with vertical banks, the ratio h_z/h_y is the slope m of the primary ray. For channels without vertical banks, such as trapezoidal channels, the slope of the primary ray is easily found using h_z/h_y and the slope of bank itself. Although the slope of the primary ray can be obtained using a similar method with the empirical rays, the simple linear method yields results for the primary ray angle that are within a few degrees of the numerical results of Shimizu.

To illustrate the significant effect large-scale roughness has on the distribution of near-bank boundary shear stress, a comparison is made between the stress in hypothetical vegetated and unvegetated channels having similar dimensions and roughness sizes as those found in the Clark Fork River in the Deer Lodge Valley. In this example, the cross-section is rectangular with mean depth, h_o, equal to 0.84 m. More general cross-sections will be treated in a later example. The bed material is made up of cobbles with D_{84} = 1 cm (z_{oSF} = 0.1 cm). The bank material of both channels consists of gravel and cohesive sediments having a roughness length equal to the bed roughness. In addition to this roughness, the vegetated channel contains willow shrubs considered to be regularly spaced 6 m apart. The root balls of these trees extend 1 m into the flow and can be approximated as Gaussian curves. Using the bank form drag algorithm, the total roughness length of the vegetated channel is calculated to be 8 cm. The slope of the primary ray for the unvegetated channel (y_o/z_o = 1.0) is 45 degrees. The increased wall roughness in the vegetated channel (y_o/z_o = 79) pushes the primary ray away from the bank to an angle of 16 degrees from horizontal. The increased friction on the walls of the vegetated channel significantly reduces the near-bank bed shear stress from that of the unvegetated channel as shown in Figure 3.

COUPLING TO CURVED CHANNEL FLOW MODEL

The near-bank boundary shear stress algorithm is imbedded into the curved channel flow model of Smith and McLean (1984). This model assumes frictionless banks which do not affect the flow. Coupling the near-bank algorithm to this model must be done in a way that is fluid mechanically consistent with the underlying assumptions of the model. The curved channel model was constructed using a regular perturbation expansion founded on an interior flow scaling. The frictional near-bottom flow could have been included in the model in two ways. The most mathematically consistent way requires a singular perturbation theory, which would

match the turbulent boundary layer to the interior velocity field above each point on a spatially variable bed. This method is only practical for the geophysically uninteresting case of a flat bed. The second, and more practical way, is to impose the velocity field for the fully frictional flow on the inviscid interior, which results in a velocity field that is accurate to first order.

Consistent with the original formulation of the model, a frictional boundary layer can be added next to the vertical banks. This is similar to matching a frictionally dominated near-bottom flow to the nearly inviscid outer flow. A mathematically consistent approach, following a singular perturbation theory, would require matching the inner and outer velocity profiles along each isovel-perpendicular ray. This approach is impractical and can be avoided to first order, in analogy with the procedure of the curved channel model, by imposing the boundary layer structure on the interior flow. The approach is further approximated by imposing the wall boundary layer only a distance 0.2 L into the flow, where L is the length of the primary ray. Beyond 0.2 L, the friction is taken to be due to the bed only as in the original curved channel model. This approximation reduces the calculation time without much loss of accuracy.

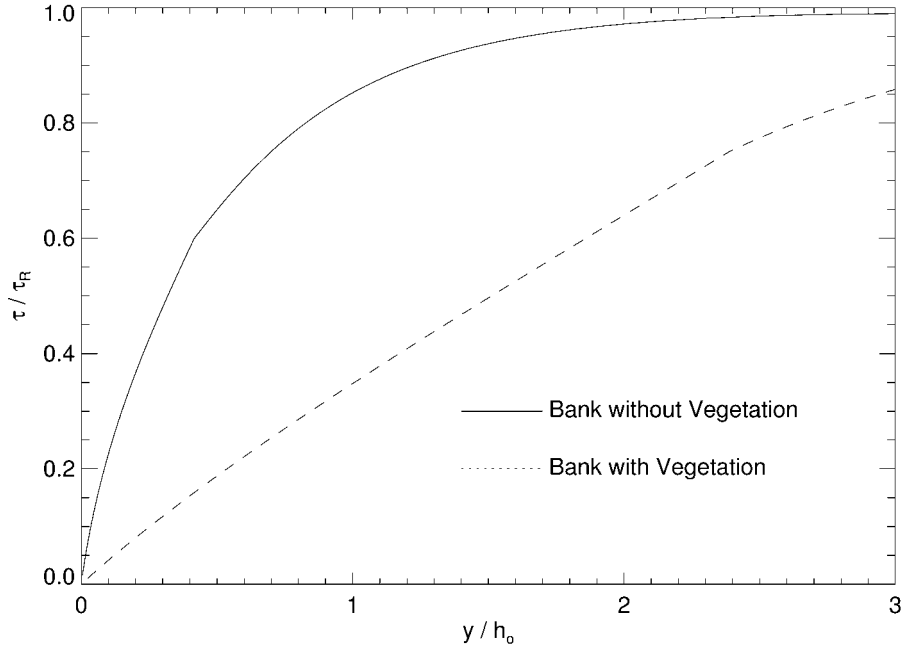

Figure 3. Comparison of near-bank boundary shear stresses in a hypothetical channel with and without large-scale roughness due to vegetation. Shear stress is normalized by the depth-slope product, t_R, which equals $r\ g\ h_o\ S$. The distance from the bank is normalized by the depth at the cut bank, which, in this case, equals h_o. The form drag created by the vegetation reduces the boundary shear stress a distance of $h_o/2$ away from the bank by 71%.

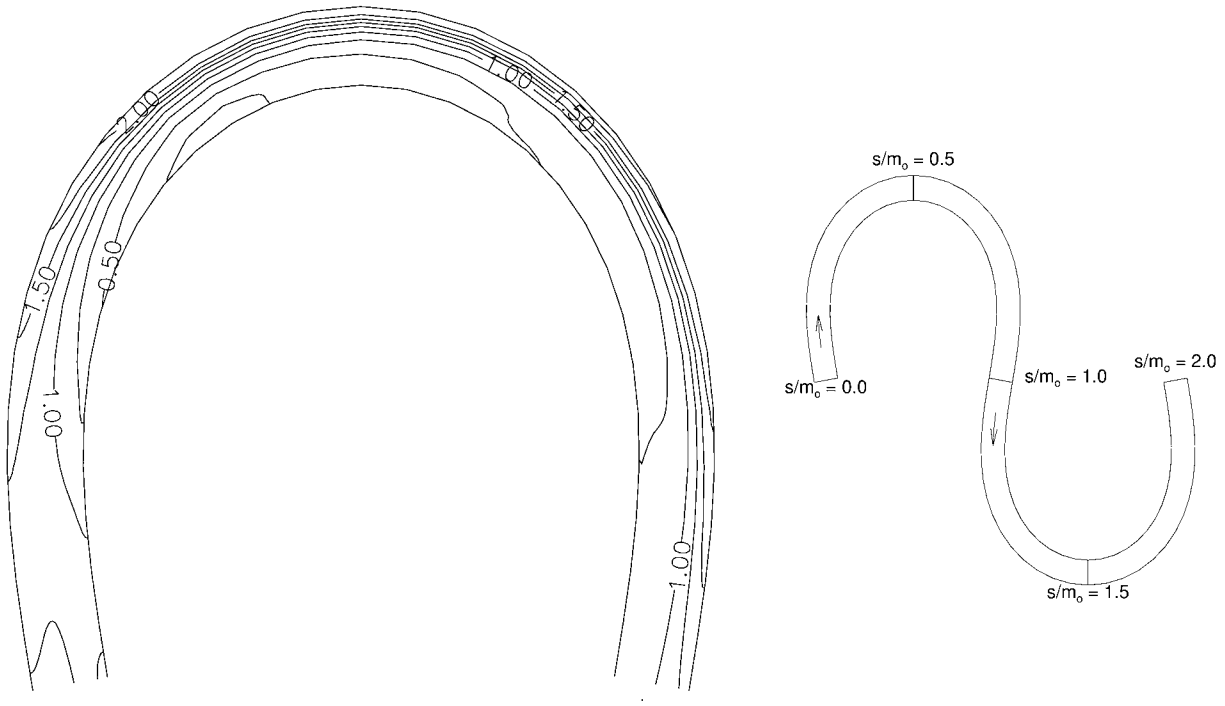

Figure 4. Bottom topography and planform geometry of a bend series typical of the Clark Fork River. Bed elevation contours are non-dimensionalized by the mean depth, h_o, which was 0.84 m. The mean width, w_o, is 19.3 m, and the half wavelength measured along the channel centerline, m_o, is 383 m. The planform geometry corresponds to sine-generated curve with Ω = 100 degrees. The bank irregularities due to vegetation are not shown.

APPLICATION TO THE CLARK FORK RIVER

The results of this coupled model are given for a repeating series of meander bends of the structure shown in Figure 4. These bends approximate a series of 10 bends in the Clark Fork River in the upper Deer Lodge Valley. The banks and the bed of the model channel have the same skin-friction roughness lengths as in the previous example. In addition, the modeled banks are shaped as if vegetated with equally spaced willow shrubs 6 m apart. The scale in which the root balls extend into the flow is taken to approximate bank undercutting and slumping processes. High cut banks with willows are more prone to undercutting and slumping than low banks, and hence, tend to have root balls that extend further into the flow. In order to approximate this effect, the protrusion distance into the flow is taken to be proportional to the local flow depth at the base of the cut bank. At the deepest point along the cut bank, the root balls are modeled to extend 0.6 m into the flow. At the crossing (s/m_o = 1.0), where the local depth is half of the maximum value, the roughness elements extend only 0.3 m into the flow. Figure 5 shows the distribution of the wall and near-wall bed shear stresses along the bank of one full meander and compares these values to the value of bed shear stress in a channel containing no vegetation and having frictionless walls. Bed load transport is dependent on the magnitude of the boundary shear stress to approximately the 3/2 power, and erosion depends on the divergence of the bed load transport rate. This comparison, therefore, demonstrates the importance of including form drag produced by bank irregularities in models that are to be used to calculate 1) cut bank erosion and 2) the geomorphic properties of bends in meandering rivers.

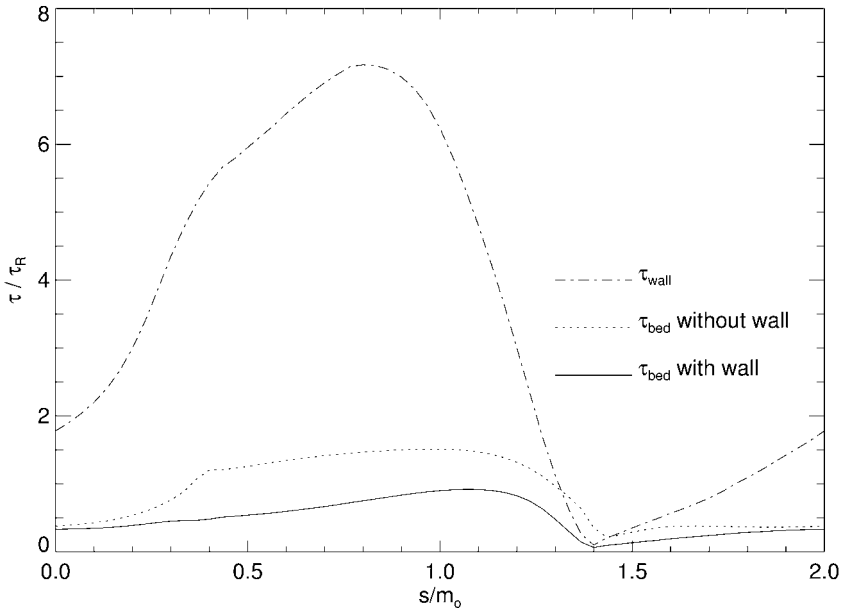

Figure 5. Comparison of wall and near-wall bed stresses for a channel with and without wall friction. The stresses are shown for the left side of the channel in Figure 4b. Flow is at bank full (Q = 31.2 m^3/s). The wall friction is due to skin friction and form drag from vegetation. The wall stresses are at half the local depth, and the bed stresses are at a distance 0.1 L away from the wall. Stresses are normalized by the depth-slope product for the channel without wall friction (S = 0.0024). The form drag of the vegetation along the cut bank produces high wall shear stress, which significantly reduces the near-bank bed shear stress. For much of the channel length, the near-bank bed stress is about 50% less than the bed stress that would be there if there were no wall friction.

SUMMARY AND CONCLUSIONS

The importance of including bank irregularity in models designed to provide boundary shear stress for near-bank sediment transport and bank erosion is demonstrated using a bend typical of meander sequences in the Clark Fork of the Columbia River in the Deer Lodge Valley, Montana. The effects of bank irregularity are included in our model using a boundary layer on vertical and near vertical banks that includes form drag on sequences of bank protrusions using sequences of Gaussian shapes. This approach permits a fluid mechanically consistent model that can be usefully applied to natural bends and series of bends in meandering rivers.

REFERENCES

Hopson, T.H., 1999, The Form Drag of Large Natural Vegetation Along the Banks of Open Channels, Unpublished Master' s thesis, University of Colorado, 114 p.

Kean, J.W., 1998, A Model for Form Drag on Channel Banks, Unpublished Master' s thesis, University of Colorado, 56 p.

Shimizu, Y., 1989, Effects of Lateral Shear Stress in Open Channel Flow, report for the River Hydraulics and Hydrology Laboratory, Civil Engineering Research Institute, Hokkaido, Japan, 22 p.

Smith, J.D., and McLean, S.R., 1984, A Model for Flow in Meandering Streams, Water Resources Research, v. 20, p. 1301-1315.

USING THE PHOTO-ELECTRONIC EROSION PIN (PEEP) AUTOMATIC MONITORING SYSTEM TO DEFINE BANK EROSION EVENT TIMINGS: THE R. WHARFE, UK

By D. M. Lawler[1]; Couperthwaite, J. S.[1]; Leeks, G. J. L.[2]

[1] Fluvial Geomorphologist, School of Geography & Environmental Sciences, The University of Birmingham, UK
[2] Centre for Ecology & Hydrology, Institute of Hydrology, Wallingford, Oxfordshire, OX10 8BB, UK

Abstract: Despite numerous bank erosion *rate* studies, there is a distinct lack of information on bank erosion *events*, especially their temporal distribution in relation to the controlling forces. To help tackle these problems, this paper describes the first automatic erosion monitoring technique to be developed - the Photo-Electronic Erosion Pin (PEEP) system - which can help to clarify the magnitude, frequency and timing of individual bank erosion events. It reports recent improvements to the technique, including increased appropriateness for larger-scale sites, enhanced installation flexibility, and addition of thermistors for temperature monitoring. Example bank erosion event sequences from the active R. Wharfe, UK, in 1996-97 are related to flow, bank temperature, turbidity and suspended sediment concentration series. These show how the PEEP system can for the first time (a) quantify the impact of *individual*, rather than *aggregated*, flow events (b) reveal the full complexity of bank response to given driving forces; and (c) help to disentangle competing ideas on the dominant processes responsible. The concept of *thermal consonance timing* (TCT) to fine-tune the timing of erosion events is also introduced. The paper also calls for further technical research to develop new methods for the automatic and continuous monitoring of erosion and deposition events.

INTRODUCTION

Bank erosion processes are still not well understood or specified in river dynamics and sediment flux models. The field is particularly complicated by the operation of both fluvial and non-fluvial erosion processes in channel systems, the change in bank material erodibility over different timescales which induces complex bank responses to similarly-sized flow events and - the specific focus here - the lack of bank erosion data *at the event timescale*. The main goals of this short paper are to: (1) describe the Photo-Electronic Erosion Pin (PEEP) automatic erosion monitoring system, including recent improvements; (2) demonstrate its potential to establish more clearly the timing of individual bank erosion events; and (3) outline the general importance of automatic erosion and deposition monitoring, and the need for further technical research to address this need. Examples below are drawn from the LOIS project results.

The need for an automatic erosion monitoring technique: When studying erosion systems, we rely on the availability of continuous, automatically-monitored data on, for example, stage, discharge, precipitation intensity and turbidity recorded with pressure transducers, automatic raingages and turbidity meters. However, the weakest part of the investigation is likely to be the monitoring of the erosional or depositional change itself. Because of the limitations of existing measurement methods, little knowledge has yet emerged of the *dynamics* of bank erosion and deposition *events* at a time resolution comparable to that available for flow and sediment transport rates (Lawler, 1992). Conventional, *manual*, field monitoring methods (e.g. erosion pins or cross-section resurveys (Lawler, 1993)) merely reveal *net* change in the position of a bank or gully surface since the previous measurement: they do not quantify the precise *temporal distribution* of that change. This means that erosion event timing and the precise bank response to *individual* flow or meteorological events is generally uncertain. Clearly, bank erosion process explanations and model building and testing efforts will be more securely based when (a) the full episodicity of bank change is detected, including event timings and (b) information on specific erosion and deposition events can be related to continuous information on the temporal fluctuations in the suspected driving forces.

THE PHOTO-ELECTRONIC EROSION PIN (PEEP) SYSTEM

The Photo-Electronic Erosion Pin (PEEP) system was originally developed in the early 1990s to help address these measurement problems (e.g. Lawler, 1991, 1992). The PEEP sensor is a simple optoelectronic device containing a row of overlapping photovoltaic cells connected in series, and enclosed within a waterproofed, transparent, acrylic tube of 12 mm I.D. and 16 mm O.D. (Fig. 1A). The sensor generates an analogue voltage proportional to the total length of PEEP tube exposed to light. A reference cell is used to adjust outputs for variations in light intensity (Fig. 1A). Small networks of PEEP sensors are normally inserted into carefully pre-augered holes in the bank face, and connected to a nearby datalogger set to record PEEP mV outputs at 15-min intervals, though any frequency is possible (Fig. 1B). Most dataloggers are compatible with PEEPs. Subsequent retreat of the bank face exposes more cells to light, which increases sensor voltage output (Fig. 1B). Deposition reduces voltage outputs. Data recovered from the logger thus reveal the magnitude, frequency and timing of individual erosion and deposition events much more clearly than has been possible before (Lawler, 1992), as will be shown below for LOIS project sites (Fig. 2).

Figure 1: The Photo-Electronic Erosion Pin (PEEP) erosion monitoring system: (A) The PEEP sensor, which now includes two reference cells and two thermistors; (B) typical installation of a PEEP sensor and datalogger assembly at a river bank site

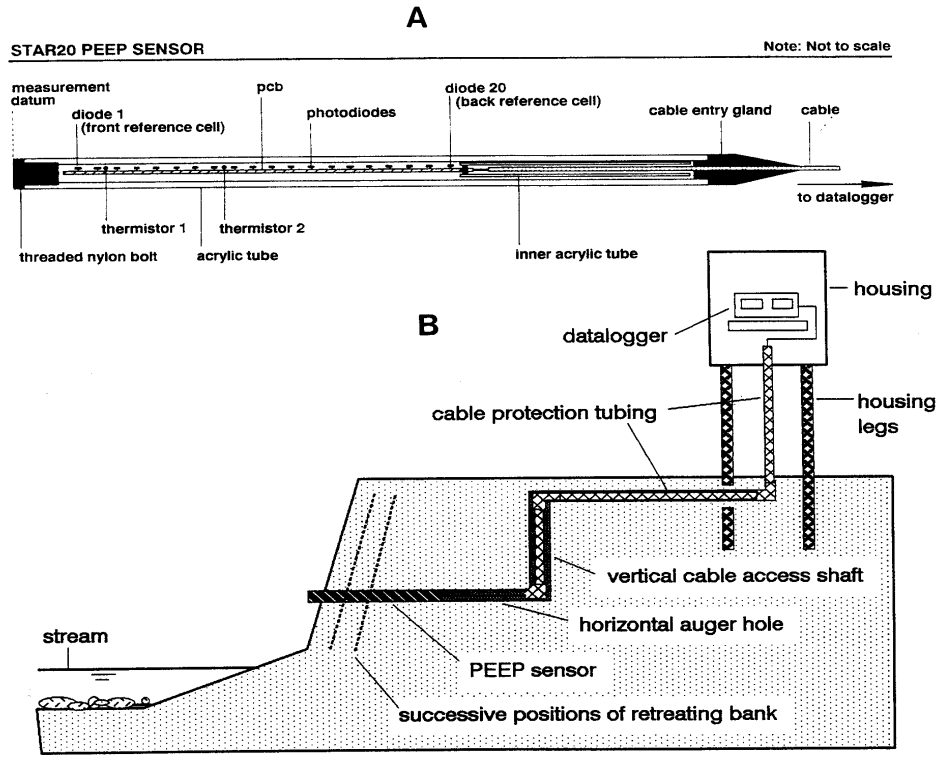

Various PEEP designs are possible to suit the application (e.g. bank, gully wall, channel bar, hillslope, cliff, dune, beach). The early generation of PEEP sensors were 0.40m long, and were equipped with an array of 10 photovoltaic cells to provide an active length of ~90mm. The PEEP sensors were redesigned in 1996 as follows (Fig. 1): (a) sensors were lengthened to 180mm active length and 0.66m total length to allow for higher bank retreat rates; (b) a second reference cell was added to permit inverted installation, and to confirm minimum erosion magnitudes for large events; and (c) two thermistors were incorporated to generate bank temperature data at the sediment surface and at 68 mm depth, to help evaluate bank freeze-thaw, desiccation and biological (e.g. vegetation growth) processes. For example, two freeze-thaw events are detected in the bank temperature time series of Fig. 3. Thermistors also allow erosion events to be better timed through the use of *thermal consonance timing* (TCT), as discussed below.

Laboratory calibration establishes relationships between PEEP outputs and exposed tube lengths. These relationships are encouragingly strong: the position of the sediment surface is generally known with 95% confidence to within $\pm$ 2-4 mm (Lawler, 1992), although low light conditions can reduce confidence. Further details of PEEP system measurement principle, design, calibration, installation and applications can be found in Lawler (1991, 1992, 1994, Lawler et al. 1997a).

Advantages and limitations of the PEEP System: Advantages of the PEEP system are listed in Table 1. They allow a more precise picture of the temporal distribution of erosional and depositional activity to be established. PEEPs have great potential in defining shifting threshold stresses required for erosion, because the geomorphological impact of virtually every hydrological or meteorological event can be ascertained. They should permit relationships between bank sediment supply and sediment transport to be defined more readily. PEEP sensors can also be linked to data telemetry platforms to generate *real-time* data which can aid scheduling of fieldwork, provide early warnings of erosion problems and assist with management issues.

Table 1. Advantages and potential of the Photo-Electronic Erosion Pin (PEEP) sensor

Advantages	Potential
* No power needed; PEEP based on solar cells	* Temporal distribution of erosion established more clearly
* Reference cells normalise for light levels	* Process inference and model testing stronger
* Easy to connect to dataloggers	* Threshold identification more definitive
* Simple and reasonably robust	* Magnitude-frequency analysis more comprehensive
* Temperature and light monitoring capability	* Relation of erosion to sediment dynamics possible
* Sufficiently inexpensive for networks (e.g. 4-8)	* Erosion-warning capability via telemetry systems viable
* Applicable to many erosion/deposition contexts	* Real-time monitoring for research or management

Research is proceeding, however, to address certain limitations of PEEP systems. For example, being a visible-light system, nocturnal events are not detected until the following morning, although temporal resolution is still much better than with traditional manual methods. Data gaps at night could be plugged with programmed bursts of artificial light. Also, as with traditional erosion pins, PEEPs are invasive (although their small size minimises this), and they may be less suitable for gravel materials or for large mass-failure situations. The addition of data transmitters to PEEP sensors will obviate the need for cabling and backfilled access holes (Fig. 1B). Some PEEP data are occasionally lost or degraded in low-light conditions, or when the bank is covered by snow, snagged vegetation or highly turbid water.

METHODS

Project and Study Area: The bank erosion research reported here was undertaken as part of the UK Land-Ocean Interaction Study (LOIS) study, 1994 - 2000. The aims of LOIS were to understand the fluxes and dynamics of sediments, contaminants and nutrients from the land surface (northern England) to the ocean (North Sea) (e.g. Leeks et al., 1997). We focused bank monitoring on the fluvial and estuarine part of the Swale-Ouse-Wharfe river system in northern England (Fig. 2) from January 1996 - April 1998. This short paper concentrates solely on the R. Wharfe PEEP site at Easedike, for which flow and suspended sediment concentration data are available from Tadcaster, 2 km downstream (Fig. 2). At Tadcaster, the Wharfe drains an area of 818 km^2 (Webb et al., 1997), including part of the Pennine Uplands, and it is a largely rural, cool, humid temperate basin (Jarvie et al., 1997). Average annual precipitation (1961-1990) is 1139mm, rising to over 1500mm in the headwater areas. Bank materials are fine-grained.

Monitoring methods: A total of 26 representative fine-grained eroding bank sites (16 fluvial; 10 estuarine) were established for bank monitoring (Fig. 2). Grid networks of ~30->100 erosion pins were installed and re-read at ~20-day intervals for between 1 and 2.25 years. Repeat survey was used to quantify major changes in bank position. For a clearer picture of erosion events, we deployed the Photo-Electronic Erosion Pin (PEEP**)** *automatic* erosion-monitoring system at up to six strategic points at eight key bank sites near LOIS Core Monitoring stations (5 fluvial; 3 estuarine) (Fig. 2). We focus here simply on example PEEP results for the site at Easedike, for which continuous flow, turbidity and suspended sediment concentration data were available at nearby Tadcaster (Fig. 2). All sensors, including PEEPs, were connected to Campbell-Scientific CR10X dataloggers programmed to scan at 1-minute intervals and store data as 15-minute means. An Automatic Water Sampler was used within the LOIS Core monitoring programme to assess temporal changes in suspended sediment concentration (SSC) and for turbidity meter calibrations (Leeks et al., 1997). Flow and meteorological data were obtained from nearby UK Environment Agency stations. All timings are in GMT (Greenwich Mean Time).

EXAMPLE BANK EROSION EVENT SEQUENCES

Erosion dynamics: This was one of the most comprehensive river bank erosion investigations ever undertaken, in terms of the holistic basin approach adopted, the number of sites and points monitored, and the temporal resolution of measurement achieved. Around 15,000 manual erosion pin measurements were made over the 2.25-year monitoring period, plus 15-min PEEP readings. Some early data are published in Lawler et al. (1999) and Mitchell et al. (1999).

Much bank erosion took place in discrete, episodic events, rather than as a slower, continuous process. Moreover, in most cases, these bank erosion events were virtually instantaneous, and generally took less than 15 minutes to be completed (i.e. the logger scan interval). This underlines the need to adopt an automatic (quasi-) continuous approach to the monitoring of erosion in fluvial and other systems. Space permits here a brief focus on two example bank erosion events at Easedike (Fig. 2) to illustrate the how the PEEP system can clarify bank erosion event timings with respect to the hydrograph.

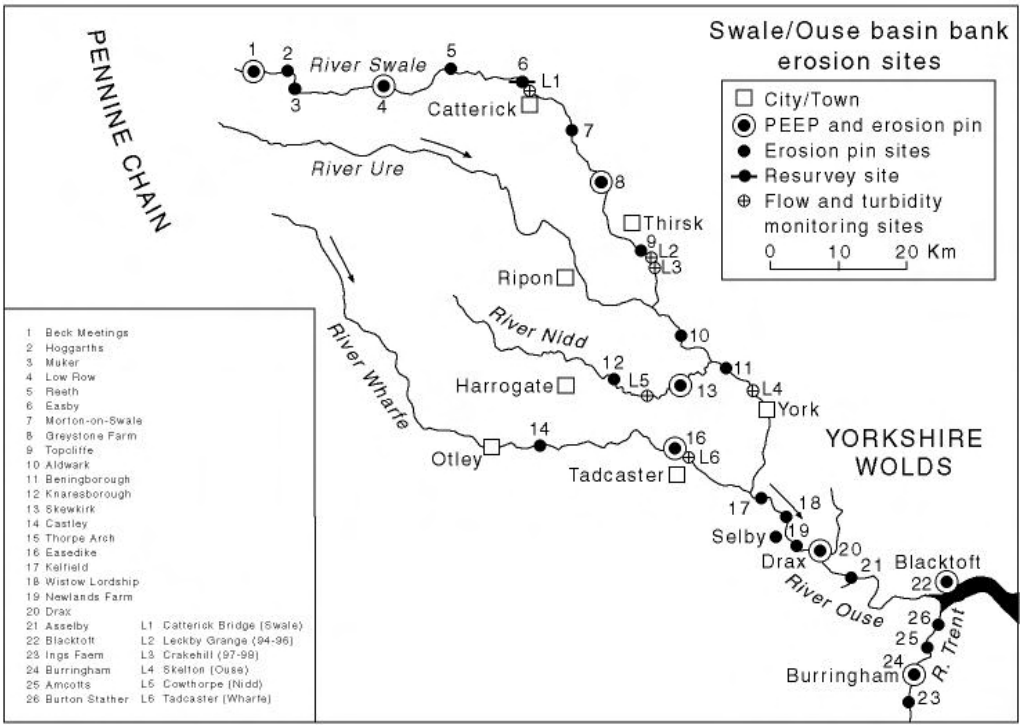

Figure 2. Location of the bank erosion sites and monitoring stations of the LOIS project. This paper is concerned with Easedike PEEP site (station 16) and Tadcaster gaging station (L6) on the River Wharfe

November 1996 Event: Fig. 3 illustrates a typical PEEP diurnal data sequence. The sudden increase in PEEP series outputs, with respect to a largely constant reference cell signal, clearly reveals that a large (>150 mm) erosion event occurred during a flow rise in early November 1996. Maximum readings for the PEEP back reference cell also confirm that the complete active length of the sensor has been exposed by bank retreat. The pattern of PEEP outputs also indicates that the erosion event took place within an 18-hour 'window' between 14.15 h on November 6 and 08.15 h on November 7 (Fig. 3), i.e. around the time of the flow and suspended sediment concentration peak.

Thermal Consonance Timing (TCT): Although defining the 'erosion event window' as above is very useful, and a significant improvement over conventional methodologies, the moment of material removal can be further fine-tuned through what we term *thermal consonance timing* (TCT). PEEP sensors carry two thermistors, one at the bank surface and one at 68 mm depth (Fig. 1B). Under normal conditions, micrometeorological theory and empirical data suggest that thermal regimes at the soil surface (which acts as a radiation exchange surface) are much more extreme than at depth. This is precisely what we record: note how, before the November 6 flood, bank surface temperatures tend to be higher during the day and lower during the night than the bank interior (e.g. November 1-6, Fig. 3). However, once erosion 'exposes' both thermistors so that they experience very similar microclimates, thermal differences are minimised and the thermistors achieve *thermal consonance*. The time when thermal consonance is first established, therefore, reveals the precise moment of material removal. This is especially useful for those periods when PEEPs do not produce strong signals (e.g. when in nocturnal 'sleep' mode or if inundated by turbid water). A simple plot of the temperature difference time series (e.g. Fig. 3) reveals when *thermal consonance* has been established, i.e. when differences become low and constant. For example, in Fig. 3, TCT suggests that the bank erosion event which exposed both thermistors occurred on November 6 at 15.00 GMT - 1.5 hours after inundation, 1 hour before the suspended sediment concentration peak, and 2 hours before the flow peak. In this case, therefore, at least 68 mm of the 150 mm bank erosion recorded was achieved as a *rising limb* event. Data on the timing of material removal with respect to the hydrograph can help to understand the minimum stresses required for entrainment.

February 1997 Event: Figure 4 shows a triple-peaked hydrograph event in February 1997, along with time series for PEEP erosion, suspended sediment concentration and bank temperature. The clear increase in PEEP outputs after the 18 February flow event indicates bank erosion of 140mm (Fig. 4). The increase in PEEP back reference cell outputs confirms this. A key point, however, is that bank erosion was a *delayed retreat* incident, occurring *at least* 6

hours after the flow peak of 12.45 h on February 18 (Fig. 4). The PEEP data place the erosion event in the latter stages of the recessional limb of the first hydrograph rise, during a 13.5-hour nocturnal event 'window' between 19.00 h on February 18 and 08.30 h on February 19 (Fig. 4). TCT evidence is not as conclusive here as for the November 1996 event above. However, it suggests that the main bank retreat occurred towards the end of this window, as indicated by the arrow in Fig. 4, within a 6-hour period between 02.15 h and 08.15 h on February 19, and probably just before 08.15, i.e. between 13 and 19 hours *after* the discharge peak. Further erosion ($\geq$ 20mm) then took place during the second flow event on February 20 (Fig. 4). This is again confirmed by maximum outputs from the back reference cell.

Delayed retreat events, well after the discharge peak, suggest that direct *fluid entrainment* is not the main erosion process in this case. Instead, such delays are usually taken as the signature of *a mass failure* or bank collapse process, and reflects either the removal during or following the hydrograph recession of transient lateral buttressing support to the bank provided by the flood waters themselves, or time-lags in the attainment of the critical pore-water pressure conditions necessary for geotechnical instability (e.g. Lawler et al., 1997b). Although there is some anecdotal evidence in the literature to suggest that delayed bank retreat events can occur, it is significant that the PEEP data are able to quantify such delays to confirm the phenomenon. Thus, PEEP data on erosion *timing* can help to suggest or eliminate certain controlling processes. Future parallel investigations of the variables driving such mechanisms should therefore provide a method of evaluating competing hypotheses, and testing erosion and sediment transport models.

DISCUSSION AND CONCLUSIONS

This application of the PEEP system to a large river system has demonstrated that bank erosion event details can be determined much more clearly with this technique than was possible hitherto - especially the magnitude, frequency and timing of erosional and depositional activity in relation to fluctuations in river flow and hydrometeorological conditions (Figs 3 and 4). The study has yielded new and hitherto elusive information on the time-dependent behaviour of bank erosion. The two sequences show how the PEEP system can (a) quantify the impact of *individual*, rather than aggregated, forcing events, (b) reveal the full complexity of bank response to flow sequences, and (c) help to identify likely driving processes. The occurrence of *delayed* bank retreat events, up to 19 hours after the flow peak and indicating mass failure processes rather than fluid entrainment mechanisms, has been confirmed and quantified.

Further examples of how the PEEP system improves the temporal resolution of erosion and deposition monitoring on the banks of other rivers can be found in Lawler (1991, 1994; Lawler et al., 1997a, 1997c). PEEP systems have also been applied to other contexts, including snow ablation and accumulation, beaches, tidal systems, drainage ditches and artificial channels (e.g. Mitchell et al., 1999; Prosser et al. 2000; Stott, 1999).

Such high-resolution information on the temporal distribution of bank erosion is vital to a sound process understanding of: the mechanics of bank instability, the fate of failed material, basal clean-out cycles, and the delivery and storage of bank sediment to river systems, especially time-lags between hydrograph peaks, erosion events, and sediment injection to rivers. In particular, given the importance of knowing the *timing* of inputs and outputs, coupling PEEP systems with concurrent flow and turbidity monitoring (e.g. Figs 3 and 4), should help in future studies to evaluate the relations between erosion, sediment supply and sediment transport in fluvial (and other) systems.

There is an urgent need for further research, however, to refine existing techniques and to develop new methods for the continuous monitoring of erosion and deposition events in many geomorphological contexts. Such research could usefully exploit recent developments in micro-electronics, communications and data acquisition systems.

ACKNOWLEDGEMENTS: We are very grateful for funding from the UK Natural Environment Research Council (Land-Ocean Interaction Study ST 231; GST/02/1184), and help from Robert Brown, James Grove, Richard Johnson, Steve Mitchell, Kevin Burkhill and UK Environment Agency with data collection, provision and graphics.

Figure 3. PEEP series showing bank erosion event, flow, suspended sediment concentration (SSC) & bank temperature series: the R.Wharfe at Easedike, UK, October 31 - November 18 1996

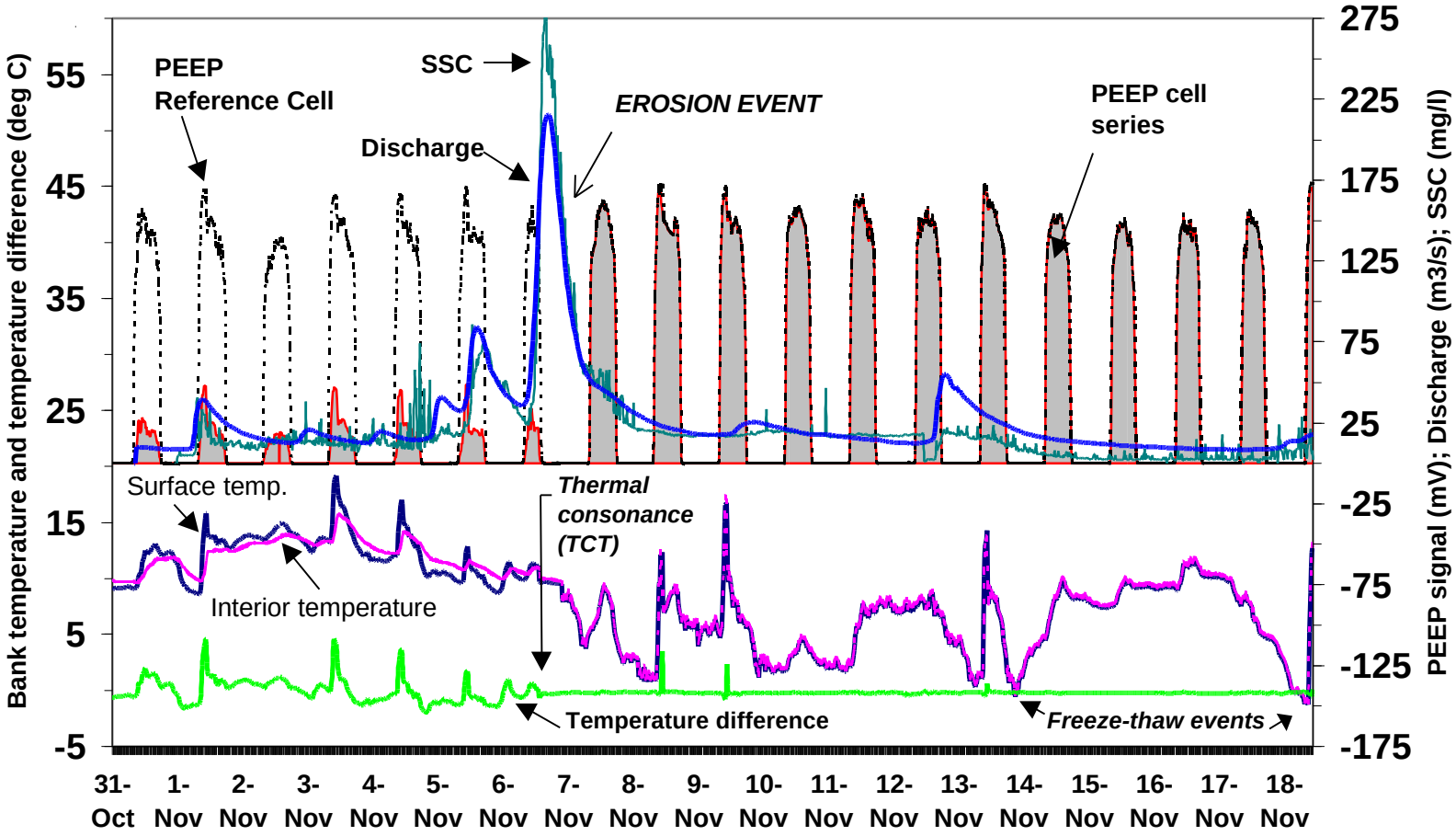

Figure 4. PEEP series showing bank erosion events, flow, suspended sediment concentration (SSC) & bank temperature series: the R.Wharfe at Easedike, UK, February 16 - 26, 1997

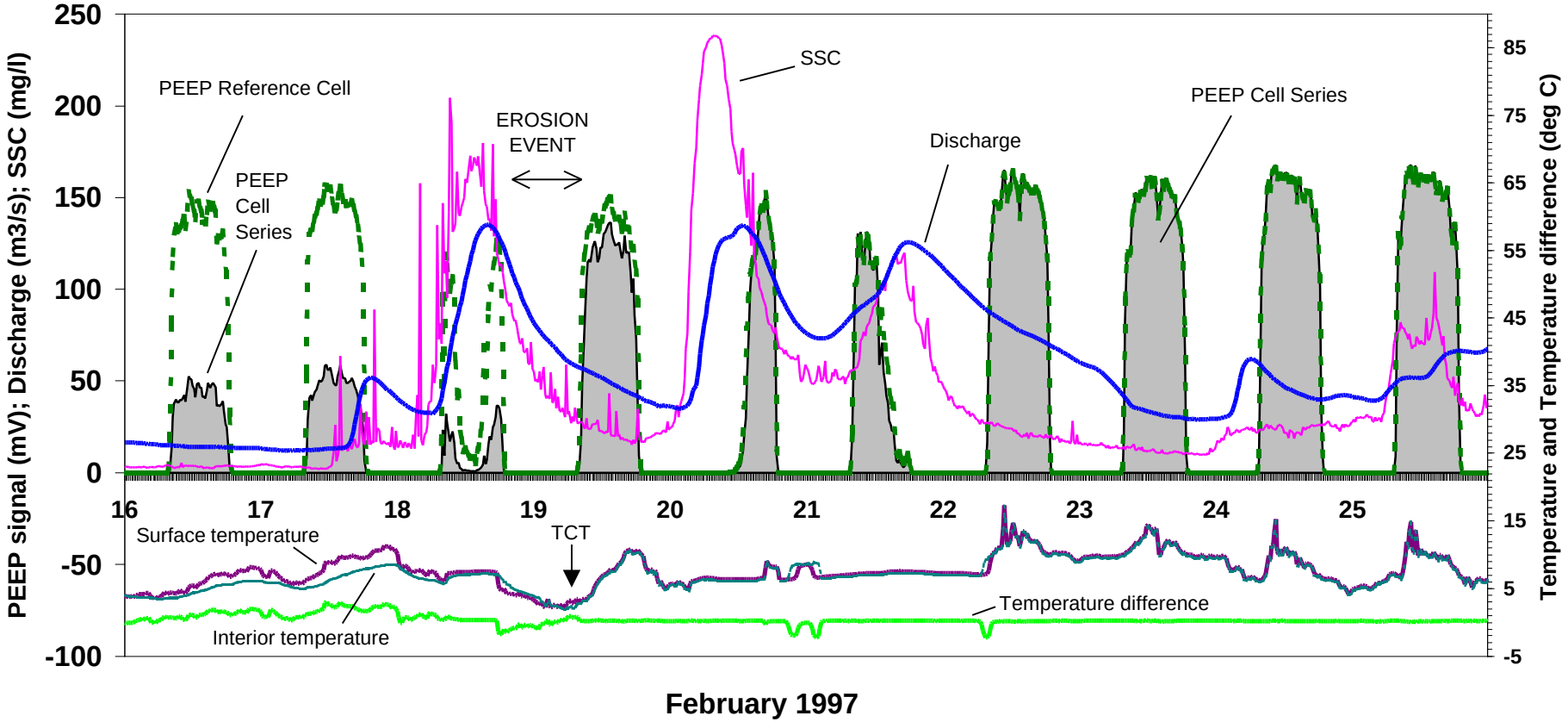

REFERENCES

Jarvie, H.P., Neal. C., Robson, A.J., 1997, The geography of the Humber catchment. Sci. Total Environ. 194/195: 87-99.

Lawler, D.M., 1991, A new technique for the automatic monitoring of erosion and deposition rates, Water Resources Research 27, 2125-2128.

Lawler, D.M., 1992, Design and installation of a novel automatic erosion monitoring system, Earth Surface Processes and Landforms 17, 455-463.

Lawler, D.M., 1993, The measurement of river bank erosion and lateral channel change: a review, Earth Surface Processes and Landforms 18 (9), 777-821.

Lawler, D.M., 1994, Temporal variability in streambank response to individual flow events: the River Arrow, Warwickshire, UK, In: Olive, L. et al. (Eds) Variability in Stream Erosion and Sediment Transport, Int. Ass. Hydrol. Sci. Publication No. 224, 171-180.

Lawler, D.M., Harris, N., Leeks, G.J.L.,1997a, Automated monitoring of bank erosion dynamics: applications of the novel Photo-Electronic Erosion Pin (PEEP) system in upland and lowland river basins, In Wang, S.Y.; Langendoen, E.J.; Shields, F.D., Jr. (Eds), Management of Landscapes Disturbed by Channel Incision, The University of Mississippi, Oxford, Mississippi, 249-255.

Lawler, D.M., Thorne, C.R., Hooke, J.M., 1997b, Bank erosion and instability, In Thorne, C.R., Hey, R.D. and Newson, M.D. (Eds) Applied Fluvial Geomorphology for River Engineering and Management, Wiley, 137-172.

Lawler, D.M., Couperthwaite, J., Bull, L.J., Harris, N.M., 1997c, Bank erosion events and processes in the Upper Severn basin, Hydrology and Earth System Sciences 1, 523-534.

Lawler, D.M., Grove, J., Couperthwaite, J.S., Leeks, G.J.L., 1999, Downstream change in river bank erosion rates in the Swale-Ouse system, northern England, Hydrological Processes 13, 977-992.

Leeks, G.J.L., Neal, C., Jarvie, H.P., Casey, H., Leach, D.V., 1997, The LOIS river monitoring network; strategy and implementation. Sci. Total Environ. 194/195, 101-109.

Mitchell, S.B., Couperthwaite, J.S., West, J.R., Lawler, D.M., 1999, Dynamics of erosion and deposition events on an intertidal mudbank at Burringham, River Trent, UK, Hydrological Processes 13, 1155-1166.

Prosser, I.P., Hughes, A.O., Rutherfurd, I.D., 2000, Bank erosion of an incised upland channel by subaerial processes: Tasmania, Australia, Earth Surface Processes and Landforms 25, 1085-1101.

Stott, T., 1999, Stream bank and forest ditch erosion: preliminary responses to timber harvesting in mid-Wales, In: Brown, A.G. and Quine, T.A. (Eds.), Fluvial Processes and Environmental Change, Wiley, 47-70.

Webb, B.W., Phillips, J.M., Walling, D.E., Littlewood, I.G., Watts, C.D., Leeks, G.J.L., 1997, Load estimation methodologies for British rivers and their relevance to the LOIS RACS programme. Sci. Total Environ. 194/195, 87-99.

***Author contact details**: Dr Damian M. Lawler, School of Geography and Environmental Sciences, The University of Birmingham, Birmingham B15 2TT, UK. Tel: +44-121-414-5532/5544; Fax: +44-121-414-5528; Email: **D.M.Lawler@bham.ac.uk**; Internet: http://www.bham.ac.uk/geography*

SCIENTIFIC BASIS FOR STREAMBANK STABILIZATION USING RIPARIAN VEGETATION

Andrew Simon, Research Geologist, USDA-ARS National Sedimentation Laboratory, Oxford, MS; and Andrew Collison, Visiting Scientist, King' s College London, UK

USDA-ARS National Sedimentation Laboratory, 598 McElroy Drive, Oxford, MS 38655, Ph. (662) 232- 2918, simon@sedlab.olemiss.edu

Abstract Stabilization of streambanks using riparian vegetation offers numerous potential benefits, and some potential problems. These can be separated into mechanical and hydrological effects and though widely discussed, they are rarely quantified. To determine these combined impacts, monitoring and modeling of unstable streambanks is underway in Goodwin Creek, Mississippi. Mechanical reinforcement has been quantified through measurements of root tensile strength, used to calculate increased soil cohesion. Hydrological effects of vegetation are monitored using interception plots and tensiometers under three covers: a cropped grass ' control' cover, clumps of eastern gamma grass, and a deciduous woody-vegetation stand. The measurements have been applied in a numerical model to assess the individual and combined effects of vegetation on streambank stability. On April 4th 2000 prolonged rainfall at the field site caused bank failure at the control cover plot, providing useful validation data for the analysis. The resulting factor of safety (F_s) values (incorporating both hydrological and mechanical effects) were 1.04, 1.64 and 2.18, respectively. Results show that the main contribution of the woody-vegetation to bank stability during the study period was hydrological rather than mechanical, and that the build up of matric suction at depth during the summer months persisted throughout the winter and spring. This effect was due to transpiration rather than canopy interception losses, which were only 2% of rainfall during the study period. The beneficial hydrologic effect of woody vegetation may not be the case during wetter winters; more rapid loss of matric suction beneath woody-vegetation suggests that this bank may become less stable than the control or clump grass treatments due to enhanced infiltration of rainfall.

INTRODUCTION

Channel widening occurs by a combination of hydraulic-induced bank-toe erosion and mass-bank failure. In addition to its effects in modifying hydraulic scour, and its undoubted benefits in terms of environmental quality, vegetation is widely believed to increase the stability of streambanks (see for example Thorne, 1990). Stabilizing effects include reinforcement of the soil by the root system and the reduction of soil moisture content because of canopy interception and evapotranspiration. However, studies of vegetation' s impact on the stability of hillslopes have highlighted the potential for some destabilizing effects (Greenway, 1987; Collison *et al.*, 1996). These include higher moisture contents during and after rainfall events due to increased infiltration capacity. Though many authors have evaluated the mechanical benefits of vegetation (see for example Abernethy and Rutherford, 2000) few have quantified the hydrologic effects, or considered the balance between potential stabilizing and destabilizing effects under different scenarios. This paper reports a field monitoring and computer-modeling investigation that has been carried out in northern Mississippi to quantify the separate and combined hydrologic and mechanical effects of different vegetation covers on streambank stability.

Bank stability processes in incised channels Channel widening by bank collapse is a common process in incised river channels, which are found throughout much of the Midwestern United States (Simon and Rinaldi, 2000). An important feature of bank stability in deeply incised channels is the significance of negative pore-water pressure (matric suction) above the water table in maintaining sufficient soil strength to withstand destabilizing forces (Casagli *et al.*, 1997; Simon and Curini, 1998; Simon *et al.*, 1999). The strength of saturated soil can be described by the Mohr-Coulomb criterion:

$$\tau_f = c' + (\sigma - m_w) \tan f' \qquad (1)$$

where τ_f = shear stress at failure (kPa); c' =effective cohesion (kPa); σ = normal stress (kPa); m_w = pore-water pressure (kPa); and f' = effective angle of internal friction (degrees).

Matric suction (negative pore-water pressure) above the water table has the effect of increasing the apparent cohesion of a soil. Fredlund et al., (1978) defined a functional relationship increasing soil strength with increasing matric suction. The rate of increase is defined by the parameter f^b, which is generally between 10º and 20º, with a maximum value of f' under saturated conditions (Fredlund and Rahardjo, 1993). Apparent cohesion incorporates both electro-chemical bonding within the soil matrix and cohesion due to surface tension on the air-water interface of the unsaturated soil:

$$c_a = c' + (m_a - m_w) \tan f^b = c' + y \tan f^b \quad (2)$$

where c_a = apparent cohesion (kPa); m_a = pore-air pressure (kPa); and y = matric suction (kPa).

The term f^b varies for all soils and for a given soil with moisture content (Fredlund and Rahardjo, 1993; Simon *et al*., 1999). Data on f^b are particularly lacking for alluvial materials. However, once this parameter is known (or assumed) effective cohesion (*c'*) in the soil can be estimated by measuring matric suction with tensiometers or other devices and by using equation 2.

Effects of vegetation on bank stability Soil is generally strong in compression, but weak in tension. The fibrous roots of trees and herbaceous species are strong in tension but weak in compression. Root-permeated soil therefore makes up a composite material that has enhanced strength (Thorne, 1990). Numerous authors have quantified this enhancement using a mixture of field and laboratory experiments. Endo and Tsuruta (1969) used *in situ* shear boxes to measure the strength difference between soil and soil with roots. Wu (1984) and Gray and Leiser (1982) used laboratory-grown plants and quantified root strength in large shear boxes. Wu *et al*., (1979) developed an equation that estimates the increase in soil strength (c_r) as a function of root tensile strength, areal density and root distortion during shear:

$$c_r = T_r.(A_r / A) (\cos q \tan f + \sin q) \quad (3)$$

where c_r = cohesion due to roots (kPa); T_r = tensile strength of roots (kPa); A_r/A = area of shear surface occupied by roots, per unit area (root-area ratio); q = shear distortion from vertical (degrees); and f = friction angle of soil (degrees).

Root tensile strength can be measured in the laboratory or field and is highly variable, with typical values in the thousands to millions of Pa (see Greenway, 1987, for a comprehensive review of published data). Most authors note a non-linear inverse relationship between root diameter and strength, with smaller roots contributing more strength per unit root area. Our current research indicates, however, that although stronger per unit area than larger roots, great numbers of small roots still may lack sufficient total area to contribute significantly to increases in c_r. It is unclear whether the optimum species for bank stabilization are grasses and herbaceous plants, rather than trees. Clump grasses such as Vetiver (*Vetiver zizinades*) and eastern Gamma grass (*Tripsacum dactyloides*), which have proved successful in reducing surface erosion (Dabney *et al*., 1997), have been advocated as potential bank-stabilizing species, in addition to woody riparian covers.

Although many authors have measured root tensile strength for a variety of upland woody and herbaceous species, little work has been done on riparian species and still less has been carried out on the root architecture of riparian vegetation. Abernethy and Rutherford' s (2000) study in Australia stands out as an exception. Available data suggest that most roots are found within the upper 50-cm of the soil profile (Jackson *et al*., 1986; Sun *et al*., 1997; Tufekcioglu *et al*., 1999). More data are needed, however, to quantify the root-area-ratio (A_r / A) and shear distortion terms.

The hydrological effects of riparian vegetation are even less well quantified. Although data are available on canopy-interception rates for many riparian tree species, there is little useful data on the degree to which vegetation dries out the material comprising streambanks. Canopy interception for deciduous trees species is typically in the range of 10-20%, (see Coppin and Richards, 1990) but these figures are annual averages. A point that tends to be overlooked when discussing vegetation effects on bank stability is that most bank failures occur during the winter or spring, when deciduous vegetation is dormant and canopies have died back. In addition, the high rainfall events likely to be associated with bank failures tend to have the lowest canopy interception rates, since canopy interception is inversely proportional to rainfall intensity and duration. The hydrological behavior of streambanks is particularly important in deeply incised channels since these banks are normally unsaturated. Decreases in shear strength due to a loss of matric suction are a leading cause of bank failures in incised channels (Simon *et al*., 1999). In non-incised channels, however, streambanks may be expected to reach saturation during typical winter conditions, yet remain stable because they are not particularly high. Any detrimental hydrological effects are unlikely to be significant, because standard hydrologic conditions already represent a ' worst case' . However, for high, incised streambanks the ' normal' winter condition is likely to be unsaturated. Adding moisture due to increased infiltration capacity may therefore reduce bank stability.

METHODOLOGY

In order to assess the effects of vegetation on streambank stability, data were collected on the hydrologic and mechanical properties of three test plots on an unstable incised streambank in northern Mississippi. The data collected include intrinsic soil-mechanical properties (cohesion, friction angle, and unit weight), matric suction and

pore-water pressure under three vegetation treatments, and root tensile strength and distribution. The three vegetation treatments were control (short cropped turf), clump grass (Eastern Gamma Grass) and mature riparian trees (a mixture of sycamore, river birch and sweetgum).

Field data collection The research was carried out at the Goodwin Creek experimental watershed in the Loess Hills region of northern Mississippi. Channel straightening on the Tallahatchie River and its tributaries beginning around the start of the 20th century led to upstream channel degradation and associated bank widening. The study reach has been intensively monitored since 1997. The channel in the study reach is incised approximately three meters to a current depth of about five meters. For at least the last four years the channel has been relatively stable in terms of depth, with slight aggradation accompanying lateral migration by mass failures on the outside of meander bends. Dendrochronology and a geomorphic evaluation on the opposing point bar indicates that lateral migration has been occurring for at least 30 years at an average rate of about 0.5 m/y (Simon and Darby, 1997). The bank cross section is steep, generally between 70 and 90º.

An Iowa Borehole Shear Test (BST) device was used to measure the *in situ* strength of bank layers at different depths in a series of boreholes augered into the streambank. The BST enables direct measurements of apparent cohesion and friction angle to be made at ambient pore-water pressures. By measuring matric suction in an undisturbed core removed from the point where the BST was operated, it was possible to calculate effective cohesion using equation 2. Core samples were also analyzed for unit weight and particle size distribution.

Bank hydrology was monitored using tensiometers which recorded pore-water pressure (positive and negative) every ten minutes. At each of the three vegetation treatment plots, a nest of five tensiometers was installed, at depths of 30, 100, 200, 270 and 433 cm (corresponding to different sedimentary layers within the bank profile). Streamflow level was also recorded every ten minutes using two submerged pressure transducers mounted in the channel. Open sky rainfall, stemflow and canopy throughfall under the riparian tree plot were recorded on tipping bucket rain gages every ten minutes, with an additional array of 12 manual rain gages (10 in the woody stand and two in the open) measuring rainfall and throughfall every day on which rain occurred.

To obtain data to parameterize the root-reinforcement equation, a series of trenches was dug alongside riparian trees of different ages and species outside the monitored plots. Roots were exposed and tested for tensile strength using a technique developed by Abernethy and Rutherford (2000). The diameters of individual roots were measured using calipers, and the roots were then attached to a load cell using a cable grip. Stress was applied to the load cell using a winch, and the load and displacement were recorded electronically. Stress was increased until the root failed, either by snapping or by pulling out. Peak stress at failure and root diameter was then recorded. The location and depth of each root was noted to enable depth-root area relationships to be developed for each species. Attempts were made to measure the tensile strength of the eastern gamma grass, but these failed due to difficulties in gripping such small roots.

Numerical modeling of bank stability To assess vegetation effects on bank stability hydrologic and mechanical data were used in a numerical model of bank stability. The model used is a wedge failure type developed by Simon and Curini (1998) and Simon *et al*., (1999), and represents further refinement of the models developed by Osman and Thorne (1988) and Simon *et al*., (1991). The model is a Limit Equilibrium analysis in which the Mohr Coulomb failure criterion is used for the saturated portion of the wedge, and the Fredlund *et al*., (1978) criterion is used for the unsaturated portion. In addition to positive and negative pore-water pressure, the model incorporates various soil layers, changes in soil unit weight based on moisture content, and external confining pressure from streamflow. The model divides the bank profile into a number of user definable layers with unique geotechnical properties.

The factor of safety (F_s) is given by (Simon *et al*., 1999):

$$Fs = \frac{\sum c_i' L_i + [S_i \tan f_i^{\,b}] + [W_i \cos b - U_i + P_i \cos(a - b)] \tan f_i'}{\sum W_i \sin b - P_i \sin[a - b]} \qquad (4)$$

where c_i = effective cohesion of i^{th} layer (kPa); L_i = length of the failure plane incorporated within the i^{th} layer (m); S = force produced by matric suction on the unsaturated part of the failure surface (kN/m); W = weight of the i^{th} layer (kN); U = the hydrostatic-uplift force on the saturated portion of the failure surface (kN/m); P = the hydrostatic-confining force due to external water level (kN/m); a = failure-plane angle (degrees from horizontal); and b = bank angle (degrees from horizontal).

When driven with temporally and spatially distributed pore-water pressure data from the tensiometer nests, the output is a time series of F_s. In this study the model was parameterized with data from each of the three vegetation plots. Identical intrinsic soil-strength properties (c' , f' , g_s, $f^{\,b}$) were used for all three plot simulations (Table 1),

while measured pore-water pressures and c_r properties were applied uniquely to each plot (with the exception of cohesion for the grass plot, as outlined above).

Table 1. Geotechnical data used in bank-stability modeling

Depth below surface (cm)	c' (kPa)	ϕ' (degrees)	γ_s (kNm^{-3})	ϕ^b (degrees)
0-50	1.41	33.1	16.9	†17.0
50-100	2.70	28.1	19.3	10.2
100-200	13.0	28.5	20.0	†17.0
>270	0.0	32.8	19.7	†17.0

† No data available - estimated values used

FIELD RESULTS

Inspection of the bank profile and boreholes revealed four layers within the bank. The stratigraphy can be divided into two major layers, representing early and late Holocene deposition units. At the base, the bank lies on a coarse layer of cemented gravel. Strength testing shows the upper Holocene layer to be largely frictional with little or no cohesion (<2.7 kPa). Most of the apparent cohesion in this layer is due to matric suction. The lower Holocene unit by comparison has considerable cohesion, and acts as a semi-permeable boundary below the upper layer, contributing to the development of higher moisture contents and pore-water pressures in the upper Holocene during rainfall.

Root tensile strength varies widely, with several orders of magnitude variability. Comparison of root tensile strength with diameter reveals a set of non-linear inverse relationships similar to those found by other investigators (Figure 1). The data fall into two broad categories with Sycamore having the greatest average strength and willow amongst the lowest. The root architecture study revealed that most roots are found in the top 50-cm of soil, with an exponentially declining concentration of roots below the upper 10-cm. Average root area ratio for mature sycamore was 0.18%. Cohesion due to roots calculated using Wu *et al*., (1979) equation gives a value of 9.8 kPa, averaged over the upper 50-cm.

Assessing the mechanical contribution of the eastern gamma grass was difficult, and after one year little root growth had occurred at the field site, partly due to predation by mice. Plots of gamma grass elsewhere in northern Mississippi have performed well, and suggest that dense root growth can be expected down to at least 50 cm. To provide an idea of the potential effect of grass roots once they are established, a c_r value of 20 kPa was assumed, based largely on the greater relative strengths of small roots.

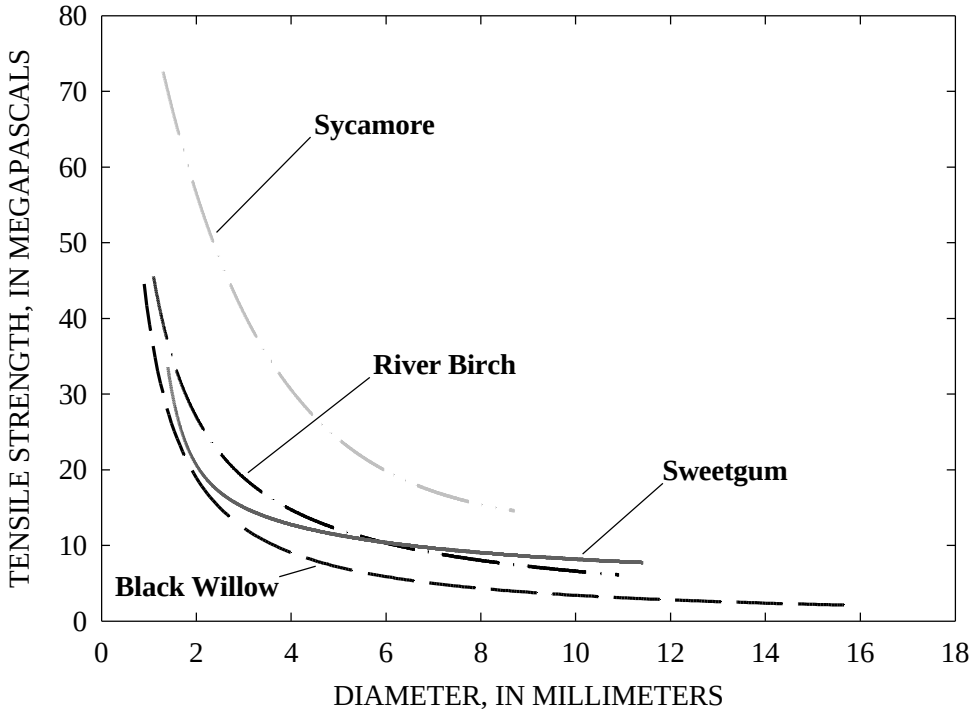

Figure 1. – Relation between root strength and root diameter for four riparian species.

PORE-WATER PRESSURE UNDER DIFFERENT VEGETATIVE COVERS

Pore-water pressure monitoring reveals significant differences between the three vegetative covers (Figure 2). Note that due to an artificial irrigation experiment during July 2000, data for this period have been removed from the record. At 30-cm there is little difference between the plots, although the tree cover is slightly wetter (lower matric suction) than either clump grass or the control site from December 1999 until May 2000. A striking feature of all of the records below 30 cm is the difference between the tree plot and the other two plots prior to the onset of the winter, wet season. Matric suction the tree plot is 40 to 60 kPa higher than under the other treatments. The tree cover experiences brief periods of negative suction (positive pore-water pressure) after rainfall events in the spring, indicating increased infiltration capacity and the development of a perched water table in the root zone. The steep decline in suction under this cover indicates enhanced infiltration rates via macropores, probably along root pathways. This represents one of the potential negative effects of woody vegetation although this was limited during the monitoring period because of an unusually dry winter and spring. After May, the tree site dries out faster than the other sites owing to greater rates of evapotranspiration, rising above the maximum measurable suction of 83 kPa by August.

Comparison of the tensiometer results from 100-cm reveals significant differences between all three covers. The control site and the grass plot broadly track each other, with the control consistently maintaining a suction around 10 to 20 kPa higher than the grass, indicating that stemflow may be concentrating water to depth in the grass plot (Figure 2). This is even more pronounced in the tree plot, further pointing to the potential negative effects of rapid delivery of water along root- and faunal-induced macropores. Evidence for preferential macropore flow is not confined to the vegetation covers however, with all three treatments showing response times to the April 4th event that exceed matric conductivities.

In general, the deeper the tensiometer, the slower the response to the onset of rainfall under all treatments as rainwater infiltrates from the surface downward. The tree cover shows the maintenance of the previous summer' s soil-moisture deficit through February 2000, at which point rapid wetting occurs at 100 cm. This wetting is associated with a series of relatively small rainfall events and the effect is translated to the deeper tensiometers with time as the 270 cm instrument begins to respond in early April (Figure 2).

The tensiometer data suggests that there is relatively little hydrologic difference between clump grasses and a control (cropped grass) cover. The cropped grass was observed to recover from the winter faster than the clump grass, which has a longer dormant period. There is some evidence from the tensiometers to suggest that the control cover was transpiring earlier, and that the clump grasses did not start to transpire until May. This is supported by field observations of stem growth at around the same time. However, the overall differences in matric suction are slight, and fall within the range of uncertainty due to soil heterogeneity.

Although the streambank under the tree cover maintains the greatest average values of matric suction, and, therefore, provides hydrologic benefits, rapid wetting at depth during spring suggests that under wetter antecedent conditions or under typical (wetter) springtime rainfall amounts, the net hydrologic effect may become negative and promote bank instability. This is supported by data from the relatively wet March period, when the tree plot becomes the wettest at 100 cm. Data from mid March show the onset of photosynthesis and transpiration leading to the rapid recovery of matric suction from May onwards.

MODELING VEGETATIVE EFFECTS ON BANK STABILITY

Tensiometer data for the three plots were used to drive the bank-stability model described above. Shear strength due to roots was added to the tree and grass plots based on measured and assumed values, respectively. All three data sets were modeled using identical bank profiles to ensure that any differences in F_s were solely due to vegetative effects. The resulting plots of F_s between December 1999 and September 2000 are shown with hydrologic effects only (Figure 3a) and for combined hydrologic and root-reinforcement effects (Figure 3b). As expected, both plots show a general trend of declining bank stability through the winter and spring with recovery starting in the early summer. The bank with the tree cover consistently has the highest F_s, although this drops markedly during the April 4th rainstorms. Grass consistently outperforms the control cover, though to a much lesser degree than trees. During the April 4th event the F_s for the control, grass and tress covers falls to 1.04, 1.64 and 2.18, respectively. The observed failure of the bank under the control cover suggests that the bank-stability model is performing well. At the time of failure, matric suction at 1-m depth was 13.1 kPa for the control site, compared with 4.5 and 6.2 kPa for the clump grass and tree sites, indicating that the vegetation increased infiltration rate and moisture content. However, this effect was reversed at depth, where suction values at 2.7-m were –3.9, 0.2 and 81.3 kPa respectively, indicating the beneficial effects of transpiration by the vegetative treatments, particularly in the tree plot.

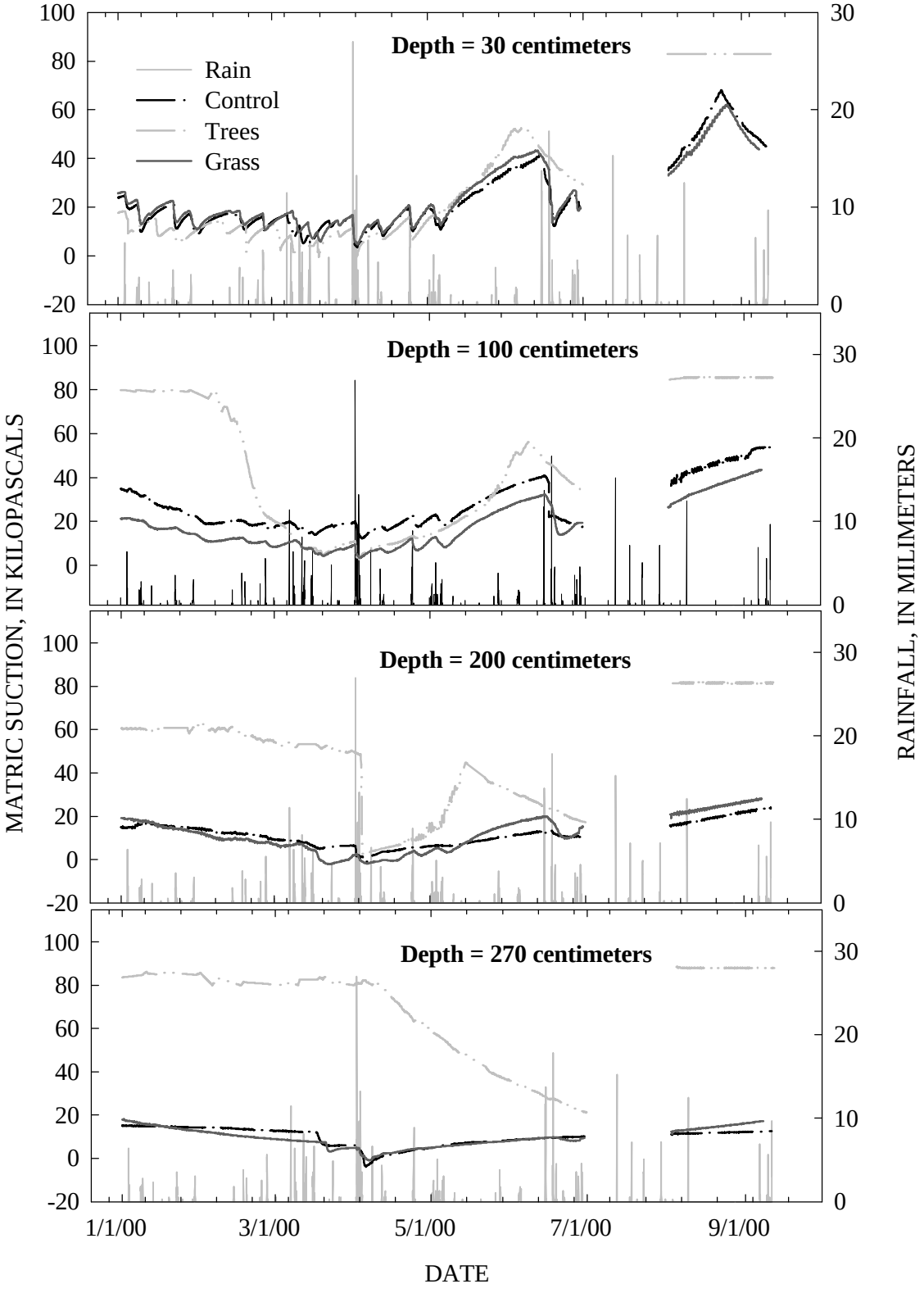

Figure 2--Tensiometer response for the three vegetative treatments.

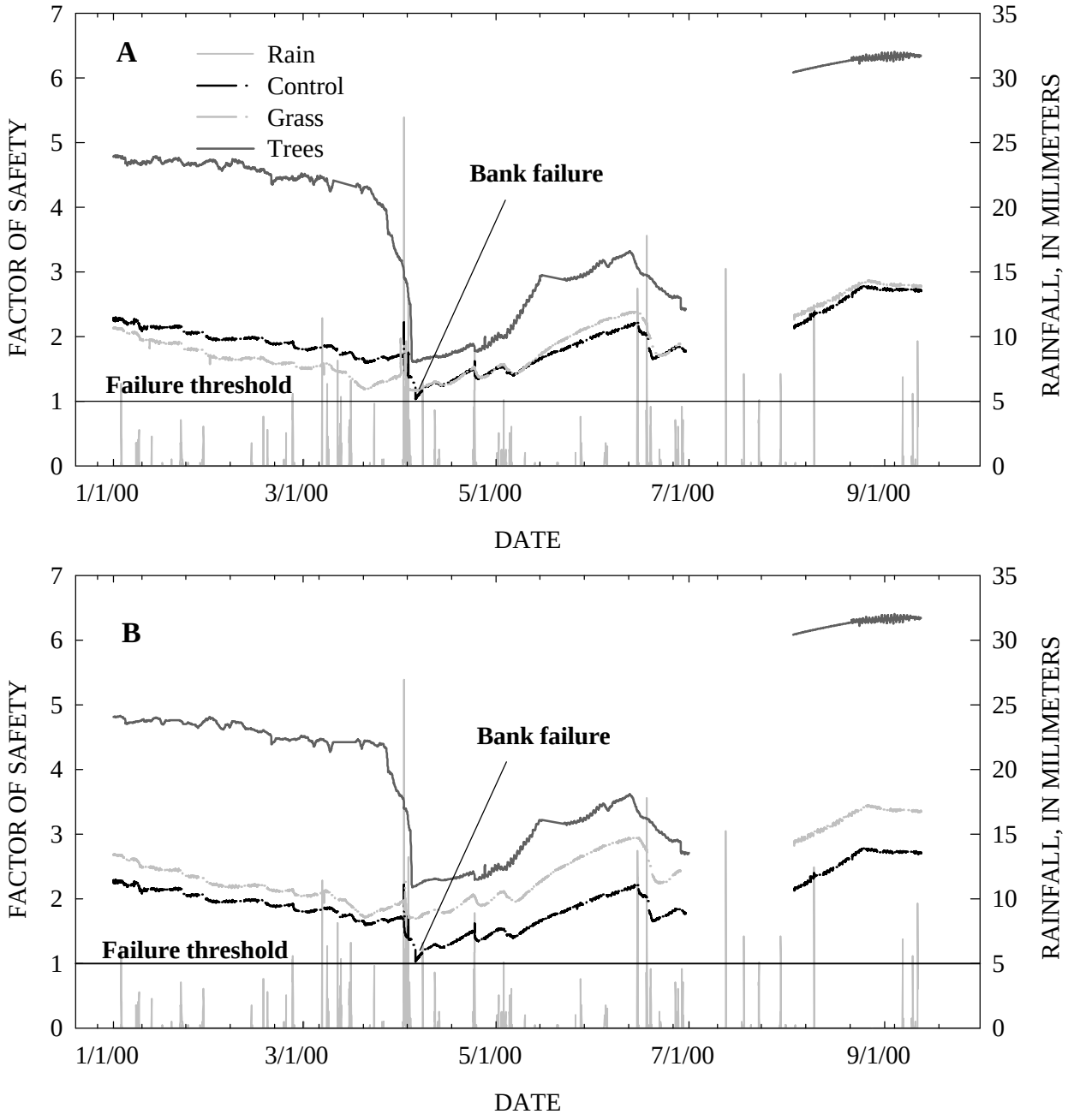

Figure 3--Factors of safety for the three vegetative treatments showing hydrologic effects (A) and combined effects (B).

Comparison of the F_s plots with the tensiometer data reveal that the difference in F_s between the control and grass plots is largely due to the assumed increase in shear strength (c_r) due to root reinforcement, whereas the increase in F_s under trees is largely a hydrologic function. By modeling F_s for each vegetative cover with hydrologic effects only, mechanical effects only and combined effects, we can observe the contribution made by each (Figure 4). For the grass-covered bank the mechanical reinforcement contributes an increase in F_s of 0.53, whilst the hydrologic contribution is only an additional 0.07. By comparison, under the tree cover the mechanical contribution to F_s is an increase of 0.26 whilst the hydrologic contribution is 0.88.

CONCLUSIONS

Hydrological and mechanical effects of riparian vegetation have been evaluated for three vegetation covers along an incised channel in northern Mississippi. The three covers were cropped grass ' control' , clumps of eastern gamma grass, and a mature stand of deciduous woody vegetation. Application of the data to a bank-stability model has shown that the effects of riparian vegetation on pore-water pressure response and bank-stability are both positive and negative. In general, however, the greatest enhancement to bank stability occurred under the tree plot as the positive effects of evapotranspiration negated the negative effects of preferential flow.

On April 4th 2000 prolonged rainfall at the field site caused the bank to fail under the control cover. The factor of safety at this time was 1.04, 1.64, and 2.18 for the control, grass, and tree treatments, respectively, showing the beneficial effects of vegetation.

For vegetation to enhance bank strength and stability the net effect must be beneficial during the most critical period of time, that being the wet seasons during winter and early spring. This is the time period, however, when deciduous vegetation is dormant, minimizing its potential positive hydrologic effects whilst maximizing the potential negative effects. If vegetation is to enhance bank stability hydrologically, its effects must come from very high values of matric suction developed during the previous summer and maintained through the wet season. Otherwise, root reinforcement would represent the only enhancement to bank shear strength and stability. The net hydrologic effect of vegetation can, therefore, be viewed as a balance between suction developed during the previous summer, operating against rapid delivery of water to depth via macropores during winter and spring rains. In this study, clearly lower than average rainfalls resulted in net positive effects, particularly in the case of a bank covered with mature trees. This, however, may not be the case in wetter years.

REFERENCES

Abernethy, B., and Rutherford, I.D., 2000, The role of riparian tree roots in reinforcing riverbanks. *Hydrological Processes*, 14, in press.

Casagli, N., Curini, A., Gargini, A., Rinaldi, M., Simon, A., 1997, Effects of pore pressure on the stability of streambanks: Preliminary results from the Sieve River, Italy. In. S.S.Y. Wang, E.J. Langendoen, and F.D. Shields Jr., (Eds.) *Management of Landscapes Disturbed by Channel Incision*, 243-248.

Collison, A.J.C., and Anderson, M.G. (1996): Using a combined slope hydrology and stability model to identify suitable conditions for landslide prevention by vegetation cover in the humid tropics. *Earth Surface Processes And Landforms*, 21, 737-747.

Coppin, N.J., and Richards, I.G., 1990, *Use of Vegetation in Civil Engineering*, Butterworths, London.

Curini, A., 1998, *Analisi dei processi di erosione di sponda nei corsi d' acqua*, Universita degli Studi di Firenze, Dipartimento di Scienze della Terra, 147, unpublished thesis, in Italian.

Dabney, S.M., Meyer, L.D., and McGregor, K.C., 1997, Sediment control and landscape modification with grass hedges. In S.S.Y. Wang, E.J. Langendoen, and F.D. Shields Jr., (Eds.) *Management of Landscapes Disturbed by Channel Incision*, 1093-1099.

Endo, T., and Tsuruta, T., 1969, On the effect of tree roots upon the shearing strength of soil. *Annual Report of the Hokkaido Branch, Forest Place Experimental Station*, Sapporo, Japan, 167-183.

Fredlund, D.G., Morgenstern, N.R., and Widger, R.A., 1978, The shear strength of unsaturated soils. *Canadian Geotechnical Journal*, 15, 313-321.

Fredlund, D.G., and Rahardjo, H., 1993, *Soil Mechanics of Unsaturated Soils*. John Wiley & Sons, Inc., New York, 517 p.

Gray, D.H., 1978, Role of woody vegetation in reinforcing soils and stabilizing slopes. *Proc. Symp. Soil Reinforcing and Stabilizing Techniques in Engineering Practice*, NSW Inst. Tech., Sydney, Australia, 253-306.

Gray, D.H., and Leiser, A.J., 1982, *Biotechnical Slope Protection and Erosion Control*. Van Nostrand Reinhold, New York.

Greenway, D.R. (1987) Vegetation and slope stability. In Anderson, M.G. and Richards, K.S. (Eds.), *Slope Stability*, Wiley, Chichester, 187-230.

Jackson, R.B., Canadell, J., Ehleringer, J.R., Mooney, H.A., Sala, O.E., and Schulze, ED., 1996. A global analysis of root distributions for terrestrial biomes. *Oecologia*, 108 (3): 389-411.

Osman, A. M., and Thorne, C. R. 1988. Riverbank stability analysis. I: Theory, *Journal of Hydraulic Engineering*, 114(2), 134-150.

Simon, A., and Curini, A., 1998, Pore pressure and bank stability: The influence of matric suction. In. S. Abt (Ed.) *Hydraulic Engineering ' 98*, ASCE.

Simon, A., Curini, A., Darby, S.E., and Langendoen, E.J., 1999, Streambank mechanics and the role of bank and near-bank processes in incised channels. In S.E. Darby and A. Simon (Eds.), *Incised River Channels: Processes, Forms, Engineering and Management*, John Wiley and Sons, London, 123-152.

Simon, A., and Darby, S.E., 1997, Bank-erosion processes in two incised meander bends: Goodwin Creek, Mississippi. In S.S.Y. Wang, E.J. Langendoen, and F.D. Shields Jr., (Eds.) *Management of Landscapes Disturbed by Channel Incision*, 256-261.

Simon, A., and Rinaldi, M., 2000, Channel instability in the loess area of the Midwestern USA. *Journal of the American Water Resources Association*, 36 (1): 133-150.

Simon, A., Wolfe, W. J., and Molinas, A. 1991. Mass wasting algorithms in an alluvial channel model, *Proc. 5th Federal Interagency Sedimentation Conference*, Las Vegas, Nevada, 2, 8-22 to 8-29.

Stone, E.L., and Kalisz, P.J., 1991. On the maximum extent of tree roots. *Forest Ecology and Management* 46, No. 1-2:59-102.

Sun, G.W., Coffin, D.P., and Lauenroth, W.K., 1997. Comparison of root distributions of species in North American grasslands using GIS. *Journal of Vegetation Science*, 8 (4): 587-596.

Thorne, C.R., 1990, Effects of vegetation on riverbank erosion and stability, In Thornes, J.B. (Ed.), *Vegetation and Erosion: Processes and Environments*, John Wiley & Sons, 125-144.

Tufekcioglu, A., Raich, J.W., Isenhart, T.M., and Schultz, R.C., 1999, Fine root dynamics, coarse soil biomass, root distribution and soil respiration in a multispecies riparian buffer in Central Iowa, USA. *Agroforestry Systems*, 44 (2-3):163-174.

Wu, T.H., 1984, Effect of vegetation on slope stability. *Trans. Res. Record* 965, Trans. Res. Board, Washington, DC, 37-46.

Wu, T.H., McKinnell, W.P., and Swanston, D.N., 1979, Strength of tree roots and landslides on Prince of Wales Island, Alaska. *Can. Geotechnical Journal*, 16 (1): 19-33.

AN ANALYTICAL APPROACH TO ESTIMATE SOIL EROSION FROM ROADSIDE DITCHES IN MOUNTAIN FOREST

By Jennifer G. Duan, Assistant Research Professor, Division of Hydrological Sciences, Desert Research Institute, University and Community College System of Nevada, 755 E. Flamingo Road, Las Vegas, NV 89119.

Abstract: Road construction has increased the run-off erosion and silt-producing potential from road cut banks and ditches along highways. Road ditches are designed to transport flow and sediment coming from bank cuts. Erosion occurs when flow-induced shear stress is sufficient to entrain bed or bank material. This paper reports the development of an analytical approach to estimate soil erosion from road cut banks and ditches. The result indicated that sediment yield could be calculated based on runoff, the slope and length of road cut banks, the longitudinal slope of road, and pavement in road ditches. Highway engineers can use this approach to estimate soil erosion in the design of roadside ditches.

INTRODUCTION

Non-point source pollutants from agricultural and forested lands have accounted for more than 50% of pollutants entering the waterways of the nation. Studies have shown that sediment is the major non-point source pollutant that causes the reduction of stream water quality. Sediment, itself, is a pollutant because its presence increases flow turbidity and reduces water clarity. It is also the carrier of contaminants, such as phosphorus, nitrogen, toxic metal, etc. These contaminants are either stored in the pore water of sediment particles or delivered by mobile bed materials. Therefore, it requires the accurate prediction of sediment discharge in order to better identify the outstanding contaminant sources and improve the accuracy in predicting non-point source pollutants.

Many of the forest watersheds in the West U.S. mountain regions have been intensively developed for recreation or industry, for example, the Lake Tahoe basin. The activities, such as logging, mining, housing, skiing, road building have changed the geomorphic settings of land surface and thus often increase runoff and erosion. Roads are constructed for these activities because it provides transportation. As a consequence, soil erosion associated with road building ranked the top of sediment source from several forest watersheds in the East U.S. (Farrish, *et al*., 1994; Swanson and Dyrness, 1975; Tysdal *et al.*, 1962). Highways in mountain forest are constructed by intercepting natural hill slopes and usually have a steeper longitudinal slope. Roadside ditches are existed for storing and transporting runoff from the upper road cut banks. These ditches are parallel to roads, therefore, often have a similar slope as that of road surface.

Since these roadside ditches convey flow not only from imperious road surfaces but also from road cut banks, if they were designed based on flow from road surfaces, erosion of their bed and banks are unavoidable. In fact, the severe bed and bank scoring of roadside ditches in several locations of the Lake Tahoe basin indicated that eroded soil in these ditches contributes considerably to non-point source pollutant. However, except for a few experimental studies in the early 1960s, there has not been a thorough theoretical analysis and no method available in the

literature to estimate soil erosion in these ditches. In this paper, the physical processes of soil erosion in roadside ditches were analyzed according to the principles of hydrology, hydraulics, and sediment transport. A conceptual model was established for the development of an analytical approach to estimate soil erosion in these ditches. Finally, the developed method was applied to predicting soil loss in a field experiment. The calculated results were compared with the field measurements and reasonable agreements were obtained.

Conceptual Model: In the mountain regions of the Southwest, highways are built by directly cutting hill slopes. Road surface is connected to the upper and lower road cut slopes (Fig.1). Runoff and eroded soil from the upper road cut banks are transported to roadside ditches and form a concentrated stream flow. Soil erosion was resulted from the concentrated flow as well as the shallow overland flow. The physical parameters that are used in this analysis are illustrated in Fig.1. They are classified as characteristics of road cut banks, dimensions of roadside ditches, road properties, and precipitation. The length of road cut banks is the distance from the top of road cut bank to the edge of roadside ditch, which is symbolized as L_0. Vegetation covering and topographic settings in these banks determine the surface roughness. Infiltration rate of this land surface influences the net runoff from these banks. Road surface inclines in both the longitudinal and transversal directions. But, the transversal slope is often small enough to be neglected. Roadside ditches are assumed to have the same slope of highway, but the width of these ditches and its vegetation covering are varied along the highway. w denotes the width of road ditch. Precipitation can be rainfall or snow. Because of the complexity of frost impact on soil erodibility, this factor was not considered in this study, but, it is indeed perhaps the dominant reason for the erosion of road cut banks. Therefore, erosion in roadside ditches would occur as soon as runoff and eroded soil from the upper road cut banks are delivered to road ditches and forms a concentrated stream flow. This stream flow erodes bed and bank of these ditches if the transport capacity of this concentrated flow exceeds eroded sediment supply from the upper road cut banks. Otherwise, if eroded sediment from upper banks exceed the flow capacity, deposition will occur in these ditches.

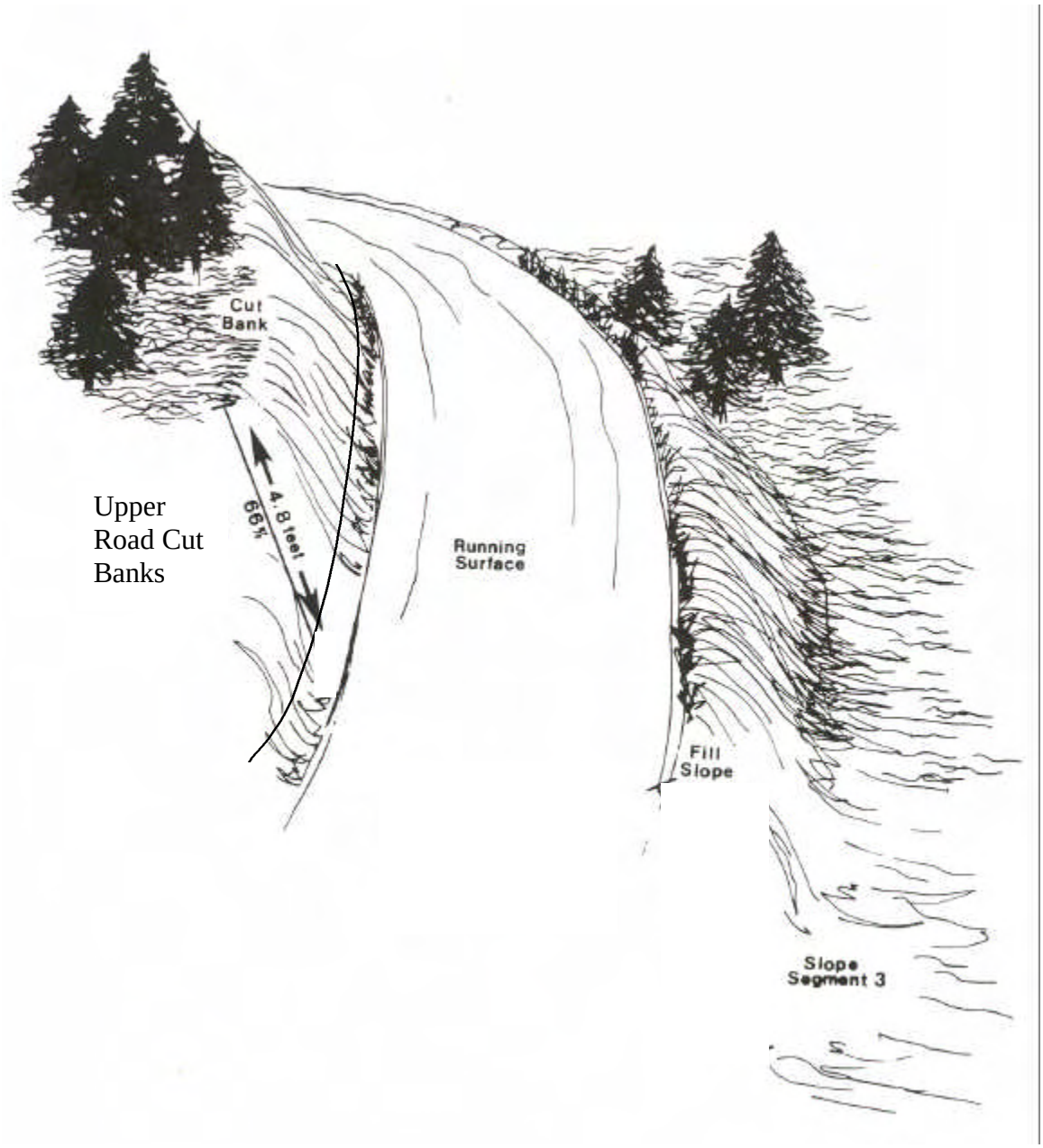

Figure 1. Schematic Diagram of Road Cut Banks and Roadside Ditches

Overland Flow on Road Cut Banks: Overland flow in a hill slope should be modeled as a two-dimensional flow because of the spatially varied microtopography, vegetation covering and soil properties. When runoff passes through land surface, rills are formed because of the irregularities and variable soil erodibility. The formation of rill has significantly increased soil erosion from these banks (Elliot and Tysdal, 1999; Poesen, 1985). Therefore, a two-dimensional unsteady hydrodynamic model (Zhang and Cundy, 1989; Gokemen and Kavvas, 1994) is required to accurately model the spatially and temporally varied overland flow. However, in engineering practices, it is preferred to get an initial approximated solution quickly and then conduct a detailed study if needed. Since the solution of two-dimensional overland flow can only be

obtained numerically, several empirical-analytical solutions (Gokemen *et al*, 1993; Govindaraju *et al*, 1988; Govindaraju *et al*., 1992) were based on the simplification of non-linear terms in the momentum equation. On the other hand, studies in the past few decades indicate that one-dimensional kinematic wave model (Stagnitti *et al*., 1992) can satisfactorily predict the averaged flow depth and hydrograph on a natural hill slope (Dunne and Dietrich, 1980) even though they are unable to account the spatial variability of flow field. In order to meet the needs of practical engineers and provide an approximated estimation of erosion from road cuts banks quickly, a simplified one-dimensional kinematic wave model is employed in this study.

The governing equations for the overland flow are the equations of continuity and momentum (Tayfur and Kavvas, 1994).

$$\frac{\partial h}{\partial t}+\frac{\partial uh}{\partial x}=I \tag{1}$$

$$\frac{\partial u}{\partial t}+u\frac{\partial u}{\partial x}+g\frac{\partial h}{\partial x}+rg(S_f-S_0)=0 \tag{2}$$

where, h is flow depth; u is velocity; g is acceleration of gravity; S_f and S_0 are surface and bed slope, respectively. I is rainfall intensity minus infiltration rate, which is approximated to be runoff. If assuming kinematic wave condition and assuming overland flow on road cut banks and channel flow in roadside ditches both satisfy Manning' s equation, that is $u=\frac{1}{n}h^{\frac{2}{3}}J^{\frac{1}{2}}$, flow depth in roadside ditches satisfies

$$\frac{\partial h}{\partial t}+k_1h^{\frac{2}{3}}\frac{\partial h}{\partial x}=I \tag{3}$$

Using the method of characteristics, Eq.3 ends up with

$$\begin{cases}\dfrac{dx}{dt}=k_1h^{\frac{2}{3}}\\ \dfrac{dh}{dt}=I\end{cases} \tag{4}$$

The infiltration rate is assumed to be a constant. In case of a rainfall event with a constant intensity and infinite time duration, the net runoff is constant. The solution of Eq.4 is given as

$$h(x,t)=\left[h(0,0)^{\frac{5}{3}}-\frac{Ix}{k_1}\right]^{\frac{3}{5}} \tag{5}$$

The boundary condition of overland flow is that $h(0,0)=0$ at the top of road cut banks. Therefore, flow depth at the bottom of bank cuts is expressed as

$$h(L_{over},t)=(\frac{IL_{over}}{k_1})^{\frac{3}{5}} \tag{6}$$

The discharge from this bank cut to road ditches is written as follows

$$q=k_1h^{\frac{5}{3}}=IL_{over} \tag{7}$$

Eq.7 is the discharge to roadside ditches from road cut banks. It is a function of runoff and the length of road cut banks.

Flow in Roadside Ditch: Runoff comes from the upper road cut bank concentrated in roadside ditches. Upon knowing the discharge, flow depth in these ditches can be obtained by solving one-dimensional momentum equation, which is written as

$$\frac{\partial H}{\partial t} + k_2 H^{\frac{2}{3}} \frac{\partial H}{\partial y} = \frac{I}{w}(L_0 + J_{road} y) \tag{8}$$

where H is flow depth, w is the width of roadside ditch, J_{road} is the slope of road ditch. $k_2 = \frac{J^{\frac{1}{2}}_{road}}{n_r}$ is flow conveyance factor. y is the distance between a cross section of road ditch and a reference cross section. Since rainfall event is assumed to have an infinite time duration, flow in these ditches is assumed to approach steady-state. The solution of Eq.8 is given as

$$H(y) = \left[\frac{IL_0}{k_2} \int_0^y \frac{1}{w}(1 + \frac{J_{road}}{L_0} y) dy \right]^{\frac{3}{5}} + \mathrm{C} \tag{9}$$

Assuming the slope of road ditch is constant and substituting the boundary condition, that is, flow depth equals to zero ($H=0$) at $y=0$. Eq.9 reduces to

$$H(y) = \left[\frac{IL_0{}^2}{2k_2 J_{road}} \frac{1}{w}(1 + \frac{J_{raod}}{L_0} y)^{\frac{1}{2}} \right]^{\frac{3}{5}} \tag{10}$$

Sediment Transport in Road Ditches: When runoff entered roadside ditches, it carries eroded soil from the surface of road cut banks. If flow-induced shear stress acting on the bed or bank of these ditches is enough to entrain sediment, bed or bank will be eroded. After obtaining flow depth and velocity, sediment discharge in these ditches can be estimated by empirical formulas. There are a number of empirical formulas to calculate the transport rate of sediment in channels. Among them, Ted Yang' s formula was used in this study because it includes the transport of bed and suspended load and is valid for a large size range of sediments. The transport formula of Ted Yang (1996) is written as follows,

$$\log C_{ts} = 5.165 - 0.153 \log \frac{wd}{n} - 0.297 \log \frac{u_*}{w} + (1.78 - 0.36 \log \frac{wd}{n} - 0.48 \log \frac{u_*}{w}) \log \frac{VJ_{road}}{w} \tag{11}$$

where C_{ts} is the concentration of sediment laden flow, w is the falling velocity of sediment particles, d is mean diameter of sediment particles, n is kinetic viscosity, V is the averaged velocity, u_* is the shear velocity that can be calculated by Eq. 12.

$$u_* = \sqrt{gH(y)J_{road}} \tag{12}$$

Obviously, by using Eq. 10, flow in the channel is assumed to be quasi-uniform and steady flow. The mean falling velocity of sediment particles can be calculated as follows (Ted Yang, 1996)

$$w = F\left[dg\left(\frac{g_s - g}{g} \right) \right]^{\frac{1}{2}} \tag{13}$$

in which g_s and g are the density of sediment and water, respectively. F is a coefficient whose value depends on the size of sediment particle. F equals 0.79 when the diameter of sediment particle is greater than *1mm*. After determining these coefficients, sediment discharge in these ditches can be calculated as

$$V_{sed} = C_{ts} Q = \frac{C_{ts} w}{n_r} H(y)^{\frac{5}{3}} J_{road}^{\frac{1}{2}} \tag{14}$$

where n_r is the Manning' s roughness coefficient of road ditch. The sediment discharge can be calculated by Eqs.11-14. It is obvious that sediment discharge is determined by flow depth, road slope, and roughness in road ditches as well as sediment falling velocity. The impact of runoff, the slope and length of road cut banks, and the roughness of road cut bank surface were reflected in the expression of flow depth in road ditches (Eq.10).

VERIFICATION BY EXPERIMENTAL DATA

Diseker and Richardson (1961) conducted a field experimental study in Cartersville, Georgia. One objective of their study is to measure the soil and water losses from highway cuts. Six roadside plots, in pairs with approximately 1:1, 1:2, 1:3 side slopes and a similar soil type, Cecil clay soil, were selected as suitable sites. The ditch grades vary from 2.8 to 5.0 percent. The bank heights at the highest point varied from 10 to 16 ft with lengths from 206 to 363 ft. The six runoff areas were 0.16, 0.27, 0.21, 0.20, 0.18, and 0.23 acres per plot. The width of these ditches varies from 9 to 13 ft. Masonary head walls, two sidewalls and a concrete apron were installed for each of the measuring devices at the lower end of the runoff plot ditch. Runoff as measured by water-stage recorders was used as a basis for calculating the runoff that passes through the H flume. Sediment samples were taken from each tank after runoff occurred to measure sediment concentration. Runoff and erosion from these six plots were measured from Nov. 1, 1958 to Dec. 31, 1959. The observed data showed that the sediment discharge of steep cut slope is much bigger than the one from a flatter slope. In order to verify the approach presented by Eq.11-14, soil loss is calculated at each study site. The monthly averaged runoff and the length of road cut slopes were used in Eq.10 to calculate flow depth in these ditches. The Manning' s roughness is 0.002 for roadside ditches. The slope of these ditches is 3.9%. The averaged width of these ditches is 11ft. Eq.11-14 is employed to calculate sediment discharge for each ditch. The calculated and observed soil losses were plotted in Fig.2 for comparison. Fig.2 indicated that the predicted results are in agreement with the observation for site 1, 2, 5, and 6. Due to the effect of frosting, the calculated soil losses in site 4 and 5 are much less than the measurement. Therefore, the approach presented in this paper, in general, is applicable to predicting soil loss from road cut banks and road ditches where the effect of frosting is not significant.

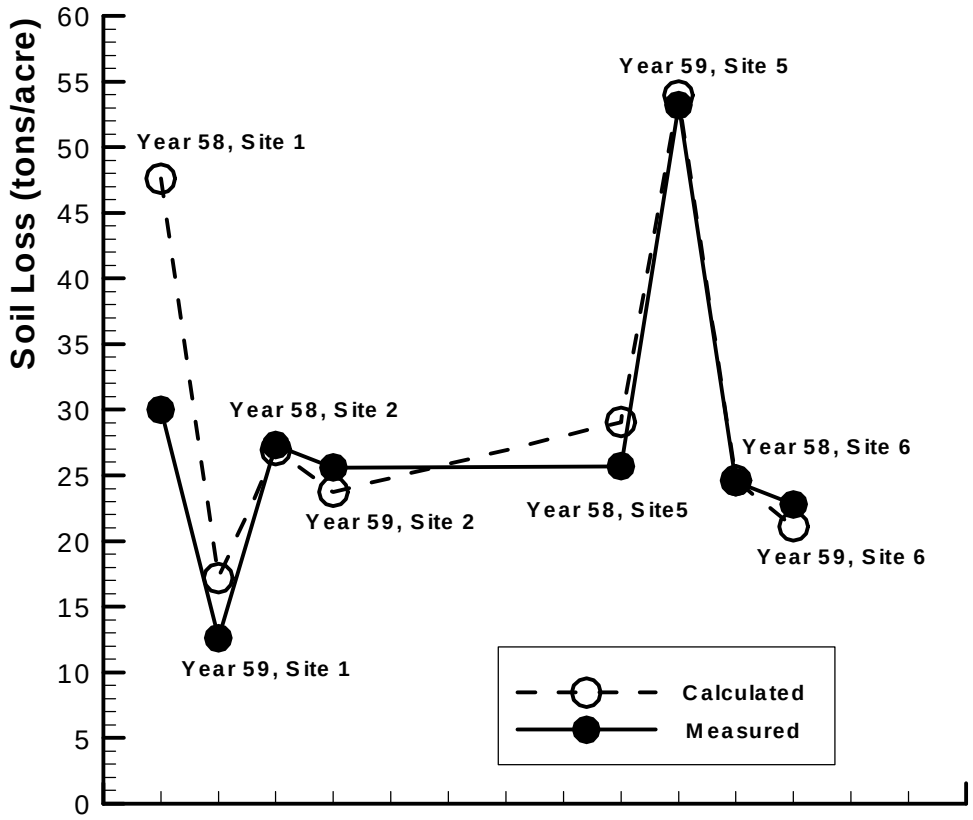

Figure 2. Comparison of Calculated Results and Measurements

CONCLUSION

An analytical approach was developed for the estimation of soil loss from road cut banks and roadside ditches in this study. One-dimensional kinematic wave model is used to solve shallow surface flow in road cut banks as well as the concentrated stream flow in roadside ditches. Soil loss from road banks can be estimated by Eq.11-14. The comparison between the calculated results and observed data indicated that the developed approach is feasible for the quick estimation of soil loss from road cut banks and roadside ditches. However, because the simplified kinematic wave method was employed and frost/defrost effect was not considered in this analysis, further research is needed in the future to enhance the capability of this method.

REFERENCES

Diseker, E. G. and Richardson, E. C., 1961, Roadside Sediment Production and Control, Transactions of the ASAE, November, 62-68

Elliot, J. W. and Tysdal, M. L. 1999, Understanding and Reducing Erosion from Insloping Roads, *Journal of Forestry,* August, 30-34.

Farrish, K. W., Aqdams, J.C., and Thompson, C.V. 1994, Soil Conservation Practices on Clearcut Forest Lands in Louisiana, *Journal of Soil and Water Conservation*, 48(2), 136-139.

Gokmen G. T., Kavvas, M. L., Govindaraju, R. S., and Storm, D. E., 1993, Application of St. Venant Equations for Two-dimensional Overland Flows Over Rough Infiltration Surfaces, *Journal of Hydraulic Engineering*, Vol. 119, No.1, January, 51-63.

Gokemen T., Kavvas M. L., 1994, Spatially Averaged Conservation Equations for Interacting Rill-interrill Area Overland Flows, *Journal of Hydraulic Engineering*, Vol. 120, No. 12, Dec, 1426-1447.

Govindaraju, R.S., Jones, S. E., and Kavvas, M. L, 1988, On the Diffusion Wave Model for Overland Flow 1: Solution for Steep Slopes, *Water Resources Research*, Vol. 24, No.5, May, 734-744.

Govindaraju, R. S., Kavvas, M. L. and Tayfur, G.,1992, A Simplified Model for Two-Dimensional Overland Flows, *Advances in Water Resources*, Vol.15. 133-141.

Poesen J. 1985. An Improved Splash Transport Model. *Z. Geomorph.* N. F., 29, 193-211.

Swanson, F.J. and Dyrness, C. T., 1975. Impact of Clearcutting and Road Construction on Soil Erosion by Landslides in the West Cascade Range, Oregan, *Geology*, 3:393-396.

Stagnitti F., Parlange, J., Steenhuis, T. S., Parlange, M. B., and Rose, W. C., 1992, A Mathematical Model of Hillslope and Watershed Discharge, *Water Resources Research*, Vol. 28, No.8, August, 2111-2122.

Tysdal, M. L., Elliot, J. W., Luce, H. C., and Black, A. T., 1652, Modeling Erosion from Insloping Low-Volume Roads with WEPP Watershed Model, *Transportation Research Record*, Vol. 1652, 250-256

Yang C. T., 1996, Sediment Transport, Theory and Practice, McGraw-Hill Companies, Inc.,141-208.

Zhang, W., Cundy, W. T., 1989, Modeling of Two-dimensional Overland flow, *Water Resources Research*, Vol.25, No.9, 2019-2035.

SEDIMENT DYNAMICS AND CONTAMINANT ACCUMULATION IN NEW YORK BIGHT

Marilyn Buchholtz ten Brink, Bradford Butman, Courtney Harris, Ellen Mecray, and William Schwab.

Coastal and Marine Geology, Northeast section
U.S. Geological Survey
384 Woods Hole Road,
Woods Hole MA 02543

Contact information for corresponding author:
Marilyn Buchholtz ten Brink email mtenbrink@usgs.gov phone: 508-457-2392

Topic: Results from regional wave-current sediment transport modeling, contaminant dispersal measurements, mooring deployments, and sediment accumulation studies (1993-2000) in the New York Bight Apex.

The coastal waters offshore of New York City have been used for disposal of sewage and dredge-spoils throughout the last century and also receive atmospheric and river-borne pollutants from the nearby metropolitan areas. The U.S.G.S. Coastal and Marine Geology Program has 1) mapped the seafloor geology and the distribution of contaminants in the sediments of New York Bight and 2) used moored instruments to measured water currents and sediment transport during winter 2000. These maps, measurements, and numeric models are being used to predict the fate of the contaminated sediments present in the Bight and the potential for adverse effects on the ecosystem in the future.

Sediment deposition and erosion occur episodically and vary spatially within the Bight. Fine-grained sediment with high concentrations of metal and organic pollutants that was dumped on the seafloor, primarily in the 1970-1980s, has been extensively reworked on the sandy shelf (25 m water depth), transported up to 100-km from disposal sites, and focused into bathymetric depressions (60-90 m) in the Hudson Shelf Valley (HSV) (Figure 1). The sites of accumulation, defined by chemical profiles and high-resolution seismic data, are focused in small depositional areas while saddles and the surrounding shelf have both lesser deposition rates and higher sediment mixing rates. In the valley, accumulation rates for contaminated sediment decrease with increasing distance from the source from 2 cm/yr to less than a mm/yr.

Modeling results indicate that the coastline orientation and shelf bathymetry exert a strong control on the response of shelf circulation and sediment resuspension to wind events. Winds from the northeast appear to drive weak flow down the HSV, while winds from the west appear to drive strong up-valley, landward, flow. The contaminant accumulation down-valley occurs because of the downstream flow that predominates during strong NE storm events, when large amounts of sediment are resuspended. Data from the moorings (Figure 2), combined with wave and wind climatology, will allow determination of the net flux and dispersal patterns for sediment in the HSV and adjacent areas.

The biological communities that exist in the contaminated regions are exposed to metals concentrations that can induce toxic effects, yet communities appear to be moving through typical recovery phases.

FIGURES

Figure 1: Seafloor features (sidescan & multibeam data: gray), Pb in surface sediments (dots), bathymetry (blue), and dumpsites, i.e. sources (pink). Core profiles show Pb accumulation (red is above background).

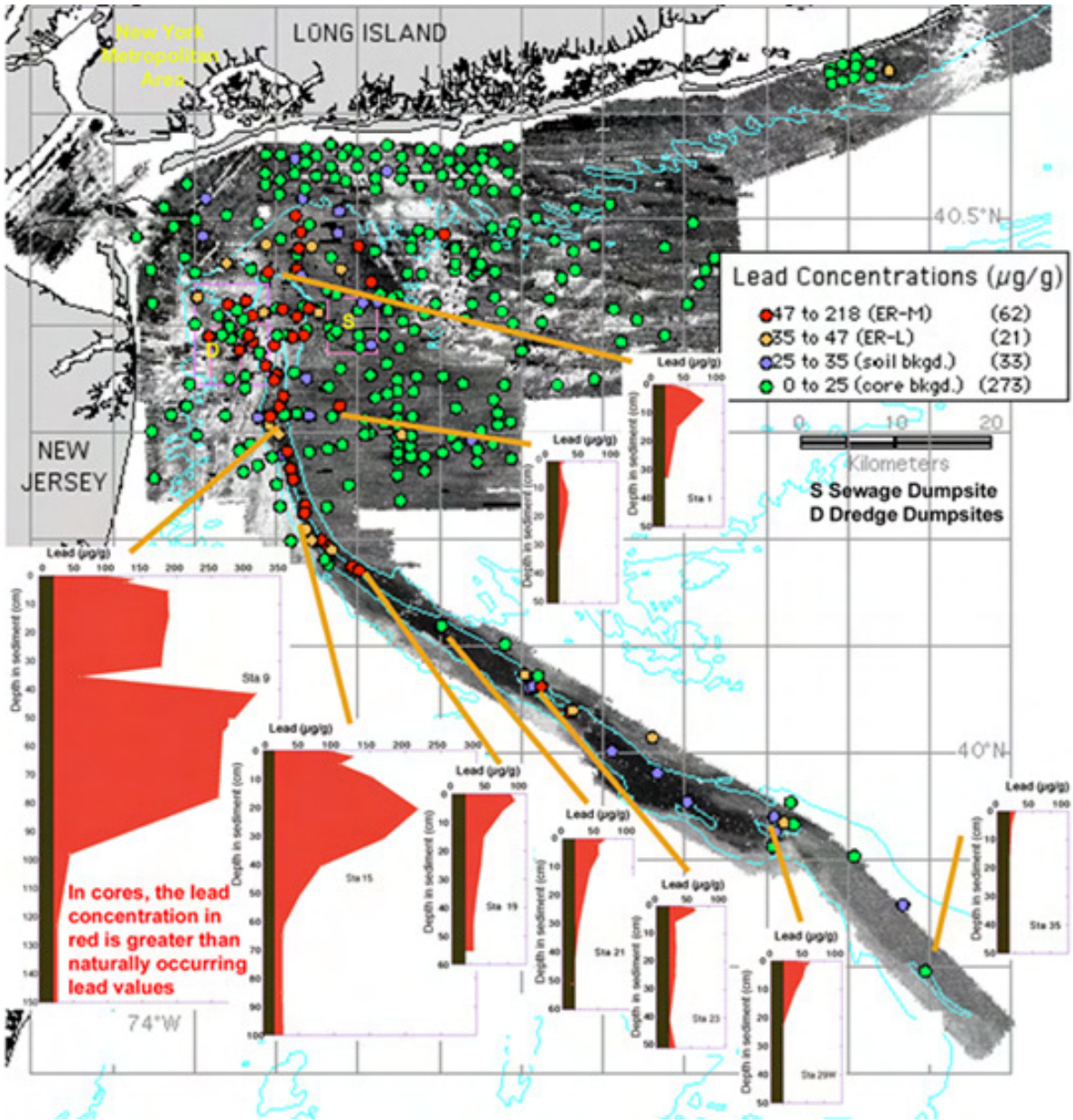

Figure 2: Location of USGS instrument sites (triangles). Eight USGS instrument packages were deployed in winter 1999-2000; tripods were located at sites A–F and moored instrument arrays were located at sites B and C. Blue arrows indicate near-bed current velocities during a representative up-valley flow event. Red arrows represent wind stresses inferred from wind measurements at National Oceanographic and Atmospheric Administration buoys (circles). Depth contours are in m.

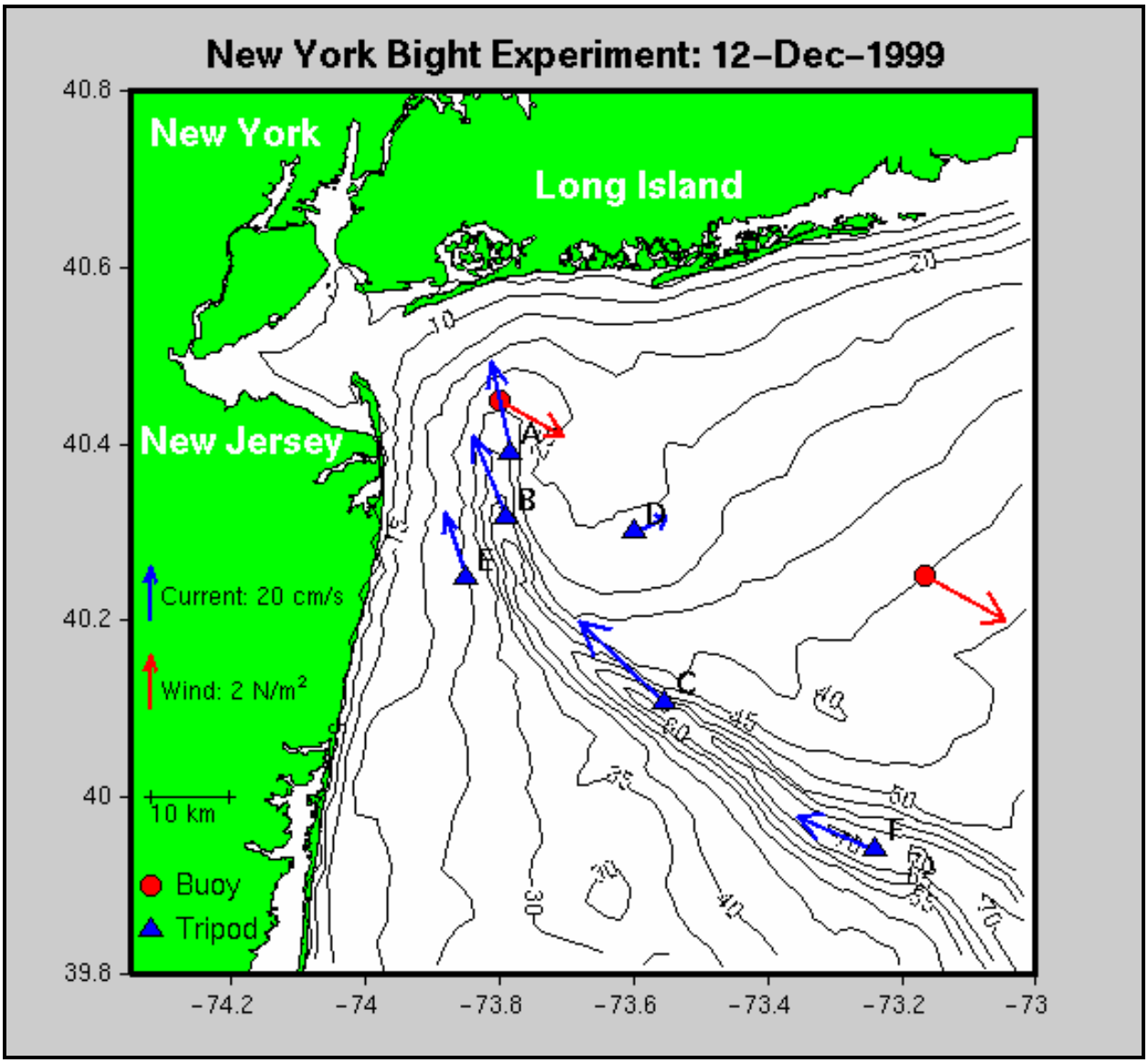

EFFECTS OF TRAFFIC AND DITCH MAINTENANCE ON FOREST ROAD SEDIMENT PRODUCTION

Charles H. Luce, Research Hydrologist, and Thomas A. Black, Hydrologist, USDA Forest Service, Rocky Mountain Research Station, Boise, Idaho
316 E. Myrtle St., Boise, ID, 83702, cluce@fs.fed.us, 208-373-4382.

Abstract: Observations of sediment yield from road segments in the Oregon Coast Range show that either heavy traffic during rainfall or blading the road ditch will increase erosion from forest roads. For the fine soils and high quality aggregate surfacing on the study plots, ditch blading increased sediment yield more than traffic equivalent to 12 log trucks per day. The combination of ditch blading and heavy traffic did not produce significantly more sediment than simply blading the ditch, a finding with important implications for sediment modeling and erosion control design. Increases in sediment production caused by traffic persisted after traffic ceased.

INTRODUCTION

Road maintenance and traffic are two of the primary activities affecting sediment production from forest roads. Given the large base of existing roads in forestlands, it is important that we understand how these activities affect sediment yield from road systems. While it is generally agreed that either traffic or ditch maintenance increase sediment production, observations showing the combined effects relative to individual effects are lacking.

Maintenance keeps roads in a condition suitable for travel and prevents severe erosion from failure of the drainage system. Unfortunately, road grading can break up armor layers on the road surface or the ditch and temporarily increase road surface erosion (Burroughs and King, 1989; Black and Luce, 1999; Luce and Black, 1999). Burroughs and King (1989) noted increased erodibility of the traveledway following road grading operations. However, Luce and Black (1999) noted that blading of only the traveledway on an aggregate surfaced road with well vegetated ditches yielded no increase in sediment production from a complete road segment, while blading of the ditch, cutslope, and traveledway substantially increased sediment yield from road segments. The recovery from ditch blading occurs rapidly during the first three years (Luce and Black, 2001) in an exponential pattern similar to that found by Megahan (1974) for new roads. Observations of vegetation and ditch particle size suggest that much of the reduction over time is due to armoring rather than revegetation (Black and Luce, 1999).

The role of traffic in increasing road sediment production is likewise well recognized and has had attention from several researchers (Reid and Dunne, 1984; Swift, 1984; Bilby et al., 1989; Burroughs and King, 1989; Coker et al., 1993; Foltz, 1999; Ziegler et al., 2001), who report a range from doubled sediment production to 30 times as much. Results are commonly reported as ratios between yields from roads with and without traffic, conceptually normalizing for precipitation and allowing generalization of the results beyond the particular events studied. Many of the studies are from rainfall simulation; some experiments were on the entire road prism, and some isolated sediment from the traveledway. Those studies where concentration samples were taken show a relatively brief effect from traffic passing during a storm, with significant recovery occurring on a time scale of tens of minutes. The postulated processes for

the increase in sediment yield are through an increased availability of fines caused by crushing the road surfacing and by pressing larger particles down through a matrix of finer sediment.

An important question left unanswered by these studies is the combined effect of ditch maintenance and traffic. One hypothesis is that the effects are cumulative. Some models use the ratios from the studies to estimate the effect, one factor is applied for the time since construction or disturbance of the ditch and another is applied for the traffic level (e.g. Cline et al., 1984; and Washington Forest Practices Board, 1995). Another way to model the effect is through addition, where the traveledway and ditch contributions are calculated separately based on their individual treatments and then added. A third alternative would suggest that there might be tradeoffs, that the total effect may be less than the sum of the parts. Increasing the availability of sediment in the ditch and on the traveledway may be somewhat redundant. If the sediment transport capacity of the ditch is fully sated by material easily detached in the ditch, the additional available fine material on the traveledway may have little effect on the segment sediment yield.

Consideration of the flowpath is important in estimating the effects of treatments to roads. Burroughs and King (1989) showed an effect on traveledway sediment yield from blading, but Luce and Black (1999) found nearly no effect on sediment yield from an entire road segment given the same treatment. One explanation may be that sediment from the road surface was trapped in the well vegetated ditch, implying that grading the ditch would not only allow ditch erosion, but also allow passage of the traveledway sediment. This logic would support the idea that there is a positive non-linear interaction (e.g. multiplicative) between road surface treatments and ditch treatments on sediment yield. Alternatively, Burroughs and King (1989) noted that substantial reductions in traveledway sediment production by placing rock aggregate (~80%) did not reduce total plot sediment production as much (~30%) because of increased sediment detachment in the unprotected ditch. This observation suggests that high sediment yields can come from either unprotected ditches or unprotected (or heavily traveled) traveledways, supporting the tradeoff hypothesis. Another observation is that traffic forms ruts, causing sediment produced on the road surface to travel on the road surface independently of ditch sediments, supporting a simple additive model. Some would be quick to point out, however, that this also robs the ditch of much of its water as well, and if the road surface is constructed with material that is less erodible than the ditch, traffic could conceivably reduce sediment yields on roads with freshly cleaned ditches.

Because the earlier studies on the individual effects of traffic and maintenance are used as the basis of sediment yield models, forest practice regulations, and best management practice design, it is important that some of the uncertainty associated with the question of combined effects be reduced. Unfortunately, the question cannot be answered with physically based models, because any of the three hypotheses can be generated using different choices of parameter values and flowpath. Observations showing the individual and combined effects of traffic and maintenance are needed to understand the interaction.

METHODS

The effects of traffic and ditch maintenance were examined on twelve road segments in the Oregon Coast range about 20 km northwest of Eugene, Oregon. The twelve plots were broken

into four categories, those with no traffic and no ditch grading (NTNG), those with traffic and no ditch grading (TNG), those with no traffic but with a graded ditch (NTG) and those with both traffic and a graded ditch (TG). Traffic was applied to one contiguous set of six road segments for practical reasons, and the grading treatment was assigned randomly.

The road segments all had similar characteristics otherwise. All had lengths of 80 m and were isolated by ditch dams and rubber-flap/wood-box water bars and runoff was diverted into sediment traps. Road gradient was between 9 and 10 percent, and cutslope heights were approximately 2 m on all road segments. The roads were constructed on a silty clay loam soil over weathered sandstone. The roads were surfaced with high quality basalt aggregate and had inboard ditches. The traveledway was freshly bladed on all plots. All ditches and cutslopes were seeded with grass during the previous spring, and the ditches were bladed on October 14, 1999 for the segments with that treatment. The reader is referred to Luce and Black (1999) for more details on plot construction and soil attributes.

Traffic was provided by a short log truck and, later, a dump truck. Both vehicles had similar wheel arrangements, with two axles in the rear with dual tires and a front steering axle. The rear sets of duals carried 15,840 kg (33,850 lbs.) and the front axle carried 5,610 kg (12,340 lbs.). These weights are similar to those on full sized log trucks. The trucks made 10 round trips per weekday over the 6 traffic plots during the period November 15 to December 14. During this period traffic occurred on both rainy and dry days and on saturated and dry road surfaces. The traffic was roughly equivalent to 12 loaded full-length log trucks per day. On each day of traffic, 5 round trips (10 passes) were made over a 1 hr period with a 30-minute break followed by another 5 round trips.

Sediment was collected from the tanks on January 11th and again on June 13th. Tanks with the greatest amounts of sediment were weighed with sediment and water, emptied and weighed again filled only with water to obtain the submerged weight of sediment (see Luce and Black, 1999 for details). For tanks with little sediment, we decanted the clean water off of the tanks using a siphon (avoiding disturbance of the sediment). The sediment was transferred to small steel buckets for weighing on a more precise scale, allowing a more precise determination for the small sediment amounts. Precipitation between Nov 15 and Dec 14 was 351 mm. 151 mm fell between Dec 14 and Jan 11. 589 mm fell between Jan 11 and Jun 13. Average precipitation depths for these periods in Eugene, Oregon are 218, 170, and 551 mm respectively.

During one day of traffic, water samples were collected from the wheel ruts immediately following a vehicle pass to capture the peak sediment concentration. An additional sample was taken 20 minutes into the break between sets of passes, and three samples were taken at 20 minute intervals following cessation of traffic to see how concentration in the wheel rut at the base of the plot changed with time. In addition, concentration samples were taken from the plot outflow (ditch plus tread) at the same time.

We used t-tests on the log transformed sediment yields to test the statistical significance of specific contrasts. The transformation was used because earlier research has suggested that erosion is log-normally distributed (Megahan et al., 2001).

RESULTS AND DISCUSSION

Mean sediment yield during the first sample period, Nov. 15 to Jan. 11, was least for the plots with no traffic and no ditch grading, followed by the plots with traffic but no grading, and the plots with grading but no traffic, and the mean sediment yield was the greatest for segments with both traffic and a graded ditch (Figure 1). All contrasts were statistically significant except for the difference between the traffic and no traffic plots given a graded ditch (Table 1). These results suggest that blading the ditch has a greater effect than traffic on the sediment yield. This particular result may differ given a different soil texture in the ditch or poorer aggregate quality. More significant is the result that the traffic effect depends on whether the ditch is graded. Given that the statistical tests were for log transformed data and the low power inherent in a design with three samples per treatment, we can reject the multiplicative cumulative effect hypothesis, but we cannot statistically discern between the simple additive cumulative effect and the tradeoff hypothesis. Looking at the pattern of the scatter from the No-Traffic-Graded (NTG) plots, we can see that the mean and scatter are strongly influenced by one plot with low sediment yield (Figure 1). The other two NTG plots actually produced more sediment than any of the plots with both traffic and grading. It is worth noting that the sediment production of the one plot is uncharacteristically low for a graded plot given earlier observations (Black and Luce, 1999; Luce and Black, 1999, 2001) and concurrent observations from similarly treated plots. For example three shorter plots (42 m, 42 m, and 60 m) with slightly steeper, 10%, slopes, graded ditches, and no traffic measured during the same period produced 2467, 4533, and 2970 kg/km respectively. Armed with this additional information, removing some weight from the low observation, there is greater support for the tradeoff hypothesis than for the simple additive effect hypothesis.

These results underscore the importance of collecting observations of sediment yield from the entire portion of road prism that is contributing water and sediment when evaluating the effects of treatments, an idea also suggested by Burroughs and King (1989). Observations of individual

Figure 1: Sediment yield from road segments during the traffic period, November 15, 1999 to January 11, 2000. Bar graphs show mean and data points show specific observations.

Table 1: Statistical Significance of specific contrasts.

		p value	
Effect of	Given	Nov--Dec	Jan-Jun
Grading	No Traffic	0.02	0.02
Grading	Traffic	0.03	0.02
Traffic	No Grading	0.02	0.04
Traffic	Grading	0.49	0.53

parts of the road prism can be misleading if there is potential for interaction of water and sediment from different parts of the road prism. It is also important to recognize the condition of the ditch and the cutslope/ditch contribution to the road segment sediment yield when interpreting results from studies. For example, it is useful to know that the results of Reid and Dunne (1984) showing substantial effect from traffic had little contribution from ditch and cutslope erosion.

Implications for modeling are fairly clear; independent factors applied for ditch maintenance and traffic are not appropriate. Nor would it appear that separate calculation of traveledway and ditch/cutslope contributions is the best option. The stronger support for the tradeoff hypothesis implies that sediment yield increases modeled to result from traffic must consider the condition of the ditch.

There are important implications for the design of BMPs or forest practice regulations. Ditch grading can increase sediment yields on a level comparable to or greater than wet weather hauling. Ditch grading is an important and necessary step in the maintenance of roads when significant sediment inputs (e.g. from a slump or upslope gully) block the ditch, however indiscriminate ditch grading to clean ditches may not be the best use of equipment time. The practice of placing rock in ditches and design criteria for ditch rocking were proposed by Burroughs and King (1989), and our results support their suggestion. The question of whether wet weather haul increases sediment yields on recently constructed or reconstructed roads is important for BMP design. Wet weather haul restrictions provide little and uncertain benefit on roads with recently bladed ditches. Sediment delivery control through crossdrain placement is probably the preferred design, but at locations where delivery is likely (e.g. stream crossings), thorough control of sediment would require protection of both the ditch and the traveledway. Note that the roads in this study were built well enough that the subgrade showed through the aggregate surfacing in only a few places, and the deepest ruts were about 90 mm. The results of this study do not apply to roads where the integrity of the surfacing may be severely damaged by traffic.

For the post traffic period, January 11 to June 13, rankings are similar to those seen in the traffic period, although there was less erosion (Figure 2). The reduced erosion is due in part to armoring during the previous months. The contrasts are similar in statistical significance (Table 1). The difference in graded versus ungraded plots is expected because we know that the effect of grading persists for more than one year in the increased availability from ditch grading (Luce and Black, 2001). The fact that the pattern of differences is maintained suggest that traffic effects may persist beyond the time scale of a few events. Reid and Dunne (1984) noted some persistence beyond the event time scale in their "temporary non-use" segments.

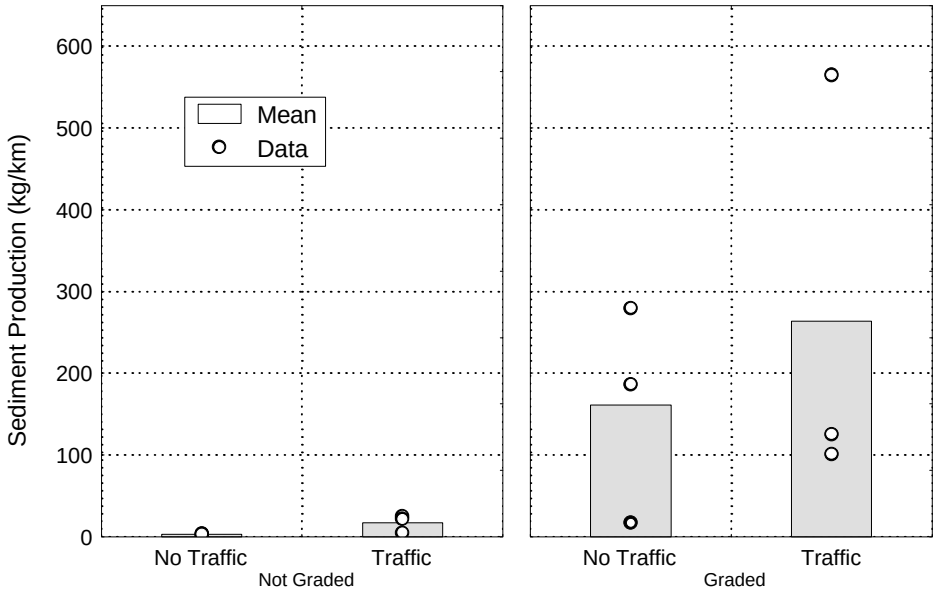

Figure 2: Sediment yield from road segments during the post-traffic period, January 11 to June 13, 2000. Bar graphs show mean and data points show individual observations.

Examination of sediment concentrations during an event showed a rise in concentration as several passes were made, and a rapid drop to lower concentrations after the traffic stopped (Figure 3). Plot runoff showed substantially lower concentrations than the peaks measured by the rut sampling because of dilution from cutslope runoff areas of the road surface where the truck had not recently passed. These patterns agree with other observations of event scale variations in sediment availability (e.g. Reid and Dunne, 1984; Ziegler et al., 2000, 2001). As the vehicle passed, fines were pressed into the tread of the tire while the lugs pressed larger pieces of gravel into the matrix of fines and gravel comprising the road bed. The treaded pattern of fine material was quickly dissipated by precipitation and flowing water. During the course of the traffic, wheel ruts developed varying in depth from 10 mm to 90 mm, and exposure of the subgrade through the aggregate was rare.

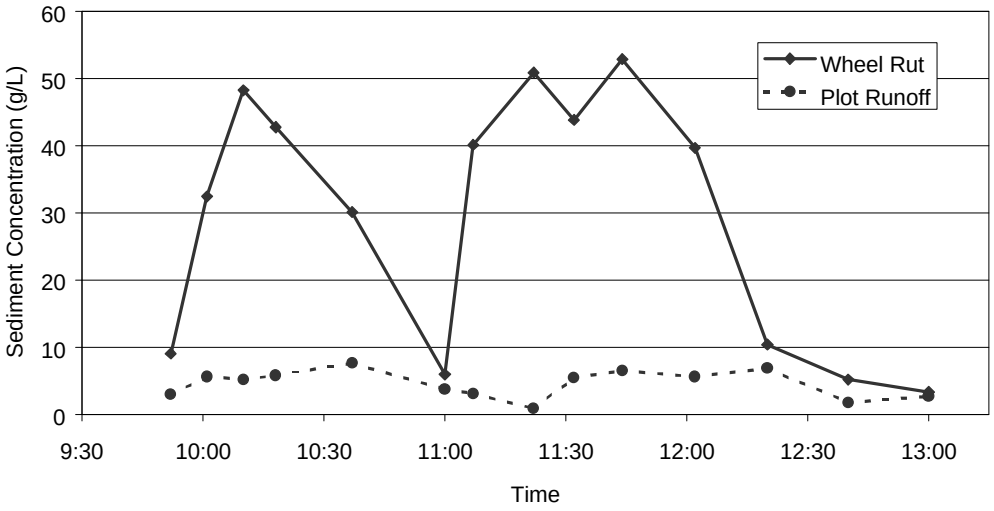

Figure 3: Concentration of sediment over time during one set of passes by a heavy vehicle.

Some persistence in availability of fines would be expected on traffic plots, as the supply of fines from the road over the traffic period would reduce the degree of armoring during that period, and the composition of the material in the ditch beds and wheel ruts should be finer at the end of the traffic period. It is not necessary that the increased availability of fine sediments persist into June for the observed differences in Figure 2. A brief period of increased erosion followed by a long period of essentially equivalent availability could account for the observations. A more likely scenario is an exponential decline in the availability of fine sediment as the finer sediments are selectively removed from the plot (e.g. Megahan, 1974).

CONCLUSIONS

Traffic and maintenance operations are activities normally experienced by forest roads at one time or another during their useful life. Both activities increase the susceptibility of a road to erosion. In order to better manage the spatial and temporal distribution of sediment inputs to streams, it is important to understand how maintenance and traffic affect sediment yield from forest roads.

Grading of the ditch increased sediment yields more than heavy traffic on a road built in a fine-grained parent material with high quality basalt aggregate. The combination of both traffic and ditch grading produced on average more sediment than either treatment alone, however the difference between grading-only and grading-with-traffic was not statistically significant with 3 samples in each treatment. A closer examination of the individual data points and results from similar plots in this year and earlier years provides support to the hypothesis that there is little difference in sediment yields between traffic and no-traffic plots given a graded ditch.

These results suggests that the multiplicative interaction model commonly used to estimate effects of multiple treatments on roads overestimates the effect of traffic on new roads or recently graded roads. A model of traffic effects that is conditional on ditch condition (e.g. time since construction or ditch grading) seems more appropriate. Although the ditch grading effect is much larger, its effect is seldom accounted for in road sediment yield modeling whereas traffic effects generally are, if only as a traffic regime. For roads with regularly scheduled maintenance, it may be desirable to model the effect of a maintenance regime.

Proscription of wet weather haul is an increasingly common best management practice that is effective in reducing sediment production from existing roads. Proscription of wet weather haul on roads with high quality aggregate and recently disturbed ditches may have little benefit. Reducing the amount of road with unnecessary ditch grading is unequivocally effective in reducing sediment production.

Observations in this study and in previous work show that sediment concentrations in runoff and, consequently, sediment yields varied on a time scale of 10s of minutes following traffic. Longer term observations in this study revealed that traffic effects may persist for longer periods, as armoring of the flow paths is prevented by the abundant fine sediment supply. This indicates that a traffic regime model may be appropriate as opposed to needing knowledge of each vehicle pass. It further indicates that any mitigations designed to trap traffic-enhanced sediment yields must be maintained after the traffic ends.

REFERENCES

Bilby, R. E., Sullivan, K., Duncan, S. H., 1989, The Generation and Fate of Road-Surface Sediment in Forested Watersheds in Southwestern Washington. Forest Science 35, 453-468.

Black, T. A., Luce, C. H., 1999, Changes in erosion from gravel surfaced forest roads though time. *in* Proceedings of the International Mountain Logging and 10th Pacific Northwest Skyline Symposium, Corvallis, Oregon,Sessions, J. and Chung, W., editors. International Union of Forestry Research Organizations and Oregon State University, Corvallis, Oregon. 204-218.

Burroughs, E. R., Jr., King, J. G., 1989, Reduction of soil erosion on forest roads, General Technical Report INT-264. U.S. Department of Agriculture, Forest Service, Intermountain Research Station, Ogden, Utah, 21 pp.

Cline, R. G., Cole, G., Megahan, W. F., Patten, R., Potyondy, J., 1984, Guide for Predicting Sediment Yield from Forested Watersheds. USDA Forest Service Northern Region and Intermountain Region, Missoula, Montana and Ogden, Utah. 42 pp.

Coker, R. J., Fahey, B. D., Payne, J. J., 1993, Fine Sediment Production from Truck Traffic, Queen Charlotte Forest, Marlborough Sounds, New Zealand. Journal of Hydrology (NZ) 31, 56-64.

Foltz, R. B., 1999, Traffic and no-traffic on an aggregate surfaced road: sediment production - differences. *in* Proceedings of the Seminar on environmentally sound forest roads and wood transport, Sinaia, Romania, Food and Agricultural Organization, Rome, Italy. 195-204.

Luce, C. H., Black, T. A., 1999, Sediment Production from Forest Roads in Western Oregon. Water Resources Research 35, 2561-2570.

Luce, C. H., Black, T. A., 2001, Spatial and Temporal Patterns in Erosion from Forest Roads, in Wigmosta, M. W. and Burges, S. J., editors, Influence of Urban and Forest Land Uses on the Hydrologic-Geomorphic Responses of Watersheds. American Geophysical Union, Washington, DC. in press.

Megahan, W. F., 1974, Erosion over Time on Severely Disturbed Granitic Soils: A Model, USDA Forest Service Research Paper INT-156. USDA Forest Service Intermountain Research Station, Ogden, Utah, 14 pp.

Megahan, W. F., Wilson, M., Monsen, S. B., 2001, Sediment Production from Granitic Cut Slopes on Forest Roads in Idaho, USA. Earth Surface Processes and Landforms 26, in press.

Reid, L. M., Dunne, T., 1984, Sediment Production from Forest Road Surfaces. Water Resources Research 20, 1753-1761.

Swift, L. W., Jr., 1984, Gravel and Grass Surfacing Reduces Soil Loss from Mountain Roads. Forest Science 30, 657-670.

Washington Forest Practices Board, 1995, Standard methodology for conducting watershed analysis, Version 3.0, November 1995. Washington State Department of Natural Resources, Olympia, Washington.

Ziegler, A. D., Sutherland, R. A., Giambelluca, T. W., 2000, Partitioning Total Erosion on Unpaved Roads into Splash and Hydraulic Components: The Roles of Interstorm Surface Preparation and Dynamic Erodibility. Water Resources Research 36, 2787-2792.

Ziegler, A. D., Sutherland, R. A., Giambelluca, T. W., 2001, Interstorm Surface Preparation and Sediment Detatchment by Vehicle Traffic on Unpaved Mountain Roads. Earth Surface Processes and Landforms 26, in press.

MODELING THE EFFECTIVENESS OF SILT FENCE

By Sherry L. Britton, Graduate Research Assistant, Biosystems Engineering Department, Oklahoma State University, Stillwater, Oklahoma; Dr. Kerry M. Robinson, Research Hydraulic Engineer, USDA-ARS Hydraulic Engineering Research Unit, Stillwater, Oklahoma; Dr. Billy J. Barfield, Professor and Department Head, Biosystems Engineering Department, Oklahoma State University, Stillwater, Oklahoma

Authors contact points: Sherry L. Britton and Dr. Billy J. Barfield, Biosystems Engineering Department, Oklahoma State University, 111 Ag Hall, Stillwater, Oklahoma, 74078. Phone number (405) 744-5431, Fax number (405) 744-6059, e-mail addresses: brittos@okstate.edu and bill@okstate.edu. Dr. Kerry M. Robinson, USDA-Agricultural Research Service, Plant Science and Water Conservation Research Laboratory, 1301 N. Western Street, Stillwater, Oklahoma, 74075. Phone number (405) 624-4135, Fax number (405) 624-4136, e-mail address: krobinson@pswcrl.ars.usda.gov.

Abstract: Research on three woven silt fence products (fabrics A, B, and C) was conducted to evaluate their effectiveness at separating sediment from runoff water. The three fabrics were tested over a range of flow rates and sediment feed rates. Sediment of known size and gradation was developed from glass beads ranging in size from 1.5 to 177 μm. Using a digital encoder, the changes in head against the fabric were measured. From the head information, the flow rate exiting the fabric was determined by calculating the volumetric changes in the model during the recession period of each test. Head versus discharge plots were developed to compare the clear water and sediment-laden flows of each fabric. Each fabric demonstrated unique clear water flow behavior. Fabric A was slightly affected by sediment-laden flow, while sediment had a dramatic influence on fabric B. The performance of fabric C fell between the other fabrics. The number and size of the fabric openings were observed to influence how much sediment passed the fabric. Preliminary modeling efforts suggest that a simple modification of the orifice equation fit the data well. The performance of the fabrics was also evaluated based on their trapping efficiencies and average sediment concentrations exiting the flume. This study provides valuable information about silt fence performance and a preliminary model of flow through the fabric.

INTRODUCTION

In recent reports, the Environmental Protection Agency (EPA) named agricultural and urban runoff as the leading pollutants in U. S. waters (EPA, 1998). Runoff transports natural and man-made pollutants such as sediment, oil, and fertilizers and deposits them into rivers, lakes, storm drainage systems, and other waterways (EPA, 1997). One of the major pollutants in waterways today is sediment with over 4 billion tons of it lost each year as a result of erosion (Brady and Weil, 1999). Deposition of sediment in waterways causes long-term ecological and economic problems in both rural and urban communities. For example, sediment in rivers and lakes inhibits light for photosynthesizing plants and depletes oxygen for aquatic life (Waters, 1995; Herzog et al., 2000). From an economic standpoint, soil deposition adds to the financial burden by causing an aesthetic distraction in the recreational use of waterways and increases a potential

for flooding and water treatment operations (Carpenter, 1999; Herzog et al., 2000). Obviously, improved sediment controls are needed.

A common practice for controlling sediment release is the use of silt fences. The objective of this research is to model the effectiveness of silt fences at separating sediment from runoff water. Specifically, this study examines the hydraulic performance of silt fences exposed to a range of sediment-laden flows. The performance of three woven fabrics was examined by mixing varying sizes of glass beads directly into the flow to represent sediment-laden conditions. The captured sediment altered the performance of the silt fence by blocking some of the filter openings in the fabric. The impounded water level behind the fence was monitored for a range of sediment feed rates and flow rates. This study provides additional information about silt fence performance.

BACKGROUND

Silt fence is a geotextile fabric fastened to wooden or steel posts, with a wire mesh fence occasionally attached for structural support (Sherwood and Wyant, 1976). Silt fence is typically used to trap sediment and to slow the erosion process on drastically disturbed lands (Britton et al., 2000). If functioning properly, silt fence acts as a screen for separating soil particles from runoff (Theisen, 1992). Soil begins to deposit in front of the fabric as well as within the fabric, making it difficult for water movement through the fabric. Because of the impedance caused by the soil blocking fabric openings, the water level behind the fence rises and allows more suspended solids to settle from the runoff water. Theisen (1992) concluded from this observation that the apparent opening size of the fabric affects the storage capacity of the fence as well as the soil deposition upstream of the fabric.

Studies in the area of silt fence have been quite limited; however, Wyant (1980), Kouwen (1990), Barrett et al. (1995), and Wishowski et al. (1998) are among the few who have performed comprehensive studies on silt fence. Wyant (1980), whose work led to the development of ASTM D 5141, examined the performance of silt fence exposed to 50-L batch mixes of sediment-laden water. Both woven and nonwoven fabrics were tested with three soil types: clayey, silty, and sandy. His studies showed average trapping efficiencies of 95% of the clayey, 92% of the silty, and 97% of the sandy soils, respectively. The majority of Wyant' s (1980) tests, however, consisted of nonwoven fabric types and low flow conditions, which would explain the high trapping efficiencies reported. Studies by Kouwen (1990), Barrett et al. (1995), and Wishowski et al. (1998) are derivatives of Wyant' s (1980) study, with variations in fabric types, soil distributions, slope approaches, and flow introductions (batch mixes versus continuous flow conditions). These studies reported trapping efficiencies ranging from 68 to 99%. Kouwen (1990), Barrett et al. (1995), and Wishowski et al. (1998) concluded that the large trapping efficiencies were a direct result of the fabric types used in the experiments because sediment clogged the fabric openings, causing the impounded water to rise behind the fabric.

The limited number of silt fence studies conducted thus far have evaluated the trapping efficiencies of fabrics. These studies contribute high trapping efficiencies to the fabric types used in the experiments. Most research suggests that sediment plugs fabric openings, causing increased impounded water levels. While these studies present valuable information, additional research should be conducted to examine the blockage of fabric openings caused by sediment.

EXPERIMENTAL SETUP

A series of tests were performed on three woven silt fence products (fabrics A, B, and C) to examine the impact clogging has on the hydraulic performance of the fabric (Table 1). Tests were conducted indoors, in an 18.7-ft long by 3.0-ft wide flume located in a model building at the USDA-ARS Hydraulics Laboratory in Stillwater, Oklahoma (Fig. 1). The flume floor was constructed with a 1-ft horizontal section upstream of the fabric, with the remainder of the floor sloping upstream at an 8% incline. An 8.0-ft long section of the flume wall was constructed of a clear acrylic material for observation of sediment deposition near the fabric barrier. The fabrics were 3 ft tall and cut in approximately 4-ft wide sections for attachment to the flume. The fabric was securely fastened to the end of the flume such that the maximum height of the fabric exposed to the flow conditions was 2.5 ft.

Tests flows were delivered to the flume in a continuous flow from a recirculation system. Flow entered a constant head tank and was then delivered through a 12-inch pipeline where the flow rate was measured with an orifice meter and differential manometer. The fabrics were tested at flow rates of 0.02 cfs (10 gpm), 0.06 cfs (25 gpm), and 0.11 cfs (50 gpm), and they were each exposed to two clear-water and one sediment-laden flow conditions. The clear-water tests typically lasted 20 minutes, and the sediment-laden test typically lasted 60 minutes. To obtain sediment-laden conditions, a sediment shaker released a glass bead mixture directly into the flow at feed rates ranging from 0.78 lbs/min to 3.44 lbs/min. A load cell and computer monitored the sediment feed rate from the shaker. The mixture of glass beads introduced into the flow for each test was always mixed in the same fashion, with four sizes of beads used. The bead mixture usually ranged in size from 1.5 μm to 177 μm in diameter. Using the USDA soil classification system, the bead mixture typically fell in a silt loam or loam category.

To determine the fabric flow rate, the impounded water level behind the fabric was measured in two fashions: manually with a carriage mounted point gage, and electronically using a digital encoder. To use the digital encoder, a 1.5-inch diameter port was placed in the floor 6.0 inches upstream of the fabric, and a 2-inch diameter side wall port was placed 20 inches upstream of the fabric just above floor elevation. Both of these ports directed flow to a wet well where the water level was recorded with the encoder. The flow rate exiting the flume was also monitored with a strip chart recorder on a 0.75-ft H-flume downstream of the fabric. Point gage readings were manually taken at the H-flume in 5-minute intervals throughout the tests.

In addition to the flow rate, the performance of the fabrics were evaluated based on their trapping efficiencies and average exit sediment concentrations. The trapping efficiency of the fabric was estimated by taking the ratio of material fed during the test and the quantity of collected and dried material trapped by the fabric. At 10-minute intervals during the tests, 1-L samples of the flow were collected downstream of the fabric for exit sediment concentration analysis.

RESULTS AND DISCUSSION

A total of 21 were conducted on fabrics A, B, and C. The fabrics were examined based on the flow rate exiting the fabric, trapping efficiencies, and average exit concentrations. The flow rate

exiting the fabric was analyzed by calculating the volumetric changes in head for the flow recession period of each test. The recession period of the test starts when the inflow to the flume is terminated and continues until the flume has completely drained (Fig. 2). To accurately calculate the flow rate exiting the fabric, the flume volume was determined by measuring the width of the flume from top to bottom with a micrometer in vertical increments of 0.5 ft and horizontal increments of 2 ft. Strip chart recordings were also used to verify the flow calculations.

Each fabric proved to have unique flow patterns associated with it. For example, figure 3 illustrates the actual flow rates that each fabric can pass for a range of impounded heads. Each fabric in this comparison was exposed to the same inflow rate and approximately the same sediment loading rate. Figure 3 shows the differences in the clear-water flows for each fabric, indicating the fabric affects the behavior of the flow. Fabric A shows similarities between its sediment-laden and clear-water flows, suggesting that sediment has little effect on the fabric. Fabric B, however, exhibited dramatic differences between clear and sediment-laden flows. This result was expected since sediment was observed to clog the openings of the fabric, causing the impounded water level to rise. The performance of fabric C fell between the other two fabrics, which indicates sediment moderately influenced the flow behavior through the fabric.

Each fabric is unique, with variations in opening size and weave pattern. Therefore, to develop a fabric flow equation, certain physical features of the fabric had to be considered. Each fabric is comprosed of a matrix of openings. Consequently, the flow through the fabric becomes dependent upon the number and size of the fabric openings. The number of filaments in the horizontal and vertical directions was assumed to be an indicator of the number of openings exposed to a hydraulic head. Therefore, the number of openings was found using the following equation:

$$m = (hW)(vH)$$

where h equals the number of horizontal filaments per 0.328 ft (100 mm), W is the width of the fabric in feet, v is the number of vertical filaments per 0.328 ft (100 mm), and H is the impounded head on the fabric in feet. For the purposes of this modeling effort, the geometry of the opening was assumed to be a rectangular orifice opening. Therefore, the clear flow through the fabric was easily written as a modified form of the orifice equation:

$$Q = C'mA(2gH)^{0.5}$$

where Q is the flow in cfs, C' is an orifice coefficient (in this case assumed to be a sharp-edged orifice with coefficient of 0.61), A is the orifice area (ft^2), g is the gravitational constant, and H is the hydraulic head on the fabric in feet. By having a known flow and corresponding head for each fabric tested, the area of the orifice was back calculated and plotted against the square apparent opening size (AOS) of the fabrics (Fig.4). For example, a fabric denoted as an AOS No. 10 in the fabric specifications has a corresponding AOS of 2 mm (6.56×10^{-3} ft), and by assuming the apparent opening size is perfectly square, the apparent opening area (AOA) becomes 4 mm^2 (4.31×10^{-5} ft^2). Figure 4 depicts a linear relationship of AOA and the orifice area. Figure 5 compares the results of the clear-flow equation with the actual clear-flow data

collected. This plot demonstrates that the fit equation does a reasonable job of fitting the test data.

Sediment clearly has an effect on the flow behavior through the fabric. To account for the influence of soil, the clear-flow equation was modified to include a plugging coefficient, C_p:

$$Q = C_p C' mA(2gH)^{0.5}$$

Again through back calculation, C_p for each test was determined and plotted against AOS of the fabrics. Figure 6 illustrates a linear relationship between the parameters. The sediment-laden equation results were then compared with the experimental data (Fig. 7). The sediment-laden performance of fabrics A and C was predicted well. The fit for fabric B was not as good. Figure 6 illustrates the variation in the back-calculated C_p for fabric B, suggesting other factors influenced the flow through that particular fabric. The reader should recognize that this simple fit relationship does not account for variations in sediment feed rate and flow rate. From figure 6, it is apparent that the smaller-sized openings in fabric B were likely influenced by feed rate and flow rate. While further study may allow refinement of this relationship, it is important to note that the results from fabrics A and C were not greatly influenced by sediment feed rate and flow rate. Fabrics A and C are more typical of those routinely installed in the field. Since this study is limited to three fabrics, more testing is recommended to verify the results and better examine the factors influencing the sediment-laden flow through the fabrics.

Besides evaluating the fabric flow rates, the trapping efficiencies and exit sediment concentrations were also determined. The average trapping efficiency for fabric A, B, and C were 55, 66, and 65%, respectively. Even though the flow passing through each fabric is dramatically different, the fabrics still trapped approximately the same amount of sediment. The average exit concentrations for the fabrics ranged from 563 to 12,800 mg/L. For the same inflow rate and sediment loading rates, fabric B typically passed the lowest suspended solid concentration, and fabric A passed the highest suspended solid concentration. The concentrations exiting fabric C were close to those passing fabric B. Fabrics B and C have relatively small openings sizes, and fabric A has larger openings that allowed more sediment to pass through the fabric.

SUMMARY AND CONCLUSIONS

The performance of three woven fabrics was examined for a range of flow rates and sediment feed rates. The fabrics were exposed to both clear-water and sediment-laden flow conditions. A digital encoder was used to measure the impounded water level behind the fabric. The information collected from the encoder was used to calculate the volumetric changes in head for the recession period of each test. Each fabric exhibited distinct clear-water flows. Fabric A showed similarities between clear-water and sediment-laden flows, suggesting sediment had little effect on the performance of the fabric. The behavior of clear-water and sediment-laden flows for fabric B were dramatically different. The differences in flow behavior for fabric B are attributed to flow restriction caused by sediment blocking the openings of the fabric. Fabric C fell between fabrics A and B. Preliminary results show that a modified orifice equation predicts the clear and sediment-laden flows through the fabrics. More research is needed to evaluate how

particle size distribution, sediment loading rate, inflow rate, and other factors influence the flow through the fabric.

The trapping efficiencies and average sediment concentrations exiting the fabrics were examined for the three fabrics. The fabrics demonstrated similar trapping efficiencies, suggesting the fabric had little influence on the material trapped. Higher concentrations exiting the fabric were typically associated with fabric A, and lower concentrations exiting the fabric were associated with fabric B. This observation suggests the opening size influences the sediment concentration passing the fabric.

A simple modification to the orifice equation shows promising results for predicting clear and sediment-laden flow through a geotextile fabric. Additional research is needed to fine-tune this method for predicting flow through a fabric. Hopefully, this work will provide a better understanding of the hydraulic performance of silt fence and will help improve design standards and installation procedures for silt fence.

REFERENCES

Barrett, J. E., Kearney, J. E., McCoy, T. G., Malina, J. F., Charbeneau, R. J., and Ward, G. H., 1995, An Evaluation of the Performance of Geotextiles for Temporary Sediment Control. Center for Research in Water Resources, College of Engineering, The University of Texas at Austin, CRWR 261.

Brady, N. C. and Weil, R. R., 1999, The Nature and Properties of Soils. New Jersey: Prentice Hall, Inc.

Britton, S. L., Robinson, K. M., Barfield, B. J., and Kadavy, K. C., 2000, Silt Fence Performance Testing. ASAE Annual Meeting, Paper No. 002162. St. Joseph, Mich.: ASAE.

Carpenter, T., 1999, Silt Fences that Works for Designers, Installers, Inspectors. Carpenter Erosion Control: ISBN 0-9672733-0-7.

Environmental Protection Agency, 1998, The Quality of our Nation' s Waters, A Summary of the National Water Quality Inventory: 1998 Report to Congress. Environmental Protection Agency, EPA841-S-00-001.

Environmental Protection Agency, 1997, Nonpoint Pointer No. 7: Fact Sheet. Environmental Protection Agency, EPA841-F-96-004G.

Herzog, M., Harbor, J., McClintock, K., Law, J., and Bennett, K., 2000, Are Green Lots Worth More than Brown Lots? An Economic Incentive for Erosion Control on Residential Developments. J. of Soil and Water Conservation, 55, 43-48.

Kouwen, N., 1990, Silt Fences to Control Sediment Movement on Construction Sites. Downsview, Ontario: The Research and Development Branch Ontario Ministry of Transportation.

Sherwood, W. C. and Wyant, D. C., 1976, Installation of Straw Barriers and Silt Fences. Charlottesville, Virginia: Virginia Highway and Transportation Research Council, VHTRC 77-R18.

Theisen, M. S.,1992, The Role of Geosynthetics in Erosion and Sediment Control: An Overview. J. Geotextiles and Geomembranes, 3, 535-549.

Waters, T. F., 1995, Sediment in Streams: Sources, Biological Effects, and Control. Bethesda, Maryland: American Fisheries Society.

Wishowski, J. M., Mamo, M., and Bubenzer, G. D., 1998, Trap Efficiencies of Filter Fabric Fence. ASAE Annual Meeting, Paper No. 982158, St. Joseph, Mich: ASAE.

Wyant, D. C., 1980, Evaluation of Filter Fabrics for Use as Silt Fences. Charlottesville, Virginia: Virginia Highway and Transportation Research Council, VHTRC 80-R49.

TABLES AND FIGURES

Table 1. Fabric specifications given by the company.

Property	Test Method	Fabric A	Fabric B	Fabric C
Grab Tensile (N)	ASTM D 4632	350	665 x 555	550
Grab Elongation (%)	ASTM D 4632	15	15	15
Mullen Burst (kPa)	ASTM D 3786	1720	2410	2060
Puncture (N)	ASTM D 4833	130	290	290
Trapezoidal Tear (N)	ASTM D 4533	220	290 x 290	290
Apparent Opening Size (Sieve No.)	ASTM D 4751	10	40	30
Flow Rate (gal/min/ft^2)	ASTM D 4491	30	25	10
Permittivity (sec^{-1})	ASTM D 4491	0.3	0.4	0.05
UV Resistance (%)	ASTM D 4355	80	90	80

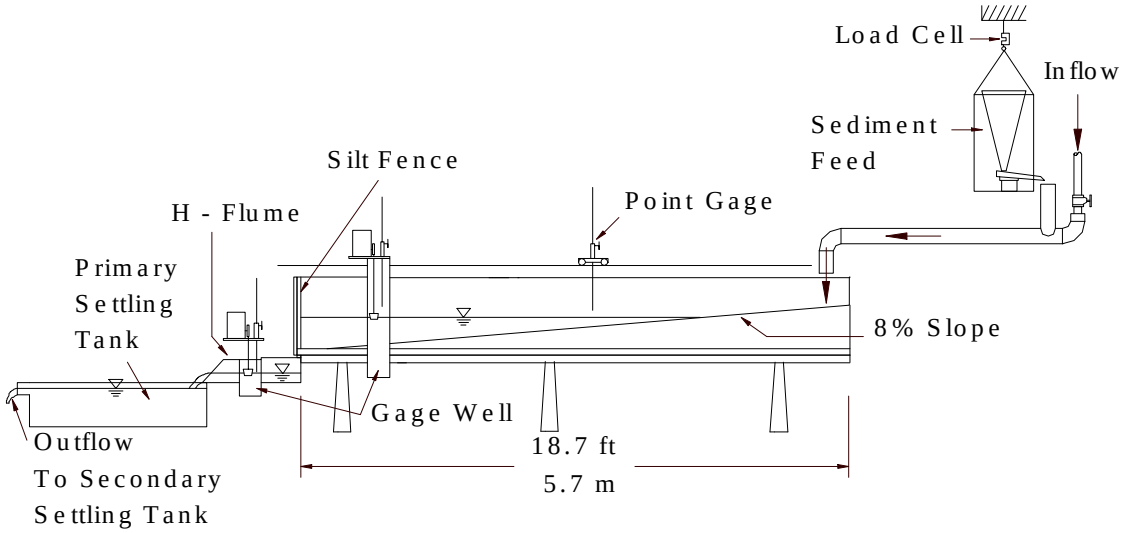

Figure 1. Test configuration (Britton et al., 2000).

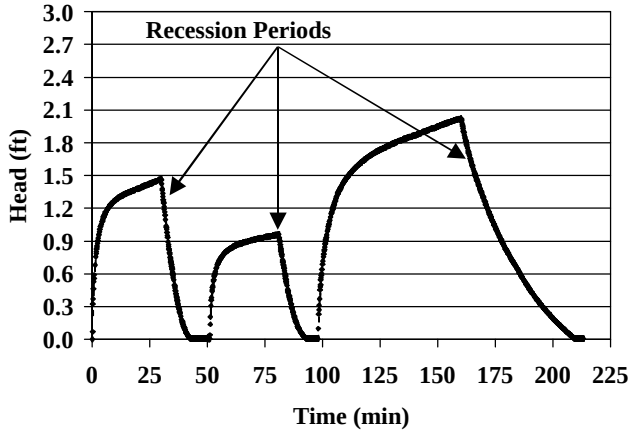

Figure 2. A typical head versus time plot of two clear-water flows and one sediment-laden flow.

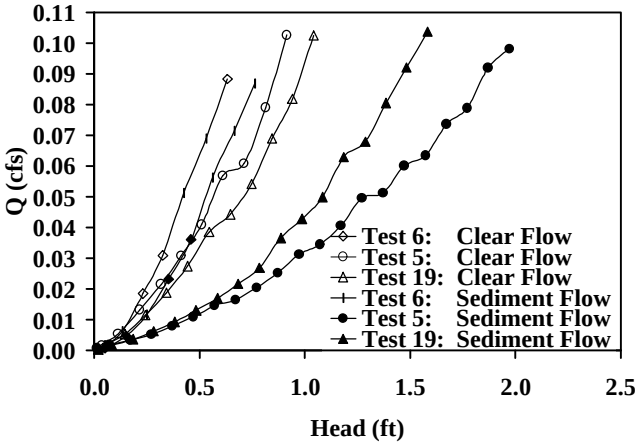

Figure 3. Head-discharge relationship. Test 6: Fabric A, Test 5: Fabric B, and Test 19: Fabric C.

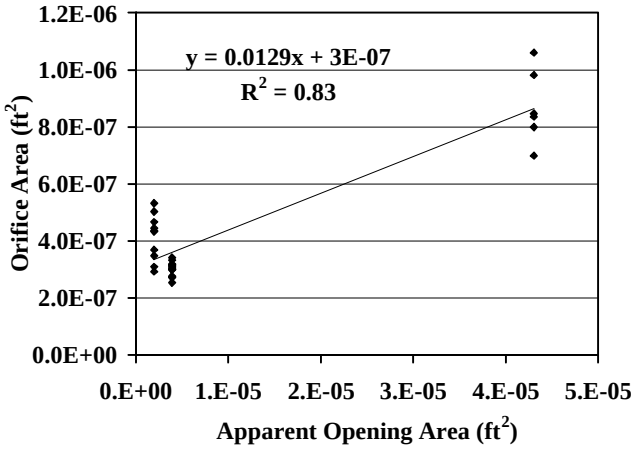

Figure 4. Orifice area versus apparent opening area.

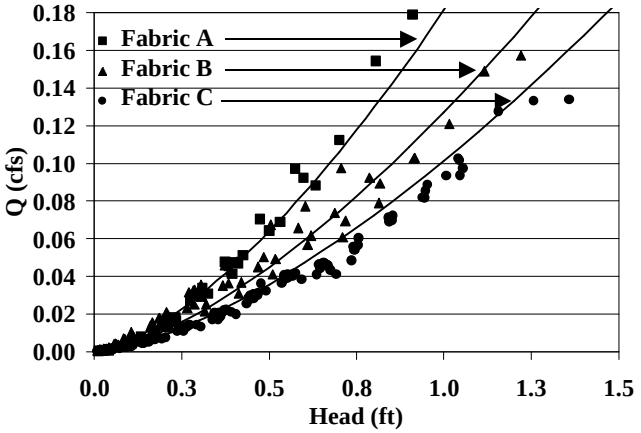

Figure 5. Clear-flow prediction versus experimental data.

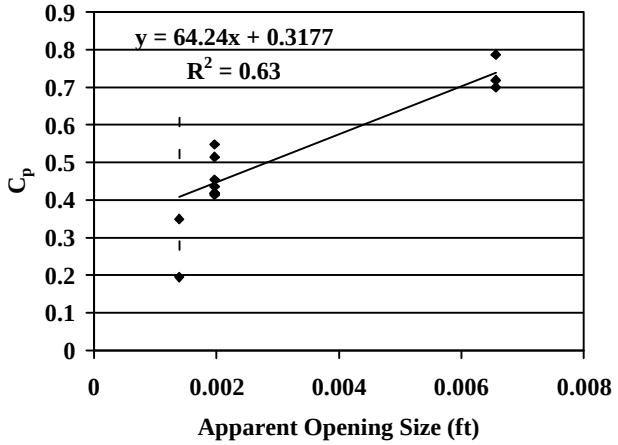

Figure 6. Coefficient of plugging versus apparent opening size.

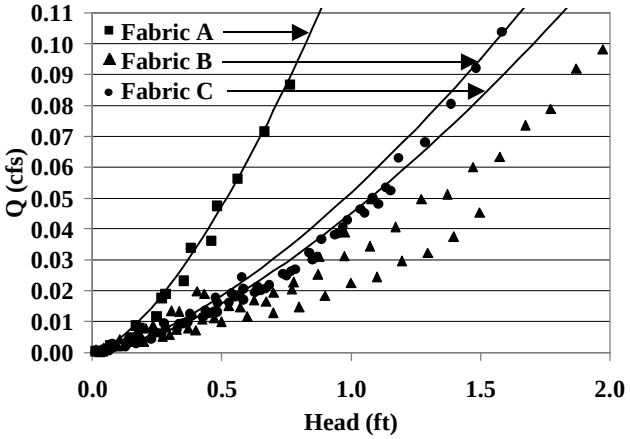

Figure 7. Sediment-flow prediction versus experimental data.

EROSION AND SEDIMENT YIELDS IN TWO SUBBASINS OF CONTRASTING LAND USE, RIO PUERCO, NEW MEXICO

Allen C. Gellis[1], Hydrologist, U.S. Geological Survey, Albuquerque, NM; Milan J. Pavich[2], Geologist, U.S. Geological Survey, Reston, VA; Amy Ellwein[3], Geologist, Austin, TX

[1]5338 Montgomery Blvd, NE, Albuquerque, NM 87109, (505) 830-7979, agellis@usgs.gov; [2]908 National Center, Reston, VA 20192, (703) 648-6963, mapvich@usgs.gov; [3]PO Box 27157, , 3312 Lafayette, Austin, TX 78722, amy.ellwein@ev1.net

INTRODUCTION

The Rio Puerco basin (16,100 km^2) (fig. 1) is the largest tributary to the Rio Grande in New Mexico, draining more than 20% of its area at San Marcial (fig. 1). The Rio Puerco contributes only 4% of the Rio Grande's average annual runoff at San Marcial, from a combination of spring snow-melt and monsoonal storms, but contributes over 70% of the Rio Grande's average annual suspended-sediment load. Data compiled for world rivers by Milliman and Meade (1983) and Zhao and others (1992) show that the Rio Puerco has the fourth highest average annual suspended-sediment concentration (fig. 2).

Three major channels have cut and filled the Rio Puerco valley in the past 3,000 years (Love and Young, 1983; Love, 1986). An interesting aspect of these cut-and-fill cycles is that the Rio Puerco channel filled to the same level in the valley that it occupied prior to each cutting event. For example, by 1880 A.D. the Rio Puerco occupied the same level in the valley that it had before its incision around 600 B.P. (Love, 1986) but incision began again in 1885 (Bryan, 1925). Recent surveys indicate that the Rio Puerco is now in a cycle of aggradation (Elliott and others, 1998; Gellis and Elliott, in press). The cycle raises questions about the sediment source(s) for this filling and the process of aggradation independent of a change in the base level of the Rio Grande.

To examine sediment sources in the Rio Puerco basin, a study quantifying a sediment budget for two subbasins, Volcano Hill Wash (9.30 km^2) and Arroyo Chavez (2.28 km^2), began in 1995 and continued through 1998. The subbasins were selected on the basis of differences in geology and land use. Volcano Hill Wash drains Cenozoic basalt flows. Soil surface textures are dominantly silty clay loam. Mesa surfaces are topped with a basalt stone pavement and underlain with silty clay loam and silt loam. Eolian silt is an important component of the mesa surface sediment. Land use in the watershed is grazing and there are no dirt roads in the basin.

The Arroyo Chavez subbasin drains interbedded shales and sandstones. Soils are derived from underlying shales and sandstones of the Cretaceous Menefee Formation and from eolian silt. Surface soil textures range from silty clay loam to sandy clay loam, both containing about 30% clay. Surface clay content, found to be important to sediment yield from local test plots (Aguilar and Aldon, 1991), appears to be similar in the upland mesa surfaces of both Arroyo Chavez and Volcano Hill Wash, although Volcano Hill Wash has a denser accumulation of stony pavement. Land use in the basin is grazing and gas pipeline activity. Portions of the alluvial valley are sparsely vegetated, and gullies and soil piping are common.

Livestock numbers in both subbasins were obtained from the Bureau of Land Management in Albuquerque, New Mexico. The 930-hectare Volcano Hill subbasin is part of a larger 29,205-hectare grazing allotment. Between 1995 and 1998 the number of livestock on the allotment ranged from 0 to 682. The average number of livestock over this time period was 293 or 1.0 animal per 100 hectares. The grazing allotment received a grazing management award in the early 1990's. The 228-hectare Arroyo Chavez subbasin is part of a larger 4,456-hectare grazing allotment. The number of livestock on the allotment from 1995 to 1998 was steady at 325 or 7.3 animals per 100 hectares.

This paper describes preliminary results of erosion and sediment yields for the Volcano Hill Wash and Arroyo Chavez subbasins used to develop a preliminary sediment budget on sediment sources and sinks.

Figure 1. Location of Volcano Hill Wash and Arroyo Chavez basin in the Rio Puerco basin.

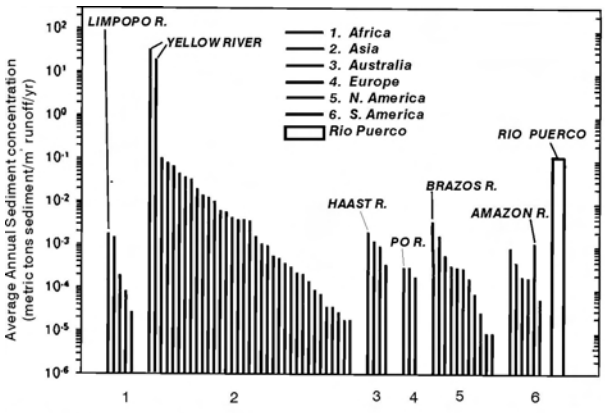

Figure 2. Average annual suspended-sediment concentrations of world rivers and the Rio Puerco, N. Mex (Milliman and Meade, 1983; Zhao and others, 1992).

METHODS

A sediment budget for a drainage basin is based on the amount of sediment leaving that basin and an accounting of the sources of that sediment (Leopold and others, 1966; Dietrich and Dunne, 1978; Swanson and others, 1982). An essential feature of a sediment budget is to define transport processes, storage elements, and linkages between the two (Swanson and others, 1982). In the Volcano Hill Wash basin, the sediment budget was generalized for five geomorphic surfaces: mesa, steep colluvial slopes, alluvium/colluvium, eolian/alluvium, and alluvium. In the Arroyo Chavez basin, seven geomorphic surfaces were identified: mesa, steep colluvial slopes, moderate sloping hillslopes, gently sloping hillslopes, alluvial fans, well-vegetated alluvium, and sparsely vegetated alluvium. The geomorphic surfaces for both basins were delineated from color aerial photographs (1:24,000 scale) and entered into a geographical information system (GIS). The GIS was used to determine the area of each geomorphic surface in each subbasin.

Both subbasins were instrumented at the basin outlets with a streamflow-gaging station and an automatic suspended-sediment sampler. Rainfall was measured at 5 and 15 minute increments at each gaging station and various areas in each basin (fig. 3). Deposition from upslope erosion was measured using sediment traps and the volume of sediment deposited behind small dams. Sediment trap design was based on a modified Gerlach Trough (Gerlach, 1967; Gellis, 1998). The traps were 68 to 85 cm long and 13 cm wide. The traps were installed flush to the ground surface with the opening parallel to the slope contour. One to three 1.27 cm diameter holes were drilled into the side of the trap and were connected by tubing to 18.9 liter collection buckets. The contributing area to each trap was bounded with metal edging.

Samples of runoff and sediment were collected in the buckets after each rainfall event. Buckets were weighed in the laboratory to determine total sediment and water (runoff). The samples were stored in the laboratory for 1 month to allow the suspended sediment to settle. Water was then decanted from the buckets and the sediment was oven dried for 24 hours at 98 ^{0}C. Samples of the water were taken to determine the amount of sediment still in suspension.

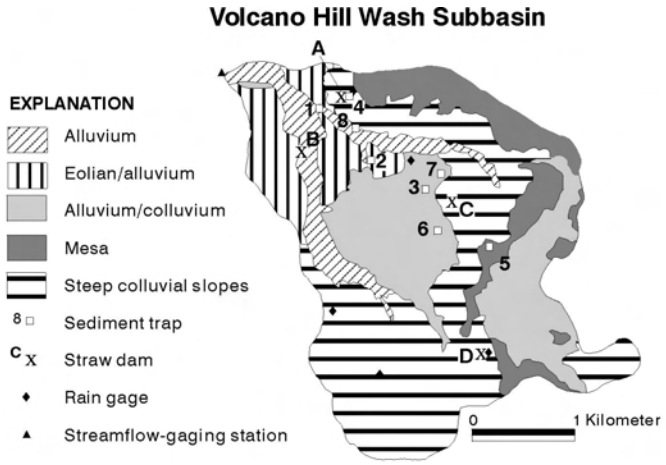

Figure 3. (A) Geomorphic surface for Volcano Hill Wash including sediment traps, straw dams, rain gages, and streamflow-gaging station.

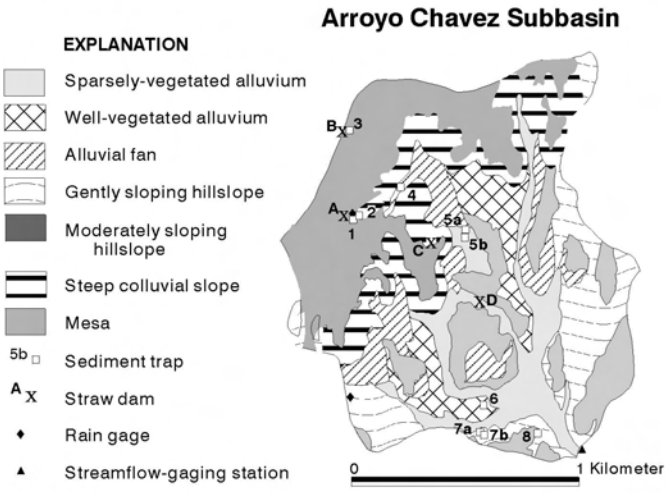

Figure 3. (B) Geomorphic surface for Arroyo Chavez including sediment traps, straw dams, rain gages, and streamflow-gaging station.

Four straw dams in each subbasin were constructed in first- and second-order channels. A notch approximately 1 m deep was dug in the channel and filled with straw bales. The bales were reinforced into the ground with steel rebar, and large rocks were piled on the downstream side, next to the straw bales to prevent the bales from toppling. The sediment pool on the upstream side of the straw bales was dug out, and four to six cross sections were monumented in the pool using steel rebar on either end. The cross sections were surveyed periodically to quantify sediment deposition.

Eight sediment traps were installed in the Volcano Hill Wash subbasin and 10 in the Arroyo Chavez subbasin (fig. 3). The contributing area to the sediment traps and the straw dams were surveyed using a total station. Drainage areas for the sediment traps ranged from 0.76 to 37 m^2; the straw dams ranged from 405 to 5,170 m^2. Contributing areas for two traps in the Arroyo Chavez subbasin, 5b and 7b (fig. 3B), were purposefully constructed at a small area, 0.76 and 1.7 m^2, respectively, to determine the effect of contributing area on sediment yield. Runoff was not recorded in these traps.

RESULTS

Streamflow and Suspended Sediment

Rainfall, runoff, and suspended sediment measured at the gaging stations are presented for water years 1996-98. A water year is October 1 of the previous year to September 30 of the current year. Volcano Hill Wash and Arroyo Chavez are ephemeral channels. Between October 1, 1995, and September 30, 1998, 31 runoff events were recorded at Volcano Hill Wash and 41 events were recorded at Arroyo Chavez.

The average annual sediment yield, water years 1996-98, for the Volcano Hill Wash subbasin was 405 tonnes/km^2/yr and for Arroyo Chavez subbasin was 981 tonnes/km^2/yr. By summing runoff and suspended-sediment load for the 3 years of collection, the total discharge-weighted sediment concentration for Volcano Hill Wash is 34,000 mg/L and for the Arroyo Chavez was 92,500 mg/L. Discharge-weighted sediment concentration is an informative way to look at sediment transport because it normalizes total sediment transport by the total amount of runoff transporting the sediment (Guy, 1964).

Dams and Sediment Traps

The sediment traps for Volcano Hill Wash operated between June 6, 1996, and August 12, 1998. The sediment traps for Arroyo Chavez operated between June 13, 1996, and October 2, 1998, except for traps 5b and 7b, which operated between March 5, 1997, and October 2, 1998. To calculate an annual sediment yield for each trap (kg/m^2/365 days), the total sediment load in grams (g), was divided by the total number of days the trap was

operating and multiplied by 365 days. The volume-weighted sediment concentration, in parts per million (ppm), for each trap was calculated by dividing the sum of the dry weight of sediment (g) for the period of collection, by the weight of sediment and water (g), and multiplied by 10^6.

The highest sediment yield and sediment concentrations recorded from the sediment traps and dams in both subbasins occur on alluvium (Table 1). Based on the sediment trap results for Volcano Hill Wash, the highest sediment yield was 0.975 kg/m^2/365 days and the highest volume-weighted sediment concentration was 25,300 ppm for the alluvium (Table 1). Based on sediment trap results for Arroyo Chavez, the highest sediment yield was 3.35 kg/m^2/365 days and the highest volume-weighted sediment concentration was 140,000 ppm for the sparsely vegetated alluvium (Table 1). In both basins the alluvial valley floor is grazed. In the Arroyo Chavez basin the portion of the alluvial valley floor that is grazed is sparsely vegetated is a gullied, soil-piped surface with many headcuts.

The lowest sediment yield recorded from the traps at Volcano Hill Wash was 0.046 kg/m^2/365 days, recorded on a steep colluvial slope (Table 1). The lowest sediment yield for Arroyo Chavez was 0.139 kg/m^2/365 days, recorded for the well-vegetated alluvium (Table 1). The lowest volume-weighted sediment concentration recorded from the traps at Volcano Hill Wash was 4,170 ppm recorded on the eolian/alluvium surface (Table 1). The lowest volume-weighted sediment concentration recorded from the traps at Arroyo Chavez was 13,800 ppm on steep colluvial slopes (Table 1).

Sediment Budget

The sediment budgets are based on the time period that the gaging stations and sediment traps operated in each subbasin. The straw dams operated over a different time period than the sediment traps. To normalize for this difference, sediment deposition in the dams was divided by the number of days in operation and multiplied by the number of days the sediment traps were operating. The traps operated for 797 days in Volcano Hill Wash (June 6, 1996, to August 12, 1998) and 841 days in Arroyo Chavez (June 13, 1996, to October 2, 1998). Two traps in Arroyo Chavez, 5b and 7b, were installed later in the project, and sediment collected at these traps was normalized in the same manner as the straw dams. The sediment yield for each geomorphic surface was calculated using the results from the sediment traps and straw dams and averaged. The average sediment yield for each geomorphic surface was multiplied by the area of each geomorphic surface to obtain total erosion in kg.

For Volcano Hill Wash the highest average erosion rate for the five geomorphic surfaces occurred on alluvium (1.145 kg/m^2), followed by mesa (0.742 kg/m^2), alluvium/colluvium (0.397 kg/m^2), steep colluvial slopes (0.166 kg/m^2), and eolian/alluvium (0.145 kg/m^2) (fig. 4; Table 2). In the subbasin, 3,630,000 kg of sediment was eroded from the landscape and 11,300,000 kg of sediment was transported out of the basin (Table 2A). Thus, 7,670,000 kg (68%) of sediment was transported out of the basin that cannot be accounted for by measured upland erosion.

For Arroyo Chavez the highest average erosion rate for the seven geomorphic surfaces occurred on sparsely vegetated alluvium (6.53 kg/m^2), followed by alluvial fan (2.16 kg/m^2), steep colluvial slopes (1.37 kg/m^2), mesa (0.899 kg/m^2), gently sloping hillslopes (0.419 kg/m^2), moderately sloping hillslopes (0.334 kg/m^2), and well-vegetated alluvium (0.321 kg/m^2) (fig. 4; Table 2). More than 3,590,000 kg of sediment was eroded from the landscape and 6,710,000 kg of sediment was transported out of the basin (Table 2B). Thus, 3,120,000 kg (46%) of sediment was transported out of the basin that cannot be accounted for by measured upland erosion.

The unaccounted sediment in both subbasins may be contributions of sediment from bed and bank erosion or from important source areas of upland sediment (such as landslides noted on steep slopes in Volcano Hill Wash) that were not measured. The amount of sediment that may be originating from sources not measured in Volcano Hill Wash is 68%. The amount of sediment that may be originating from sources not measured in Arroyo Chavez is 46%. In addition, the amount of sediment removed from both subbasins is based on suspended-sediment load computations, which do not include bedload. If bedload were measured, the amount of sediment from unreported sources would increase. Kondolf and Matthews (1991) reported that the unmeasured residuals in sediment budgets can range from 1 to more than 100%.

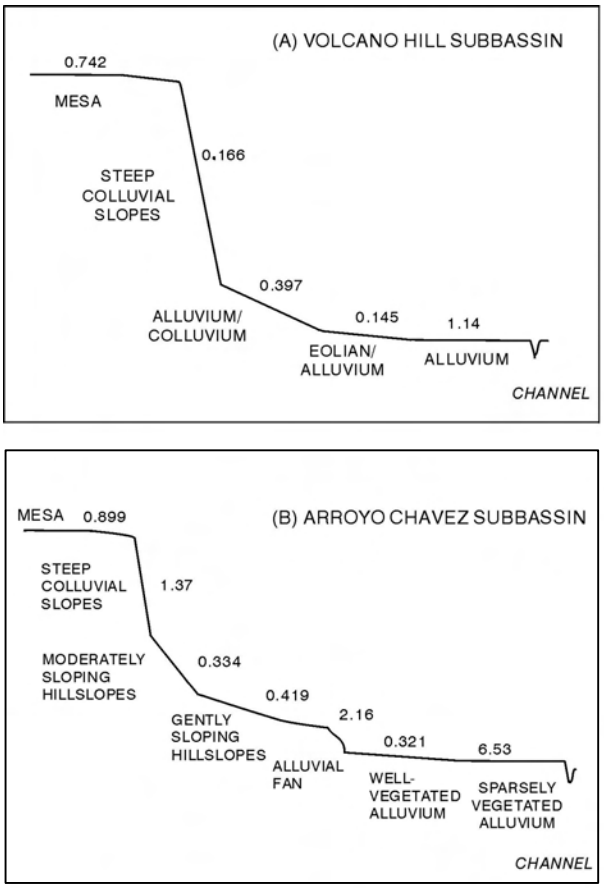

Figure 4. Erosion rates, in kilograms per square meter, on the geomorphic surfaces defined for the sediment budget in (a) Volcano Hill Wash subbasin and (b) Arroyo Chavez subbasin.

DISCUSSION

Erosion was measured in two subbasins of the Rio Puerco, each having different geology and land use. Erosion and sediment yields are higher in Arroyo Chavez subbasin compared to Volcano Hill Wash subbasin. Because geology and land use are different, these basins may represent end-members in the larger Rio Puerco drainage. The average annual sediment yield measured at the outlet of Arroyo Chavez subbasin (981 tonnes/km^2 /yr) is more than twice the sediment yield of Volcano Hill Wash (405 tonnes/km^2 /yr). The total discharge-weighted sediment concentration for the period of study at Arroyo Chavez (92,500 mg/L) was more than twice the concentration at Volcano Hill Wash (34,000 mg/L). By averaging the sediment yields and volume-weighted sediment concentrations from all sediment traps, the sediment yield for Arroyo Chavez (0.683 kg/m^2 /365 days) is more than twice the average sediment yield for all traps at Volcano Hill Wash (0.274 kg/m^2 /365 days) and the volume-weighted sediment concentration averaged for all traps at Arroyo Chavez (49,300 ppm) is more than three times greater than that at Volcano Hill Wash (11,500 ppm). The Volcano Hill Wash subbasin drains Cenozoic basalt flows with a silty eolian mantle that is protected by a basalt stone pavement.

Grazing is commonly cited as a contributor to increased erosion rates. The Arroyo Chavez subbasin is part of a grazing allotment that has livestock per 100 hectares seven times higher than Volcano Hill Wash. Visually most portions of the basin support a healthy vegetative cover. In both subbasins the major contribution of sediment is from the alluvial-valley floor. Grazing is expected to have a major effect along the valley floor where animals seek water and shade, thus grazing may play a role in differences in erosion. Other land-use factors that may be contributing to higher erosion and sediment yield in Arroyo Chavez are gas pipeline activity, including dirt roads, and trenching for the pipeline. Visually the basin is gullied with many areas of bare ground.

There are, however, observations that argue against the role of grazing as the sole factor influencing rates of erosion.

1. Storage of sediment in the alluvial valleys predates the intense grazing of the late 19th century. Alluvium in Arroyo Chavez and in the Rio Puerco yields radiocarbon dates greater than 5,000 B.P. (Pavich and others, 1997).

2. Differences in basin sediment yields are simply not due to differences in land use and upland erosion. The proportion of sediment exported from Volcano Hill Wash does not decrease in proportion to decreases in upland erosion. This may imply that sediment is being extracted from storage as upland sources are depleted and the channel attempts to maintain an equilibrium condition of sediment transport. Similar occurrences were noted for channels in the eastern United States as they maintained a stable sediment transport rate over time while upland erosion rates decreased as a result of soil conservation (Trimble and Lund, 1982).

Unraveling the complex responses of sediment transport to rainfall requires study periods longer than are possible by instrumental methods. The instrumented records do allow us to conclude, however, that erosion and sediment yields differ markedly due to geologic and land-use factors.

Table 1. Summary of data from sediment traps and straw dams for (A) Volcano Hill Wash and (B) Arroyo Chavez subbasins.

(A) Volcano Hill Wash

Sediment trap	Geomorphic surface	Number of events	Drainage area (m^2)	Runoff (g)	Sediment load (g)	Rainfall (mm)	Sediment yield (kg/m^2/365 days)	Volume-weighted sediment concentration (ppm)
1	Alluvium	39	7.2	547,240	15,220	526	0.975	25,300
2	Eolian/alluvium	28	8.3	289,820	1,210	526	0.067	4,170
3	Alluvium/colluvium	35	9.7	335,620	4,560	572	0.215	13,600
4	Steep colluvial slopes	33	4.8	64,560	490	604	0.046	7,500
5	Mesa	35	5.8	292,000	4,340	634	0.340	14,800
6	Alluvium/colluvium	34	6.6	249,550	1,830	572	0.128	7,300
7	Alluvium/colluvium	38	4.7	302,200	2,070	572	0.202	6,900
8	Alluvium	35	6.4	245,000	3,080	526	0.220	12,600

Straw dam	Days in operation	Geomorphic surface	Drainage area (m^2)	Sediment deposition (kg)	Sediment yield (kg/m^2/365 days)
A	1224	Steep colluvial slopes	5,000	1,560	0.093
B	1202	Alluvium	422	530	0.378
C	1203	Steep colluvial slopes	5,170	2,300	0.135
D	1224	Steep colluvial slopes	2,510	250	0.30

(B) Arroyo Chavez

Sediment trap	Geomorphic surface	Number of events	Drainage Area (m^2)	Runoff (g)	Sediment load (g)	Rainfall (mm)	Sediment yield (kg/m^2/365) days	Volume-weighted sediment concentration (ppm)
1	Mesa	46	37	692,390	19,000	688	0.228	27,800
2	Steep colluvial slopes	39	7.9	232,590	3,200	688	0.175	13,800
3	Mesa	47	35	487,880	29,000	701	0.353	58,900
4	Alluvial fan	52	27	726,130	59,000	688	0.937	81,400
5a	Sparsely vegetated alluvium	58	27	1,509,500	210,000	790	3.35	140,000
5b	Sparsely vegetated alluvium	34	0.76		1,300	602	1.06	
6	Well-vegetated alluvium	31	6.4	64,450	2,000	917	0.139	31,800
7a	Gently sloping hillslopes	46	28	807,660	12,000	894	0.198	15,600

7b	Gently sloping hillslopes	29	1.7		660	790	0.243	
8	Moderately sloping hillslopes	43	22	286,380	7,300	1,016	0.145	25,400

Straw dam	Days in operation	Geomorphic surface	Drainage area (m^2)	Sediment deposition (kg)	Sediment yield (kg/m^2/365 days)
A	1207	Steep colluvial slopes	2,280	2,760	0.367
B	1171	Mesa	1,420	2,690	0.590
C	1172	Steep colluvial slopes	541	2,150	1.24
D	931	Sparsely vegetated alluvium	405	4,570	4.43

Table 2. Sediment budget for (A) Volcano Hill Wash and (B) Arroyo Chavez.

(A) Volcano Hill Wash (June 6, 1996, to August 12, 1998)

	Streamflow-gaging station	Mesa	Eolian/alluvium	Alluvium/colluvium	Steep colluvial slopes	Alluvium
Sediment yield, kg/m^2	1.22	0.742	0.145	0.397	0.166	1.145
Area, m^2	9,299,309	1,260,737	991,207	2,303,337	3,878,763	865,264
Total erosion, kg	11,300,000	935,000	144,000	914,000	644,000	991,000

Total upland erosion = 3,630,000 kg
Total suspended-sediment transport = 11,300,000 kg
Difference = -7,670,000 kg

(B) Arroyo Chavez (June 13 1996, to October 2, 1998)

	Streamflow-gaging Station	Mesa	Alluvial fan	Sparsely vegetated alluvium	Well-vegetated alluvium	Gently sloping hillslopes	Moderately sloping hillslopes	Steep colluvial slopes
Sediment yield, kg/m^2	2.94	0.899	2.16	6.53	0.321	0.419	0.334	1.37
Area, m^2	2,280,679	592,593	235,198	275,445	182,117	335,654	341,173	318,499
Total erosion, kg	6,710,000	533,000	508,000	1,800,000	58,500	141,000	114,000	436,000

Total upland erosion = 3,590,000 kg
Total suspended-sediment transport = 6,710,000 kg
\ Difference = -3,120,000 kg

REFERENCES

Aquilar, R., and Aldon, E.F., 1991, Runoff and sediment rates on San Mateo and Querencia Soils, Rio Puerco Watershed Management Area, N.M. USDA Rocky Mountain Forest and Range Experiment Station, Research Note RM-506, 7 p.

Bryan, K., 1925, Date of channel trenching in the arid Southwest. Science, v. 62, p. 338-344.

Dietrich, W.E., and Dunne, T., 1978, Sediment budget for a small catchment in mountainous terrain. Zeitschrift fur Geomorphologie, v. 29, p. 191-206.

Elliott, J.G., Gellis, A.C., and Aby, S.B., 1998, Evolution of arroyos--Incised channels of the Southwestern United States. Darby, S.E., and Simon, A., eds., Incised Channels--Processes, forms, engineering and management, p. 153-185.

Gellis, A.C., 1998, Characterization and evaluation of channel and hillslope erosion on the Zuni Reservation, 1992-95. U.S. Geological Survey Water-Resources Investigations Report 97-4292, 51 p.

Gellis, A.C., and Elliott, J.G., 2000, Arroyo changes in elected watersheds of New Mexico, United States. Harvey, M., and Anthony, D., eds., Applying Geomorphology to Environmental Management, A Special Publication Honoring Stanley A. Schumm. Water Resources Publications, LLC, IN PRESS.

Gerlach, T., 1967, Hillslope troughs for measuring sediment movement. Revue Geomorphologie Dynamique, v. 4, p. 173.

Guy, H.P., 1964, An analysis of some storm-period variables affecting stream sediment transport. U.S. Geological Survey Professional Paper 462-E, 46 p.

Kondolf, G.M., and Matthews, W.V.G., 1991, Unmeasured residuals in sediment budgets–A cautionary note. Water Resources Research, v. 27, p. 2483-2486.

Leopold, L.B., Emmett, W.W., and Myrick, R.M., 1966, Channel and hillslope processes in a semiarid area, New Mexico. U.S. Geological Survey Professional Paper 352-G, p. 193-253.

Love, D.W., 1986, A geological perspective of sediment storage and delivery along the Rio Puerco. Hadley, R.F., ed., Drainage basin sediment delivery, IAHS Publication 159, p. 305-322.

Love, D.W., and Young, J.D., 1983, Progress report on the late Cenozoic geologic evolution of the lower Rio Puerco. New Mexico Geological Society Guidebook, 34th Field Conference, Socorro Region II, p. 277-284.

Milliman, J.D., and Meade, R.H., 1983, World-wide delivery of river sediment to the oceans. Journal of Geology, v. 91, p. 1-21.

Pavich, M.J., Gellis, A.C., and Aby, S., 1997, Chronostratigraphy of Quaternary alluvium, Rio Puerco basin, New Mexico. Geological Society of America, Abstracts with Programs, Annual Meeting, Salt Lake City, Utah, p. A-372.

Swanson, F.J., Janda, R.J., Dunne, T., and Swanston, D.N., 1982, Sediment budgets and routing in forested drainage basins. U.S. Department of Agriculture, Forest Service General Technical Report PNW-141, 23 p.

Trimble, S.W., and Lund, S.W., 1982, Soil conservation and the reduction of erosion and sedimentation in the Coon Creek basin, Wisconsin. U.S. Geological Survey Professional Paper 1234, 35 p.

Zhao, W., Jiao, E., Wang, M.G., and Meng, X., 1992, Analysis of the variation of sediment yield in Sanchuanhe River basin in 1980's. International Journal of Sediment Research, v. 7, p. 1-20.

FACTORS CONTROLLING STORM-GENERATED SUSPENDED-SEDIMENT CONCENTRATIONS AND LOADS IN A HUMID-TROPICAL BASIN, QUEBRADA BLANCA, PUERTO RICO

By Allen Gellis, Hydrologist, U.S. Geological Survey, Albuquerque, New Mexico

5338 Montgomery NE, Suite 400, Albuquerque, NM 87109 (505) 830-7979, Fax: (505) 830-7998, agellis@usgs.gov

INTRODUCTION

The humid tropics, which have an average annual precipitation greater than 1000 mm, cover 25 percent of the earth's surface area and by 2000 were projected to hold one-half of the world's population (United Nations Educational Scientific and Cultural Organization (UNESCO), 1990). This growing population has resulted in land-use changes and related problems of deforestation, reservoir sedimentation, channel alteration, and degradation of terrestrial and marine habitats (UNESCO, 1990; Bonell and others, 1993; World Resources Institute, 1996; Gellis and others, 1999). These land-use problems influence erosion and sediment characteristics of tropical watersheds.

Puerto Rico is an area in the humid tropics that has undergone dramatic land-use changes in the past few hundred years (Gellis and others, 1999). A large data set on suspended sediment has been collected by the U.S. Geological Survey (USGS) in Puerto Rican rivers. In 2000, 28 USGS suspended-sediment stations are operating in Puerto Rico. Many of these stations have 10 to 20 years of record. The USGS is currently involved in a study examining the role of land use on suspended-sediment characteristics of Puerto Rican rivers. This paper presents findings on factors that control storm-generated suspended-sediment concentrations and loads at one sediment station in Puerto Rico, Quebrada Blanca near El Jagual.

Background

Fifty percent of runoff to the world's oceans is contributed by low-latitude rivers (Lerman, 1985). The humid tropics are an important contributor to the oceans' dissolved and solid loads. The humid tropics supply 65% of the dissolved silica, 38% of the ionic load, and 50% of the world's solid load from rivers (Milliman and Meade, 1983; Stallard, 1988). The Langbein and Schumm (1958) curve indicates that semiarid regions have the highest sediment yields. Fournier (1960) included data from monsoonal regions and reported another spike in sediment yield in the humid tropics. Pickup and others (1981) concluded that sediment loads in the tropical rivers they studied in New Guinea were high by world standards.

Guy (1964) analyzed suspended sediment transported during storm events in seven streams in the Atlantic coast area of the United States; he found that the mean concentration of sediment (discharge-weighted sediment concentration) for a storm event was regarded as a better dependent variable than sediment load. Rainfall amounts and rainfall intensity were found to be the most important independent variables influencing suspended-sediment characteristics (Guy, 1964). Walling (1974) conducted a study of sediment characteristics during storm events and showed that suspended-sediment characteristics change with season, stage, and availability of sediment. Analysis of 102 storm events with 13 independent variables representing rainfall and discharge parameters showed peak discharge, total rainfall, rainfall energy, and time of year as the most significant independent variables explaining sediment concentrations (Walling, 1974).

Reservoir sedimentation was identified as a problem in Puerto Rico beginning in the 1940's (Nevares and Dunlop, 1948). The study area of Quebrada Blanca is a subbasin of the Lago Loiza basin (538 km^2) (fig. 1) that contains a water-supply reservoir undergoing sedimentation. Impounded in 1953, the reservoir in 1988 was experiencing accelerated sedimentation and substantial loss of storage capacity (Quinones and others, 1989). As a result, the Puerto Rican Government began a study with the USGS to quantify suspended-sediment transport in select subbasins of varying land uses in the Lago Loiza basin (Gellis and others, 1999).

Figure 1. Location of Quebrada Blanca subbasin within the Lago Loiza basin.

Setting

Puerto Rico is 180 km by 65 km and is the smallest island in the greater Antilles. Quebrada Blanca subbasin drains 8.42 km^2 in intrusive rocks (granodiorite) and volcaniclastic rocks (fig. 2a). Average annual rainfall measured at San Lorenzo, 5 km from the study subbasin (fig. 1), was 2,475 mm during 1969-93. Land use in the subbasin is rural and agricultural, and most land is used for pasture (fig. 2b); bare ground is cropland. Average slope is 33%. Land use in the subbasin is considered representative of the larger Lago Loiza basin.

METHODS

Factors that control suspended-sediment characteristics during storm-generated runoff events were examined at Quebrada Blanca near El Jagual for October 1988 to September 1993, using statistical techniques. Two dependent factors were defined to describe suspended sediment: (1) suspended-sediment load and (2) the discharge-weighted sediment concentration. Discharge-weighted sediment concentration (in mg/L) is a variable computed as total suspended-sediment load divided by total runoff of the storm event (Guy, 1964). Discharge-weighted sediment concentration is an informative way to look at sediment transport because it normalizes the total suspended-sediment load by the total amount of runoff transporting the sediment. Twenty-three independent variables believed to control suspended sediment during storms events were compiled (Table 1). The independent variables were divided into three time categories: (1) characteristics of the previous event, (2) characteristics between events, and (3) characteristics of the current event (Table 1).

Sediment characteristics were analyzed following the steps outlined in figure 3. First, the 23 independent variables were tested for normality by visually inspecting the histograms of residuals generated by linear regression (Helsel and Hirsch, 1992). Those variables found to be non-normal were log-transformed. At this point, two distinct approaches to reducing the number of variables were used to assess potential analytical and interpretive advantages . The first approach was an inspection of the Pearson's product-moment correlation matrix to remove highly correlated ($r \geq 0.80$) variables. The second approach was a more involved principal component analysis of the correlation matrix. Principal components analysis is a statistical tool used to reduce the dimensionality of the data scatter onto a new set of axes (Davis, 1973) and to compute new composite variables that are uncorrelated. The first axis explains most of the variance in the data, and subsequent axes explain the remaining variance. In factor analysis, a smaller number of principal components are selected to determine a simplified structure to the data. The smaller number of principal components was based on examination of the scree plot. A scree plot is a plot of eigenvalues against their principal component axis. The uncorrelated variables resulting from the two approaches were then subjected to forward-stepwise multiple regression, with the F-to-enter and F-to-remove level of significance set at 0.05. To avoid problems with spurious relations among the dependent and independent variables, the quickflow (runoff minus baseflow) of the current event was removed as an independent variable when examining discharge-weighted sediment concentration as a dependent variable in forward-stepwise regression analyses. Hydrograph separation techniques were used to separate baseflow from stormwater runoff into quickflow (Hewlett and Hibbert, 1967).

Table 1. Independent variables believed to influence suspended-sediment concentrations. Only those flow variables related to quickflow are shown. *[Abbreviations used in the text are in bold. ' LG' in indicates a log transformation.]*

CHARACTERISTICS OF THE PREVIOUS EVENT	**CHARACTERISTICS BETWEEN EVENTS**	**CHARACTERISTICS OF CURRENT EVENT**
Peak flow of the previous event (using quickflow or total runoff) divided by hours since the peakflow (**1-LGLSPKTI**)	Total rainfall between events divided by hours since the previous event (**9-LGPPTBTW**)	Quickflow (**12-LGQUICK**)
Sum of peakflows of the previous event (using either quickflow or total runoff) divided by hours since the previous event (**2-LGSMLSPK**)	Maximum 15-minute rainfall intensity between events divided by hours since the previous event (**10-LGINTBET**)	Total rainfall (**13-LGRAIN**)
Quickflow of the previous event divided by hours since the previous event (**3-LGQULST**)	Total runoff between events divided by hours since the previous event (**11-RNBTWTI**)	Maximum 15-minute rainfall intensity (**14-INT15**)
Combined quickflow of last 3 events divided by time over the last 3 events (**4-LGQU3EVT**)		75-% rainfall intensity (**15-LGSFIVE**)
Total rainfall of the previous event divided by hours since the previous event (**5-LGQULST**)		Baseflow at start of event (**16-LGBASE**)
Maximum 15-minute intensity of the previous event divided by hours since the previous event (**6-LGINTLST**)		Maximum peak flow (using either quickflow or total runoff) (**17-LGPK**)
75-% intensity of the previous event divided by hours since the previous event (**7-LGL75OTI**)		Sum of peakflows in event (using either quickflow or total runoff) (**18-LGSMPK**)
Sum of last 3 rainfall events divided by time over the last 3 events (**8-LGSUM3PPTI**)		Hysteresis characteristic (**19-HYSTER**) 1 = normal hysteresis loop 0 = reverse hysteresis loop
		Total rainfall on rising limb to highest peakflow (**20-LGRRISE)**
		Total rainfall on falling limb ffter highest peakflow (**21-RAINFOL**)
		Maximum rate of hydrograph rise for any peak, from preceding trough to peak (**22-LGMXTRP**)
		Maximum rate of hydrograph rise from start of event to the highest peakflow (**23-LGMXTMJPK**)

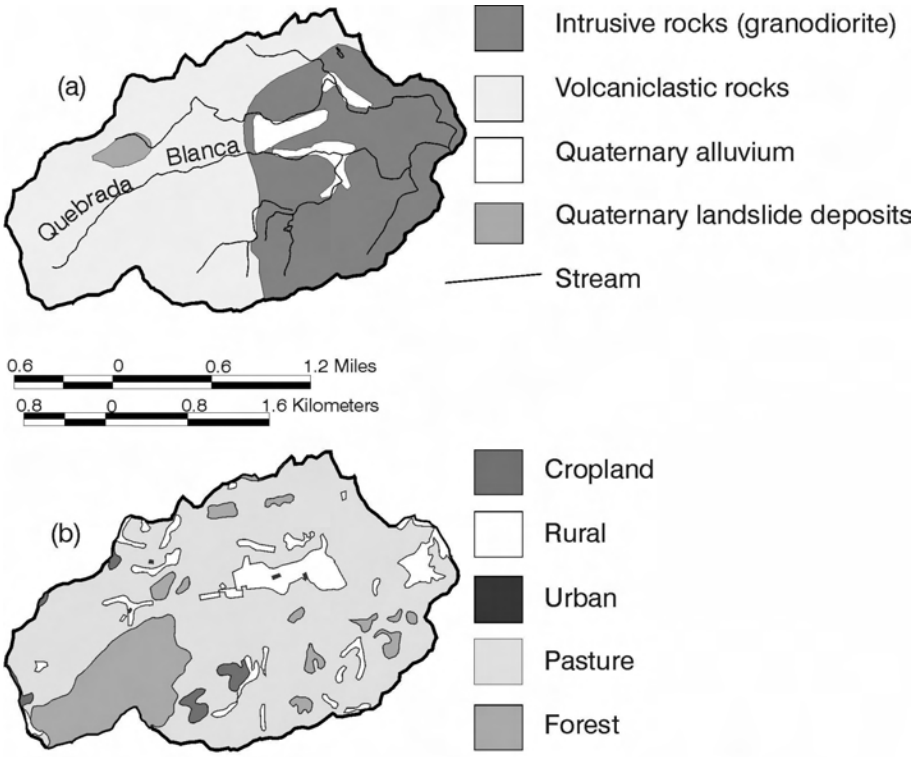

Figure 2. Quebrada Blanca subbasin (a) geology and hydrography and (b) land use.

RESULTS AND DISCUSSION

From July 4, 1989, to September 15, 1993, 23 runoff events were sampled to define suspended-sediment loads and concentrations for the storm-generated runoff hydrograph. The two dependent variables, suspended-sediment load, in tonnes, and discharge-weighted sediment concentration, in mg/L, were used to described suspended-sediment transport in the quickflow portion of the hydrograph. Tests for normality using the residuals indicated that 19 of the 23 independent variables needed a log transformation. Analysis of the correlation matrix showed a high correlation ($r > 0.80$) among five variables (1-LGLSPKTI, 6-LGINTLST, 13-LGRAIN, 23-LGMXTMJPK, and 17-LGPK) and these variables were removed. The variables are explained in table 1. Important relations of the dependent variables to the independent variables that were observed in the correlation matrix are log suspended-sediment load to 18-LGSMPK and 12-LGQUICK and log discharge-weighted sediment concentration to 22-LGMXTRP (fig. 4).

Results of forward-stepwise regression on the 18 remaining independent variables against the 2 dependent variables are shown in Table 2. The four most important variables explaining both dependent variables were related to the characteristics of the current runoff event (Table 2). 18-LGSMPK is significant in step one of the forward-stepwise regression against log suspended-sediment load. In relation to the log of suspended-sediment load, 1) the R^2 is 0.72, indicating that the correlation is high, and 2) the coefficient is positive, indicating that an increase in suspended-sediment load is related to an increase in the sum of peakflows (18-LGSMPK) (fig. 4a). The next important current event variable that appears in the forward-stepwise regression analysis is 12-LGQUICK, and the coefficient is positive (table 2).

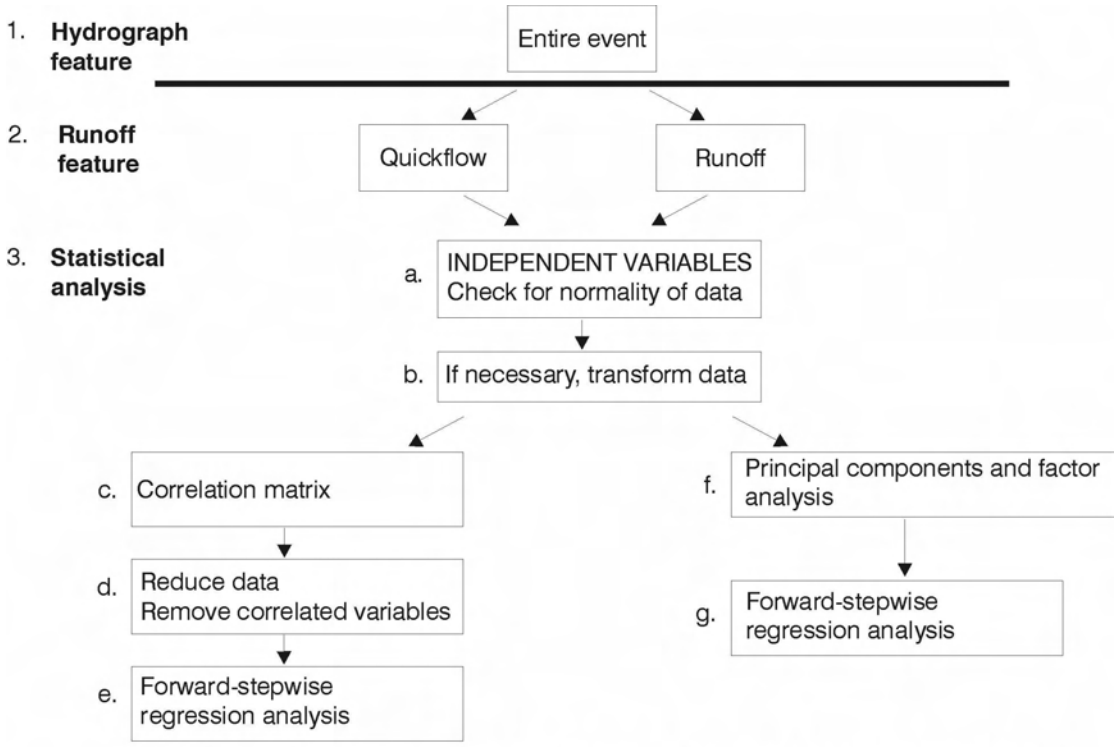

Figure 3. Steps used in the statistical analysis of suspended sediment.

Using the log discharge-weighted sediment concentration as a dependent variable indicated that 22-LGMXTRP was significant in step one (fig. 4c). 22-LGMXTRP is the maximum rate of hydrograph rise for any peak and indicates that faster rising discharge increases sediment concentration. 20-LGRRISE was important step two of forward-stepwise regression (Table 2).

Table 2. Results of forward-stepwise regression using quickflow characteristics.
[Variable abbreviations defined in table 1. mg/L, milligrams per liter]

Dependent variable	Step	Variables in the model	R2	F statistic	Slope coefficient	Constant
Log suspended-sediment load (tonnes)	One	18-LGSMPK	0.72	55.1	1.0	-0.89
	Two	12-LGQUICK	0.80	7.65	0.56	-3.65
		18-LGSMPK		17.5	0.68	
Log discharge-weighted sediment concentration (mg/L)	One	22-LGMXTRP	0.50	20.1	0.46	2.63
	Two	20-LGRRISE	0.62	6.04	0.45	2.58
		22-LGMXTRP		21.3	0.43	

Principal components analysis was performed on the data set for quickflow. More than 67% of the total variance is explained by the first three component axes. Examination of the scree plot showed eight components to be important and were selected for factor analysis. Forward-stepwise regression was performed on this data set using the dependent variables, log suspended-sediment load, and log discharge-weighted sediment concentration.

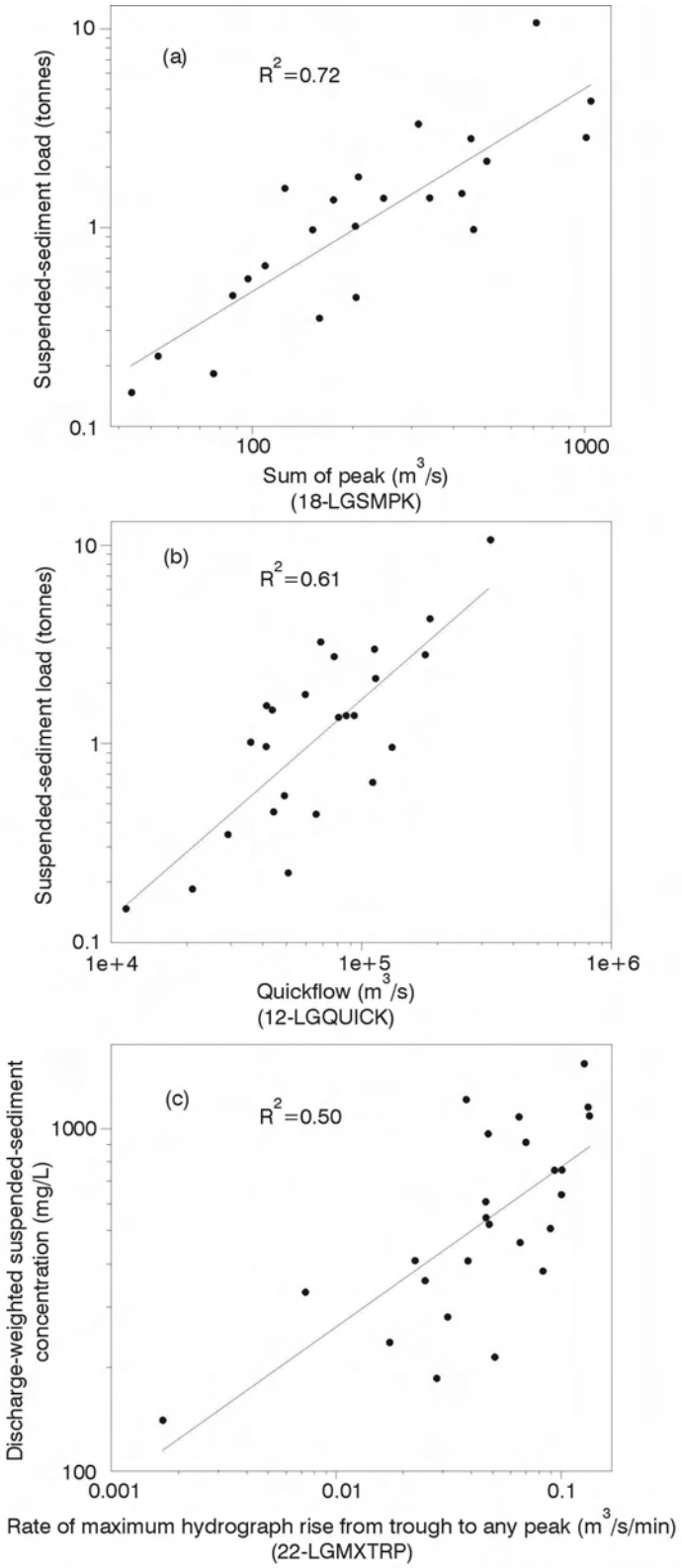

Figure 4. Relation of dependent variables for storm-generated runoff events at Quebrada Blanca showing highest R^2 values for quickflow characteristics (a), sediment load (b), and discharge-weighted sediment concentration (c).

Forward-stepwise regression was performed on the principal components against the two dependent variables (Table 3). The least-squares regression coefficients are all <0.50 for step one. Using log suspended-sediment load as a dependent variable indicated principal component 2 (PC2) as the most significant principal axis. PC2 has negative loadings (<-0.50) from rainfall (20-LGRRISE, 21-RAINFOL, and 13-LGRAIN) and flow characteristics (18-LGSMPK, 17-LGPK, and 12-LGQUICK) of the current event. Positive loadings on PC2 are from characteristics of the three previous events (8-LGSUM3PPTI and 4-LGQU3EVT) and a characteristic between events (11-RNBTWTI). The coefficient of the regression line is negative, indicating that suspended-sediment load is directly correlated to rainfall and flow characteristics of the current event and inversely correlated to characteristics of the three previous events and between the last event. The inverse relation of characteristics of the three previous events and characteristic between events to suspended-sediment load implies that as a characteristic of the previous event increases, such as the sum of rainfall for the previous three events (8-LGSUM3PPTI), suspended-sediment load decreases. The sum of the last three rainfall events would mobilize sediment on hillslopes that would be removed by the storm-generated runoff. The removal of sediment from the system would support a flushing process in which previous runoff events removed sediment from the system in Quebrada Blanca. As a variable between events increases, such as the runoff between events (11-RNBTWTI), sediment loads would also decrease. The removal of sediment from the system may also be due to flushing because higher runoff between events mobilizes and transports sediment that would otherwise be transported in the current event.

The results of forward-stepwise regression on the principal components using the log discharge-weighted sediment concentration as a dependent variable showed PC2 has high positive loadings (> 0.50) from rainfall (20-LGRRISE, 21-RAINFOL, 13-LGRAIN) and flow characteristics (17-LGPK, 18-LGSMPK) of the current event. High negative loadings (< -0.50) from PC2 are from characteristics of the previous three events (8-LGSUM3PPTI and 4-LGQU3EVT) and a characteristic between events (11-RNBTWTI). The coefficient is positive, indicating that as current event characteristics of rainfall and flow increase, the discharge-weighted sediment concentration increases. As characteristics of the three previous events and between events increase, discharge-weighted sediment concentration decreases.

The results of forward-stepwise regression analysis on the principal components, using both dependent variables, are similar to the conclusions drawn from forward-stepwise regression on the independent variables for the entire event (Tables 2 and 3). Using both dependent variables indicated that characteristics of the current event appeared to be significant in step one of forward-stepwise regression. However, 22-LGMXTRP was important in step one of forward-stepwise regression using discharge-weighted sediment concentration as a dependent variable (Table 2). 22-LGMXTRP did not appear to have high loadings on PC2.

Statistical analyses (not shown) were also performed using the total runoff of the event, which includes baseflow, on the two dependent variables, log suspended-sediment load and log discharge-weighted sediment concentration. Results were similar to the analyses using quickflow and showed characteristics of the current event as important. Results of forward-stepwise regression indicated current runoff peakflow (18-LGSMPK) as significant in step one explaining log suspended-sediment load. The log of total runoff was significant in step two of forward-stepwise regression. The results of forward-stepwise regression using discharge-weighted sediment concentration showed 22-LGMXTRP as significant in step one and a rainfall characteristic, 20-LGRRISE, as significant in step two. Principal components analysis showed PC2 as the most important principal component explaining log suspended-sediment load and discharge-weighted sediment concentration. PC2 showed the same results for each dependent variable of positive loadings on characteristics of the current event and negative loadings on previous and between event characteristics. The coefficient was positive for log suspended-sediment load and discharge-weighted sediment concentration.

Table 3. Results of forward-stepwise regression on the principal components for the entire event using quickflow characteristics. *[PC, principal component; mg/L, milligram per liter]*

Dependent variable	Step	Variables in the model	R2	F statistic	Coefficient	Constant
Log suspended-sediment load (tonnes)	One	PC2	0.48	19.1	-0.32	1.58
Log discharge-weighted sediment concentration (mg/L)	One	PC2	0.32	9.64	0.16	2.72

CONCLUSIONS

Storm-generated suspended-sediment loads and concentrations for one subbasin of the Lago Loiza basin, Quebrada Blanca (8.42 km^2), dominantly used for pasture, were statistically tested against independent variables related to three time categories: (1) characteristics of the previous event, (2) characteristics between events, and (3) characteristics of the current event. Forward-stepwise regression analysis on the independent variables and principal components showed that characteristics of the current runoff event are most important. These characteristics include magnitude of peak flows, sum of peak discharges, and maximum rate of hydrograph rise for any peak in the runoff event.

Results for the forward-stepwise regression on the principal components using log suspended-sediment load as an dependent variable are similar to the results for the log discharge-weighted sediment concentration as a dependent variable. Both results show PC2 as important in step one of forward-stepwise regression. High loadings on PC2 show current event characteristics have signs opposite to those from the previous three events characteristics and between events. This may indicate a flushing mechanism in the watershed exists, which causes suspended-sediment loads to decrease because of the previous three events and between event characteristics. Using hydrograph

separation of the storm-generated runoff event into quickflow did not improve the statistical relations compared to using total runoff.

REFERENCES

Bonell, M., Hufschmidt, M.M., and Gladwell, J.S., eds., 1993, Hydrology and water management in the humid tropics. Cambridge University Press, 343 p.

Davis, J.C., 1973, Statistics and data analysis in geology. John Wiley and Sons, first ed., 550 p.

Fournier, M.F., 1960, Climat et erosion. Paris, Presses Universitaires de France, 201 p.

Gellis, A.C., Webb, R.M.T., Wolfe, W.J., and McIntyre, S.C.I., 1999, Effects of land use on upland erosion, sediment transport, and reservoir sedimentation, Lago Loiza basin, Puerto Rico. U.S. Geological Survey Water-Resources Investigations Report 99-4010, 60 p.

Guy, H.P., 1964, An analysis of some storm-period variables affecting stream sediment transport. U.S. Geological Survey Professional Paper 462-E, 46 p.

Helsel, D.R., and Hirsch, R.M., 1992, Statistical methods in water resources. Studies in Environmental Science 49, Elsevier Science Publishers B.V., Netherlands, 522 p.

Hewlett, J.D., and Hibbert, A.R., 1967, Factors affecting the response of small watersheds to precipitation in humid areas. Sopper, W.E., and Lull, H.W., eds., International Symposium on Forest Hydrology, p. 275-290.

Langbein, W.B., and Schumm, S.A., 1958, Yield of sediment in relation to mean annual precipitation. Transactions of the American Geophysical Union, v. 39, p. 1076-1084.

Lerman, A., 1985, Weathering rates and major transport processes--An Introduction. Physical and chemical weathering in geochemical cycles, Lerman, A., and Meybeck, M., eds., Kluwer Press, p. 1-10.

Milliman, J.D., and Meade, R.H., 1983, World-wide delivery of river sediment to the oceans. Journal of Geology, v. 91, p. 1-21.

Nevares, R., Jr., and Dunlop, J.C., 1948, Some engineering and geologic data on reservoir sedimentation in Puerto Rico. U.S. Geological Survey unpublished report, 24 p.

Pickup, G., Higgins, R.J., and Warner, R.F., 1981, Erosion and sediment yield in Fly River drainage basins, Papua New Guinea. Publication of the International Association of Hydrological Sciences 132, p. 438-456.

Quinones, F., Green, B., and Santiago, L., 1989, Sedimentation survey of Lago Loiza, Puerto Rico, July 1985. U.S. Geological Survey Water-Resources Investigation Report 87-4019, 16 p.

Stallard, R.F., 1988, Weathering and erosion in the humid tropics. Physical and chemical weathering in geochemical cycles, Lerman, A., and Meybeck, M., eds., Kluwer Academic Publishers, The Netherlands, p. 225-246.

United Nations Educational Scientific and Cultural Organization (UNESCO), 1990, Water related issues and problems of the humid tropics and other warm humid regions. United Nations Environment Pogramme, 33 p.

Walling, D.E., 1974, Suspended sediment and solute yields from a small catchment prior to urbanization. Gregory, K.J., and Walling, D.E., eds., Fluvial processes in instrumented watersheds, Institute of British Geographers Special Publication No. 6, p. 169-192.

World Resources Institute, 1996, World resources 1996-97, A guide to the global environment. Oxford University Press, 400 p.

LONG-TERM RUNOFF AND SUSPENDED SEDIMENT MEASUREMENTS, REYNOLDS CREEK EXPERIMENTAL WATERSHED IN SOUTHWEST IDAHO

Frederick B. Pierson, Jr., Research Hydrologist, USDA-ARS, Boise, ID; Charles W. Slaughter, Hydrologist, USDA-ARS, Boise, ID; Clayton L. Hanson, Agricultural Engineer, USDA-ARS, Boise, ID.

USDA-ARS Northwest Watershed Research Center, Boise, ID 83712-7716
208/422-0700, fpierson@nwrc.ars.usda.gov

INTRODUCTION

The Reynolds Creek Experimental Watershed (RCEW) runoff and sedimentation program provides fundamental information for research into hydrologic processes, precipitation-runoff relationships, hydrograph characteristics, water yield, and the interactive effects of climate, vegetation, soils and land use on rangeland hydrologic response. The RCEW basic data set provides a basis for evaluating temporal variability in hydrologic regime and water yield, and for evaluating spatial variability within a"typical" upland rangeland landscape. Rangeland watersheds, with high-elevation seasonal snowpack provide a major source of runoff for spring and early summer, supply water for on-site biological production, in-stream and near-stream habitat, and downstream uses including irrigation, recreation and hydropower generation. Discharge and sediment data from RCEW are particularly valuable for understanding complex upland runoff and sediment generation processes of rain and snowmelt on snow and frozen soils [*Flerchinger et al.*, 1994], which can produce flooding and property damage throughout the northwestern United States [*Slaughter et al.*, 1997].

Early research in RCEW focused on relationships between runoff source areas and water yield [*Johnson and Hanson*, 1976; *Johnson and Smith*, 1978]. Selected source areas of varying size, elevation, aspect, climate, geology, soils and vegetation characteristics were instrumented, monitored and analyzed. The RCEW data provide a basis for investigating scale relationships in rangeland watersheds [*Seyfried and Wilcox*, 1995] and for comparison with other hydrologic systems [*Slaughter et al.*, 1996]. Recent work has emphasized runoff and erosion processes at varying scales, through use of small-scale intensively instrumented study basins within RCEW [*Pierson et al.*, 1994], and use of RCEW data as a framework for hydrologic and hydraulic process research.

The primary objectives of early sediment measurements in RCEW were to accurately sample sediment transport at key stations and to determine sediment yields from instrumented watersheds, especially during storm runoff events. Selected locations for monitoring sediment were instrumented in the mid-1960's. Bedload transport was measured at selected locations during runoff events using both Helley-Smith bedload samplers and sediment detention ponds. Bedload contributions to total sediment yields were estimated at about 20% of total sediment yield [*Johnson and Hanson*, 1976], and routine bedload measurements were discontinued.

Innovations in discharge measurement and sediment sampling have been tested and applied in RCEW. Cooperative studies with the Albrook Hydraulics Laboratory of Washington State University were successful in developing the "drop-box" weir design that can pass high sediment loads and does not require regular channel cleaning *[Brakensiek et al.*, 1979]. Drop-box weirs have performed well over a wide range of discharges and sediment loads. A variety of early sediment samplers such as the U.S. PS-69 pumping sampler [*Brakensiek et al.*, 1979] and Helley-Smith bed load samplers were tested in RCEW through cooperative efforts with other ARS locations, federal and state agencies, and universities.

WATERSHED CHARACTERISTICS

Reynolds Creek flows almost directly north from the northern flank of the Owyhee Mountains, and is a direct tributary of the Snake River. The Outlet weir, which defines the 239 km^2 Reynolds Creek Experimental Watershed, is located in a narrow canyon 11 km south of the confluence of Reynolds Creek and the Snake River. The southwestern sector of RCEW is the coolest and wettest portion of the basin, while the northeastern sector, which includes Summit Wash and Flats watersheds, is the warmest and receives the least precipitation.

The vegetation of RCEW is almost entirely sagebrush rangeland (95%). Plant communities are representative of desert, foothill, and high mountain rangelands found throughout northwestern United States. The major grass species are cheatgrass (*Bromus tectorum*), bluebunch wheatgrass (*Pseudoroegneria spicata*), bottlebrush squirreltail (*Elymus elymoides*), sandberg bluegrass (*Poa sandbergii*) and Idaho fescue (*Festuca idahoensis*). The dominant shrubs are big sagebrush (*Artemisia tridentata),* low sagebrush (*Artemisia arbuscula*), bitterbrush (*Purshia tridentata*) and rabbitbrush (*Chrysothamnus* spp.). Significant stands of coniferous forest are found only in the extreme southern (highest) sectors of RCEW. Approximately two percent of the area is covered by small stands of Douglas fir (*Pseudotsuga menziesii*), aspen (*Populus* spp.), and alpine fir (*Abies lasiocarpa*), and three percent of the area is flood-irrigated pastureland.

RCEW is developed in an eroded structural basin in which late Tertiary volcanic and sedimentary rocks overlie Cretaceous granitic basement rocks. The primary geologic formations are granitics of the Idaho Batholith, Salmon Creek volcanics, the Reynolds Basin group complex of basaltic flows, silicic tuff, diatomite, arkosic sand and gravel, and latite rhyolitic welded ash flow tuffs [*Stephenson*, 1977].

The soils of RCEW include eight soil associations and 32 soil series. Major soil associations in RCEW include Bakeoven-Reywat-Babbington (35% by area), Harmehl-Gabica-Demast (25% of the watershed), and Nannyton-Larimer-Ackmen, Dark-Gray Variant (12% by area). Soils mapping and detailed descriptions of each association and individual series are provided in *Stephenson* [1977] and the availability of those data by *Seyfried et al.* [2000].

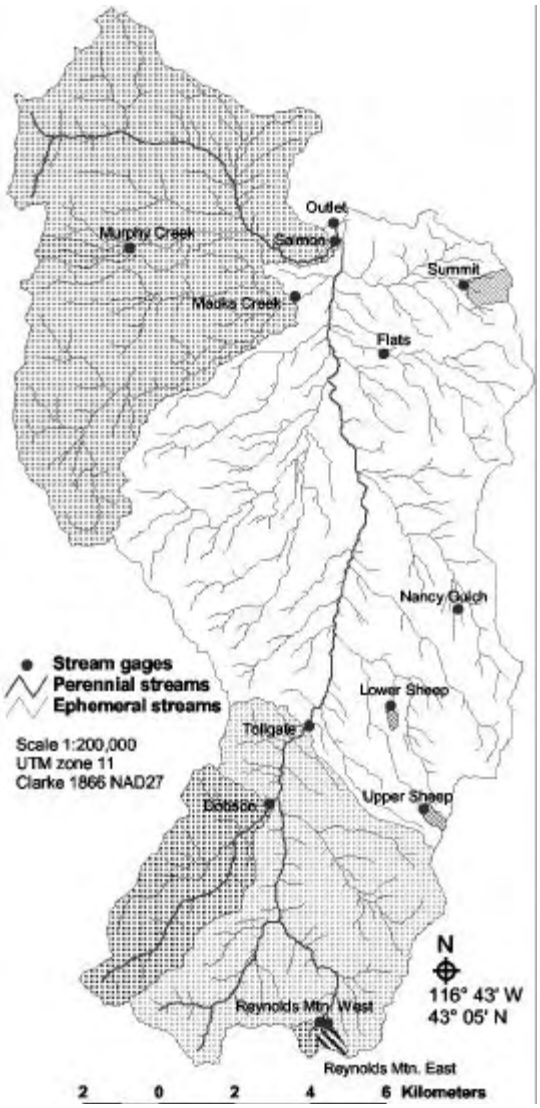

Figure 1. Stream network, watershed boundaries and weir locations on Reynolds Creek Experimental Watershed, Idaho.

Locations of all stream gauging stations within RCEW are shown in Figure 1. The drainage area, elevation range and flow characteristics for each gauged watershed are given in Table 1. A detailed description of the spatial data on soils, geology, topography and vegetation for each watershed is provided by *Seyfried et*

al. [2000]. Brief physical descriptions of each gauged watershed, based on *Stephenson* [1977] and subsequent research, are provided in *Pierson et al.* (2000).

Table 1. Watershed name, duration of record, drainage area, range in elevation, stream discharge regime characteristics and mean annual stream discharge for each gauged watershed in the Reynolds Creek Experimental Watershed, Idaho.

Watershed Name	Duration Of Record	Drainage Area (ha)	Elevation Range (m)	Stream Discharge Regime	Mean Annual Stream Discharge (m^3s^{-1})	(mm)
Reynolds Crk. Outlet	1963-1996	23,372	1101-2241	Perennial	0.560	75.7
Reynolds Crk. Tollgate	1966-1996	5,444	1410-2241	Perennial	0.424	245.9
Reynolds Mtn. East	1963-1996	40.5	2026-2137	Perennial	0.00671	523.1
Reynolds Mtn. West	1964-1984	51.0	2016-2131	Spring-fed Perennial	0.00686	424.9
Salmon Creek	1964-1996	3,638	1121-1918	Perennial	0.0823	71.4
Macks Creek	1964-1990	3,175	1145-1891	Intermittent	0.0724	72.0
Dobson Creek	1973-1980	1,409	1478-2241	Perennial	0.132	295.9
Murphy Creek	1967-1977	123.8	1383-1822	Spring-fed Intermittent	0.00752	191.7
Upper Sheep Creek	1970-1975 1983-1996	26.1	1839-2017	Intermittent	0.000756	91.6
Summit Wash	1967-1975	83.0	1260-1457	Ephemeral	0.0000181	0.7
Flats	1972-1996	0.9	1190-1198	Ephemeral	0.000000566	2.0
Nancy Gulch	1971-1996	1.3	1409-1426	Ephemeral	0.00000280	7.0
Lower Sheep Creek	1967-1984 1989-1996	13.4	1583-1653	Ephemeral	0.0000362	8.6

METHODS

Runoff

Five types of stream gauging devices are used on RCEW: (1) Self-Cleaning Overflow V-notch (SCOV) weir, (2) drop-box V-notch weir, (3) 30^o V-notch weir, (4) 90^o V-notch weir, and (5) Parshall flume [*Brakensiek et al.*, 1979]. All stations are equipped with stilling-wells and floats for obtaining instantaneous measures of stage height. Instrument shelters are heated to permit collection of discharge and sediment data during cold winter periods. Gauging stations are visited on a weekly or biweekly basis to record staff gauge readings and service all instrumentation [*Pierson and Cram*, 1998]. The lengths of discharge record for each watershed are given in Table 1.

Stage height measurements were originally recorded using Leopold-Stevens A-35 and FW-1 strip chart recorders [*Brakensiek et al.*, 1979], later supplanted by electronic data loggers. Pressure sensors are now used for redundant back-up measurements of stage height to guard against the occasional plugging of stilling well inlet pipes. Strip charts were processed by digitizing selected break-points along a recorded continuous trace to create a digital record of instantaneous stage height. Stage height was then used to create a digital record of discharge using appropriate weir calibration equations. Later use of electronic recording equipment allowed collection of more comprehensive digital data. Stage height is now monitored every ten seconds to determine if the stage is rising or falling. If the stage has significantly changed, the new instantaneous stage height value is recorded at the nearest minute. If the stage has not

significantly changed, then instantaneous stage height is recorded every fifteen minutes. Accuracy of stage height measurements is periodically checked against manual staff gauge measurements; if necessary, corrections to the recorded data are made in a linear step-wise fashion between staff gauge readings. Errors in gauge height measurements due to ice build-up in the weirs in winter are ocularly identified and manually corrected. Hourly runoff records are created from break-point runoff data using linear interpolation between break-point estimates.

Suspended Sediment

Suspended sediment samples were collected at Reynolds Creek: Outlet, Reynolds Creek: Tollgate and Reynolds Creek: Reynolds Mountain East Basin gauging stations during the period covered by this report. Suspended sediment samples were collected manually in early years using a DH-48 integrated sampler at the large weirs or simple grab samples at the smaller weirs. Automated sediment samplers were subsequently used at all stream gauging sites to collect suspended sediment samples. Chickasha, PS-67, PS-69, ISCO, Manning and Sigma pump samplers have been used to collect suspended sediment samples at different gauging stations during different time periods [*Brakensiek et al.*, 1979]. All stations are currently equipped with Sigma pump samplers. Collected sediment samples are filtered and weighed to determine sediment concentration of each sample [*Pierson and Cram,* 1998]. The types of sediment samplers used and the length of sediment record for each gauging station are given in Table 2.

Table 2. Duration of record for measured and estimated suspended sediment concentrations using different types of sediment samplers for each gauged watershed in Reynolds Creek Experimental Watershed, Idaho.

Watershed Name	Watershed ID Number	Sediment Sampler Used	Duration of Measured Concentrations	Duration of Estimated Break-Point Concentrations
Reynolds Creek Outlet	036x68	Hand	1965-1975	1967-1975
		PS-67	1975-1979	1975-1979
		PS-69	1980-1988	1980-1986
		Sigma	1989-1996	
Reynolds Creek Tollgate	116x83	Hand	1967-1969	1967-1969
		PS-67	1969-1979	1969-1979
		PS-69	1980-1986	1980-1986
		ISCO	1987-1994	
		Sigma	1994-1996	
Reynolds Mountain East	166x76	Chickasha	1969-1984	1969-1984
		Manning	1984-1986	1984-1986
		ISCO	1987-1996	

Early sediment data include only manually-sampled sediment concentrations for large events. Later, automated sediment samplers made it possible to collect more samples during all events, but samplers were often unreliable resulting in intermittent missing data during early years of automated sampling. Pump samplers have become more reliable in recent years, and when coupled with data loggers can collect sediment samples at critical points during runoff events (e.g., Figure 5 portrays a typical runoff event with corresponding sediment concentrations and sample times).

A continuous break-point record of sediment concentrations was created based upon measured sediment concentrations and runoff patterns. This record was combined with the runoff record to estimate monthly

and annual sediment yields. Both the record of measured sediment concentrations and the record of estimated break-point sediment concentrations are now available.

RUNOFF REGIME

Three stream gauging stations along the main stem of Reynolds Creek (Outlet, Tollgate and Reynolds Mountain East) constitute the backbone of the stream gauging network within RCEW. Stream discharge has been measured from Outlet and Reynolds Mountain East weirs starting with the 1963 water year and continuing uninterrupted to the present time (Table 1). Tollgate weir was installed in 1966 to represent the mid-elevations on RCEW. Ten additional stream gauging stations were subsequently installed; five of those were still active in 1996 (Table 1).

Stream discharge throughout RCEW is dominated by runoff from spring snowmelt, particularly at higher elevations (Figure 2). Average monthly discharge is greatest during May at all elevations. However, lower elevations also show the impact of rain-on-snow events during the winter months, resulting in a more even distribution of discharge from December through June. Mean annual discharge is quite variable between locations, varying with basin size, basin elevation, and specific setting within RCEW (Table 2).

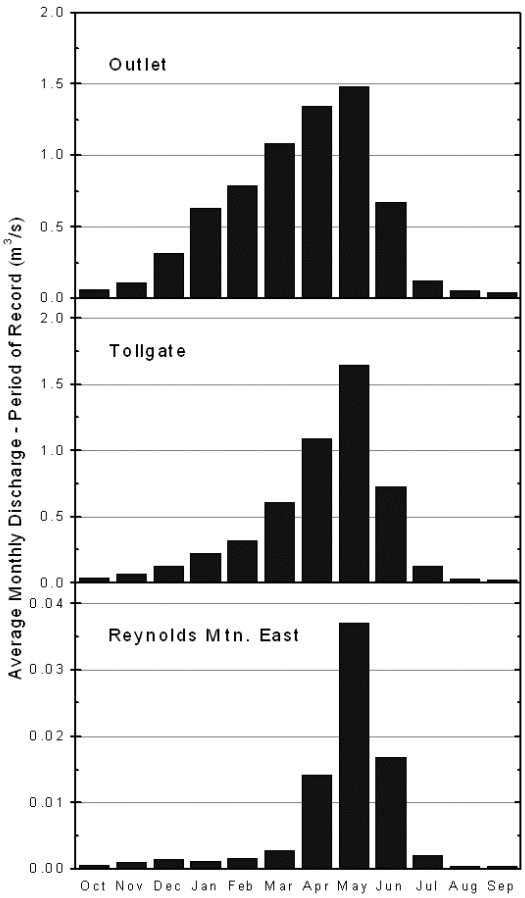

Figure 2. Average monthly discharge rate for Outlet, Tollgate and Reynolds Mountain East watersheds in Reynolds Creek Experimental Watershed, Idaho

Discharge is quite variable between years at all locations. Figure 3 shows the average daily discharge rate for Outlet, Tollgate and Reynolds Mountain East basins during years with high and low precipitation and stream discharge. During high-flow years, discharge follows the expected pattern of increasing with discharge area: Outlet has the greatest discharge, followed by Tollgate, then by Reynolds Mountain East. During low-flow years, discharge rates are generally an order of magnitude lower, with highest flows being measured at Tollgate rather than Outlet due to water being diverted from Reynolds Creek below Tollgate for local irrigation. Specific discharge rates (Figure 4) are higher for areas with greater proportions of high elevation (Table 1). The high annual variability in discharge between high- and low-precipitation years is again demonstrated in Figure 4.

Peak discharge rates for the ten greatest events recorded at Outlet, Tollgate and Reynolds Mountain East weirs are given in Table 3. The highest flows at Outlet have been driven primarily by rain-on-snow winter events, while Reynolds Mountain high flows have been dominated by rapid spring snowmelt. The winter flood in December 1964 was the highest flow recorded for both stations. Mid-elevations represented by the Tollgate weir experience both winter rain-on-snow and spring snowmelt events. Occasional intense thunderstorms can impact all elevations, but are particularly important for lower elevations and the eastern side of RCEW. The fifth-largest peak flow recorded at Outlet (Table 3) was the result of a short-duration high-intensity convective storm centered over Summit Wash, in the dry northeastern sector of RCEW.

SUSPENDED SEDIMENT REGIME

A record of suspended sediment concentrations is available for Outlet, Tollgate and Reynolds Mountain East watersheds. The record began at Outlet weir in 1965 when major runoff events were sampled using periodic grab samples throughout the duration of the event. The first pump samplers were used in 1969 increasing the number of events sampled and the number of samples taken during each event (Table 2). In current practice, sediment concentrations are intensely sampled during all events and periodically sampled during low flows. Figure 5 illustrates the frequency at which suspended sediment concentration is currently sampled at Outlet, Tollgate and Reynolds Mountain East weirs during runoff events.

Large runoff events account for most of the sediment yielded from RCEW [*Johnson and Hanson,* 1976]. Sediment concentrations are highest during the rising stages of an event and then sharply decrease until discharge rate again rapidly increases during the next runoff event (Figure 5). Sediment concentrations during low flows are generally two orders of magnitude lower than during runoff events and contribute little to the overall RCEW sediment budget. *Johnson and Hanson* [1976] reported that average sediment yields from RCEW and individual watersheds (3,200 to 23,000 ha) ranged from 1.14 to 1.9 tonnes/ha/year. Sediment concentrations and annual sediment yield increase with drainage area, as illustrated in Figure 5. During spring runoff, sediment concentrations for the entire RCEW can be an order of magnitude higher than for high elevations above Tollgate weir and two orders of magnitude higher than for Reynolds Mountain East Basin (Figure 5).

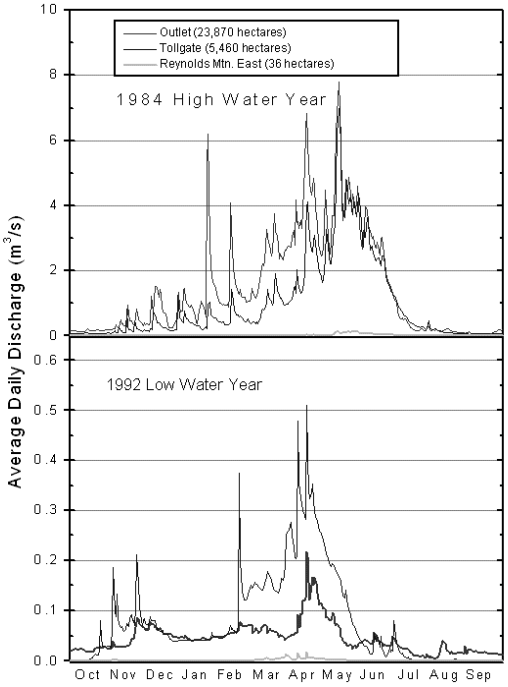

Figure 3. Average daily discharge rate for Outlet, Tollgate and Reynolds Mountain East watersheds during low (1992) and high (1984) water years in Reynolds Creek Experimental Watershed, Idaho.

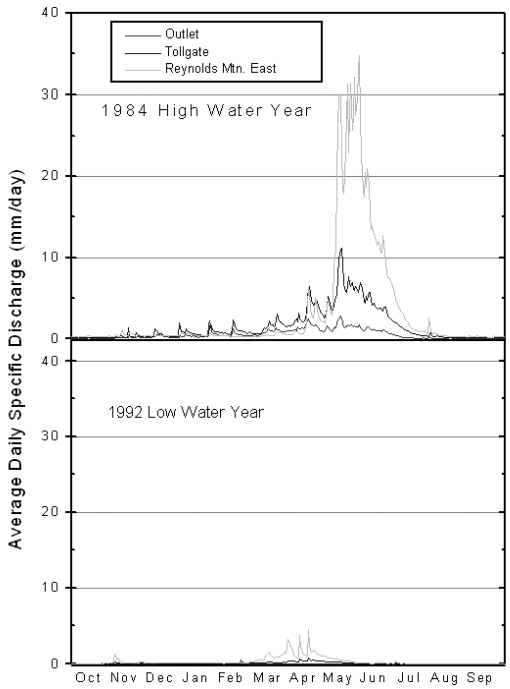

Figure 4. Average daily discharge for Outlet, Tollgate and Reynolds Mountain East watersheds during low (1992) and high (1984) water years normalized by watershed area in Reynolds Creek Experimental Watershed, Idaho.

Table 3. Top ten highest peak discharge events for Outlet, Tollgate and Reynolds Mountain East watersheds in the Reynolds Creek Experimental Watershed, Idaho.

Reynolds Creek Outlet		Reynolds Creek Tollgate		Reynolds Mountain East Basin	
Date	Peak Discharge (m^3s^{-1})	Date	Peak Discharge (m^3s^{-1})	Date	Peak Discharge (m^3s^{-1})
12/23/64	109.03	12/19/81	12.10	12/23/64	0.303
01/31/63	66.02	01/21/69	11.47	05/29/83	0.282
02/15/82	58.97	04/11/82	11.26	06/02/75	0.263
01/11/79	47.09	05/13/84	8.96	05/29/84	0.245
06/11/77	31.70	03/18/93	8.43	05/12/93	0.182
01/28/65	31.53	06/07/67	8.16	06/06/72	0.177
01/21/69	25.48	02/23/86	7.88	05/17/70	0.167
04/11/82	24.40	06/06/93	7.71	05/04/71	0.163
01/27/70	20.64	03/02/72	7.67	04/28/90	0.155
03/02/72	19.19	05/28/83	7.51	05/22/67	0.154

DATA AVAILABILITY

Discharge data from thirteen weirs located on the RCEW are available from the anonymous FTP site *ftp.nwrc.ars.usda.gov* maintained by the USDA Agricultural Research Service, Northwest Watershed Research Center in Boise, Idaho, USA [*Pierson et al.*, 2000]. Sediment data from three weirs are also available on the same FTP site and located in the same directory as the discharge data. An ASCII README file on the FTP site gives a detailed description of the file formats and contents.

DISCLAIMER

The mention of trade names or commercial products does not constitute endorsement or recommendation for use. The Agricultural Research Service (ARS) is a research organization. There are no legal mandates for the agency to collect or to distribute data collected for specific research projects. These data are being made available to the research community to promote the general knowledge of the processes relating to our country's natural resources.

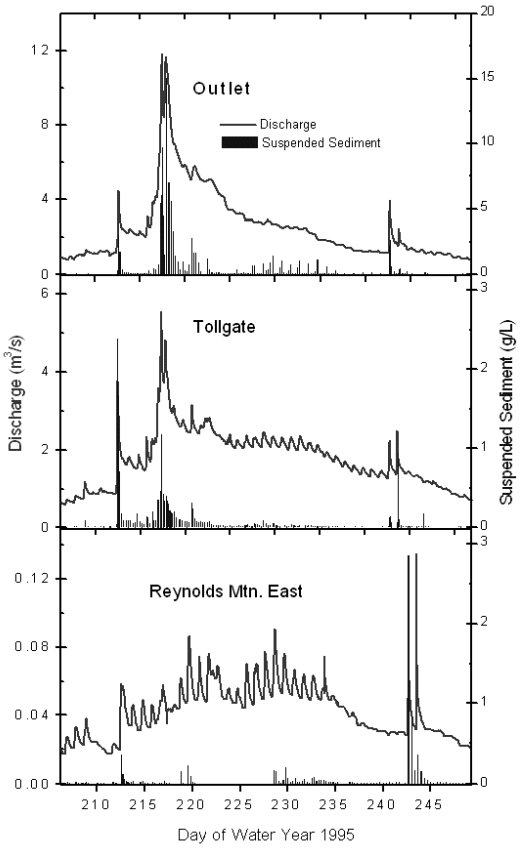

Figure 5. Discharge rate and associated measured sediment concentrations for Outlet, Tollgate and Reynolds Mountain East watersheds during spring flow 1995 in Reynolds Creek Experimental Watershed, Idaho.

REFERENCES

Brakensiek, D.L., H.B. Osborn, and W.J. Rawls, Field manual for research in agricultural hydrology, Agriculture Handbook 224, p. 550, U.S. Department of Agriculture, Washington D.C., 1979.

Flerchinger, G.N., K.R. Coolley, and Y. Deng, Impacts of spatially and temporally varying snowmelt on subsurface flow in a mountainous watershed: 1. Snowmelt simulation, *Hydrological Sciences Journal*, 39, 507-520, 1994.

Johnson, C.W., and C.L. Hanson, Sediment sources and yields from sagebrush rangeland watersheds, in *Proceedings Third Federal Inter-Agency Sedimentation Conference*, P. 1-71 - 1-80, Sedimentation Committee, Water Resources Council, Denver CO, 1976.

Johnson, C.W., and J.P. Smith, Sediment characteristics and transport from northwest rangeland watersheds, *Transactions American Society of Agricultural Engineers* 21(6), 1157-1162, 1978.

Pierson, F.B., W.H. Blackburn, S.S. Van Vactor, and J.C. Wood, Partitioning small scale spatial variability of runoff and erosion on sagebrush rangeland, *Water Res. Bulletin*, 33, 1081-1089, 1994.

Pierson, F.B., and Z.N. Cram, Reynolds Creek Experimental Watershed Runoff and Sediment Data Collection Field Manual, Report NWRC 98-2, p. 30, Northwest Watershed Research Center, USDA-ARS, Boise, Idaho, 1998.

Pierson, F.B., C.W. Slaughter and Z.K. Cram. Monitoring streamflow and suspended sediment, Reynolds Creek Experimental Watershed, Idaho, USA, ARS Tech. Bull. NWRC 2000-8, Northwest Watershed Research Center, USDA Agricultural Research Service, Boise, Idaho, 20pp, 2000.

Seyfried, M.S., and B.P. Wilcox, Scale and the nature of spatial variability: field examples having implications for hydrologic modeling, *Water Resources Research* 31, 173-184, 1995.

Seyfried, M.S., R.C. Harris, D.G. Marks, and B. Jacob, A geographic database for watershed research, Reynolds Creek Experimental Watershed, Idaho, USA, ARS Tech. Bull. NWRC 2000-3, Northwest Watershed Research Center, USDA Agricultural Research Service, Boise, Idaho, 27pp, 2000.

Slaughter, C.W., A.L. Huber, G.L. Johnson, K.R. Cooley, and C.L. Hanson, Implications of the Northwest floods of February 1996 for Southwestern Idaho, *in The Pacific Northwest Floods of February 6-11, 1996*, edited by A. Laenen, pp. 67-79, American Institute of Hydrology, Portland, Oregon, 1997.

Slaughter, C.W., K.R. Cooley, C.L. Hanson, F.B. Pierson, R.L. Hartzmann, A.L. Huber and J.B. Awang, Baseline sediment yield from dissimilar headwaters research watersheds, in *Proceedings Sixth Federal Interagency Sedimentation Conference, Sedimentation Technologies for Management of Natural Resources in the 21st Century*, pp. X30-X37, Las Vegas, NV, 1996.

Stephenson, G.R., Soil-Geology-Vegetation Inventories for Reynolds Creek Watershed. Miscellaneous Series No. 42, p. 73, Agricultural Experiment Station, University of Idaho College of Agriculture, Moscow, Idaho, 1977.